Nanomaterials as catalysts for CO2 transformation into value-added products: A review

Yakubu Adekunle Alli, Peter Olusakin Oladoye, Onome Ejeromedoghene, Owolabi Mutolib Bankole, Oyekunle Azeez Alimi, Elizabeth Oyinkansola Omotola, Clement Ajibade Olanrewaju, Karine Philippot, Adeyemi Adeleye, Adeniyi Sunday Ogunlaja

Nanomaterials as Catalysts for CO_2 Transformation into Value-added Products: A Review

Yakubu Adekunle Alli[a,b**], Peter Olusakin Oladoye[c,*], Onome Ejeromedoghene[d], Owolabi Mutolib Bankole[e], Oyekunle Azeez Alimi[f], Elizabeth Oyinkansola Omotola[g], Clement Ajibade Olanrewaju[c], Karine Philippot[a], Adeyemi S. Adeleye[h], Adeniyi Sunday Ogunlaja[e]

[a]Laboratoire de Chimie de Coordination du CNRS, UPR8241, Universite´ de Toulouse, UPS, INPT, Toulouse cedex 4 F-31077, France.

[b]Department of Chemical Sciences, Faculty of Science and Computing, Ahman Pategi University, Km 3, Patigi-Kpada Road , Patigi, Kwara State 243105, Nigeria

[c]Department of Chemistry and Biochemistry, Florida International University, 11200 SW 8th St, Miami, FL, 33199, USA

[d]School of Chemistry and Chemical Engineering, Southeast University, 211189 Nanjing, Jiangsu Province, P. R. China

[e]Department of Chemistry, Nelson Mandela University, Port Elizabeth, South Africa

[f]Research Center for Synthesis and Catalysis, Department of Chemical Sciences, University of Johannesburg, PO Box 524, Auckland Park, Johannesburg 2006, South Africa

[g]Department of Chemical Sciences, Tai Solarin University of Education, Ijebu Ode, Ogun State, Nigeria

[h]Department of Civil and Environmental Engineering, University of California, Irvine, CA 92697-2175, USA

[**]Corresponding author's e-mail address: yakubu.alli@lcc-toulouse.fr

[**]Corresponding author's address: LCC-CNRS, Université de Toulouse, CNRS, UPS, 205 Route de Narbonne, BP44099, 31077 CEDEX 4 Toulouse, France

*Corresponding author's e-mail address: poladoye@fiu.edu
*Corresponding author's address: Department of Chemistry and Biochemistry, Florida International University, 11200 SW 8th St, Miami, FL, 33199, USA

**Corresponding author's e-mail address: yakubu.alli@lcc-toulouse.fr
**Corresponding author's address: LCC-CNRS, Université de Toulouse, CNRS, UPS, 205 Route de Narbonne, BP44099, 31077 CEDEX 4 Toulouse, France

Abstract

Carbon dioxide (CO_2) is the most important greenhouse gas (GHG), accounting for 76% of all GHG emissions. The atmospheric CO_2 concentration has increased from 280 ppm in the pre-industrial era to about 417.86 ppm, and is projected to reach 570 ppm by the end of the 21st century. In addition to reducing CO_2 emissions from anthropogenic activities, strategies to adequately address climate change must include CO_2 capture. To promote circular economy, captured CO_2 should be converted to value-added materials such as fuels and chemical feedstock. Due to their tunable chemistry (which allows them to be selective) and high surface area (which allows them to be efficient), engineered nanomaterials are promising for CO_2 capturing and/or transformation. This work critically reviewed the application of nanomaterials for the transformation of CO_2 into various fuels, like formic acid, carbon monoxide, methanol, and ethanol. We discussed the literature on the use of metal-based nanomaterials, inorganic/organic nanocomposites, as well as other routes suitable for CO_2 conversion such as the electrochemical, non-thermal plasma, and hydrogenation routes. The characteristics, steps, mechanisms, and challenges associated with the different transformation technologies were also discussed. Finally, we presented a section on the future outlook of the field, which includes recommendations for how to continue to advance the use of nanotechnology for conversion of CO_2 to fuels.

Keywords: CO_2 based fuels, nanomaterials, global warming, catalysts

Table of contents

5. Conclusions and future outlook

1. Introduction

One of the primary environmental concerns today is climate change. Indicators of climate change include global warming, increased frequency and intensity of natural disasters and extreme weather events such as wildfires which was responsible for the loss of ~$650 billion between 2016 to 2018, extreme droughts in Europe, heatwaves in USA, and hurricanes in other parts of the world (Mustafa et al., 2020). Climate change is mainly attributed to increased emission of greenhouse gases into the atmosphere (Cassia et al., 2018; Solomon et al., 2010, 2009), which has led to the global surface temperature of 0.88°C (1.58°F) in September 2022 which is above the average for the 20th century of 15.0°C (59.0°F), tying September 2021 as the sixth warmest for September in the 143-year record. In addition, global CO_2 levels was 280 ppm in the pre-industrial era; it has now increased to 417.86 ppm as at October 19, 2022 according to the Global Monitoring Laboratory (daily global CO_2 trend) and it is projected to reach 570 ppm by the end of the 21st century (Mustafa et al., 2020).

In order to ameliorate global warming and other climate change indicators, it is imperative that emission of CO_2 is controlled, and the excess atmospheric CO_2 is captured. Several strategies exist for achieving atmospheric CO_2 reduction. For instance, afforestation is effective for CO_2 emission reduction and sequestration (Halder et al., 2014; Jansen et al., 2015; Li et al., 2013; Mondal et al., 2012). More so, various governmental and inter-governmental policies have been implemented to also reduce the emissions of CO_2 by putting taxes on carbon sources and fossil fuels (Atsbha et al., 2021; Herzer, 2022; Omoregbe et al., 2020; Peiseler & Cabrera Serrenho, 2022). Chemical CO_2 conversion is also effective but is a herculean task due to the

characteristic thermodynamic stability of CO_2 molecule. The stability of CO_2 arises from its structure (O=C=O) and possession of double covalent bonds with two oxygen atoms (Ateka et al., 2022). The carbon in CO_2 is extremely inactive and is kinetically inert owing to its occurrence at the highest oxidation state in CO_2 (Wang et al., 2022). As a result, the transformation of CO_2 to useful fuels and/or chemicals demands the input of substantial amount of energy to cleave the C-O bond (Pawelec et al., 2021; Sha et al., 2020)

The energy requirement for CO_2 conversion is met through three major routes: (i) the use of (nanomaterial-based) catalysts with active sites, (ii) the application of high pressure and/or temperature, and (iii) application of energy from carbon-neutral and renewable energy sources (Kamkeng et al., 2021). There are a number of technological approaches that can be employed to execute transformation of CO_2. In terms of using catalysts for CO_2 transformation, the processes and/or mechanisms involved may be photocatalytic, electrocatalytic, thermal or non-thermal etc., to lower the energy barrier and create alternative pathway for the catalytic CO_2 reduction (Ateka et al., 2022). For example, in photo-catalyzed transformation using titanium dioxide (TiO_2; a common photo-catalyst) as a catalyst, upon irradiation, a photo hole-electron pair is generated, which interacts with CO_2 and H_2O molecules to produce hydrocarbons and other value-added products. This is feasible only by appropriate catalyst selection, doping and conditions (Low et al., 2017). Scheme 1 presents the various value added-products of CO_2 transformation covered in this synthesis.

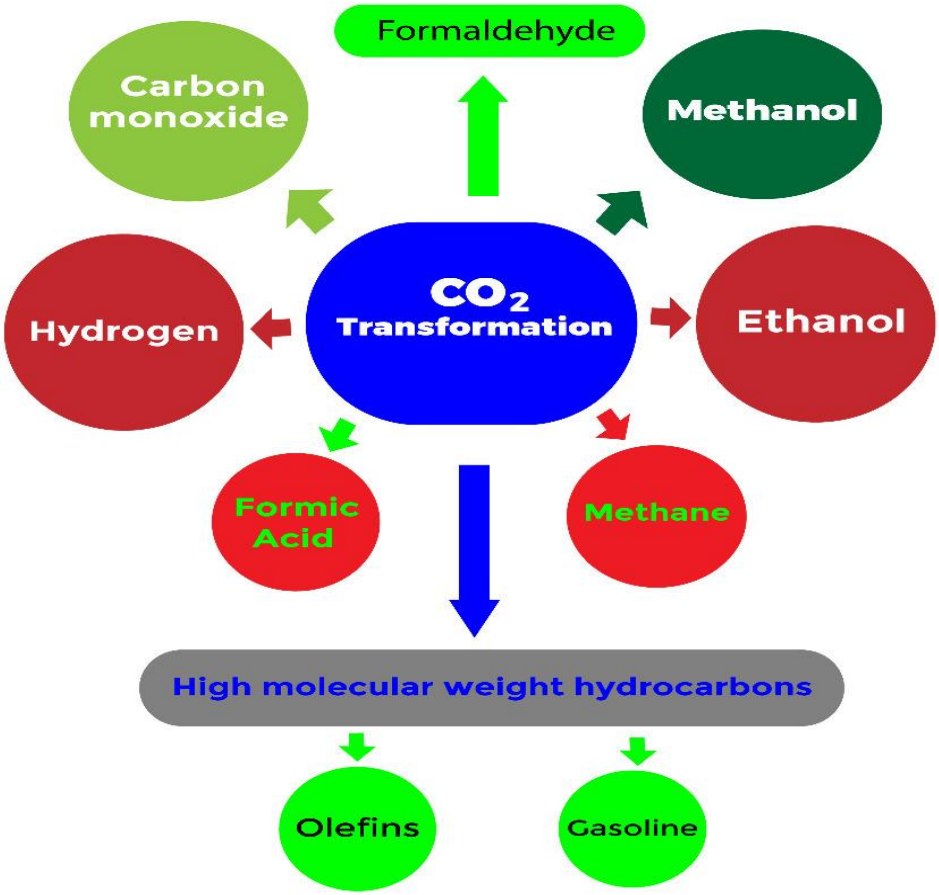

Scheme 1: Products obtained from the transformation of CO_2

A number of comprehensive, systematic and/or critical reviews on the transformation of CO_2 have been published (Kamkeng et al., 2021; Low et al., 2017; Mustafa et al., 2020; Pawelec et al., 2021; Sha et al., 2020; Wang et al., 2011; Wu et al., 2017). Although a large proportion of them are detailed with respect to application and transformation of CO_2, recent advances in technologies for CO_2 conversion have not been sufficiently covered by the existing reviews. In addition, the technical challenges facing the real-world implementation of these technologies are yet to the comprehensively explored and presented. Therefore, this synthesis on CO_2 conversion

to valued-added products attempts to provide current and comprehensive understanding on nano-enabled CO_2 conversion, routes of CO_2 conversion, fuels generated from CO_2 conversion, application, technical issues and economic implications of transformation of CO_2 into hydrocarbon fuels. The review also elaborates the research gaps that need to be filled.

2. Nanomaterials for CO_2 conversion

Nanomaterials have gotten a lot of attention in the research world because of their fascinating small size (1-100 nm), which is responsible for their improved functionality (Afolabi et al., 2022; Alli et al., 2022, 2021). In this regard, the use of nanomaterials for direct transformation of CO_2, to renewable organic fuels and other feedstocks has become a promising solution to simultaneously mitigate the global energy crisis and climatic change. Due to the thermodynamic stability, fully oxidized nature, and inertness of CO_2, various nanoscale catalysts have been developed to activate CO_2 molecules into low (C_1) and high hydrocarbon (C_1-C_9) molecules. Figure 1 depicts possible catalytic pathways for CO_2 transformation to fuels and chemical products. They include thermocatalytic reduction of CO_2/H_2 to produce CH_4/CO, electrocatalytic transformation of CO_2/H_2/electron to C_1-C_9 hydrocarbons, cycloaddition of CO_2 with epoxide to form cyclic and polycarbonates, and the emerging photocatalytic reduction of CO_2/H_2O to CH_4, CHOOH, CH_3OH, etc. The nature and kinds of nanomaterials for conversion of CO_2 also play a vital role in product selectivity to get carbon-containing fuels, in addition to process parameters such as solvent effects, reaction temperature, H_2/CO_2 ratios, and partial pressure condition of CO_2. The nanomaterials for catalytic conversion of CO_2 are range from plasmonic metal nanoparticles and metal oxides-based composites to metal-free nanoporous materials including carbon nanostructures

158 such as grapheme oxide (GO) reduced grapheme oxide (rGO) and carbon nanotubes
159 (CNT), silica, alumina, covalent organic polymers, etc.

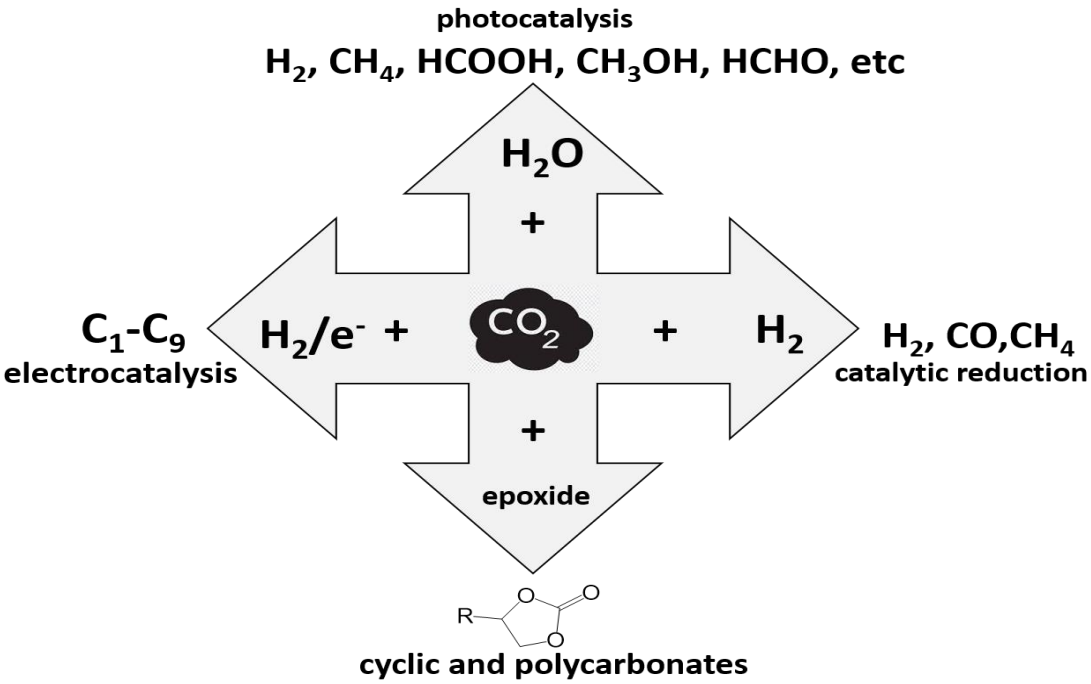

160

161 Figure 1: Pathways for catalytic conversions of CO_2 to various feedstocks

162 **3. Routes of CO_2 conversion**

163 **3.1 Photocatalytic transformation of CO_2**

164 The natural process of photosynthesis, in which plants change CO_2 and H_2O into
165 oxygen and carbohydrates when exposed to sunlight, served as the inspiration for
166 photocatalytic CO_2 reduction. This process transforms solar energy into chemical
167 bonds, which are then stored (carbohydrates). It combines light and dark reactions with
168 water oxidation and carbon dioxide reduction (or CO_2 fixation) reactions. The process
169 of photocatalytic transformation of CO_2 into value added particularly using
170 semiconductor or metal complex as catalyst can be divided into four steps: (i)
171 absorption of light greater or equal to the band gap (ii) Separation of valence band (CB)
172 and conduction band (CB) (iii) migration of electrons from the VB to CB and migration

of electrons to the surface of cocatalyst (iv) adsorption and activation of CO_2 by the photogenerated electrons (Kovačič et al., 2020)(Figure 2).

To understand the kinetic and thermodynamic point of view, the formal reduction potentials for the reactions connected to the photoreduction of CO_2 (at pH 7) is presented in Figure 12a. Due to their extremely high negative reduction potentials [$E(CO_2/CO_2^{\bullet-})$ = -1.85 V vs NHE] in relation to the CB edges of many semiconductors, one-electron reduction processes of CO_2, such as the generation of CO_2 •, are not practical (Lingampalli et al., 2017). A highly negative reduction potential results from the conversion of C's sp^2 to sp^3 hybridization. Reduction potentials for HCOOH, HCHO, CH_3OH, and CH4 production are minimal (-0.81, -0.48, -0.38, and -0.246 V) (Figure 12b) and positive relative to CB edges of various semiconductors. Proton coupled electron transfer (PCET), in which electron transfer to CO_2 is accompanied with proton transfer, is thus preferable (Kovačič et al., 2020; Lingampalli et al., 2017). A good number of works has been done recently to functionalize semiconductors and it's like as novel and effective photocatalysts. Various single and composites nanomaterial have been reported for photocatalytic transformation of CO_2. This section critically survey the scattered literatures

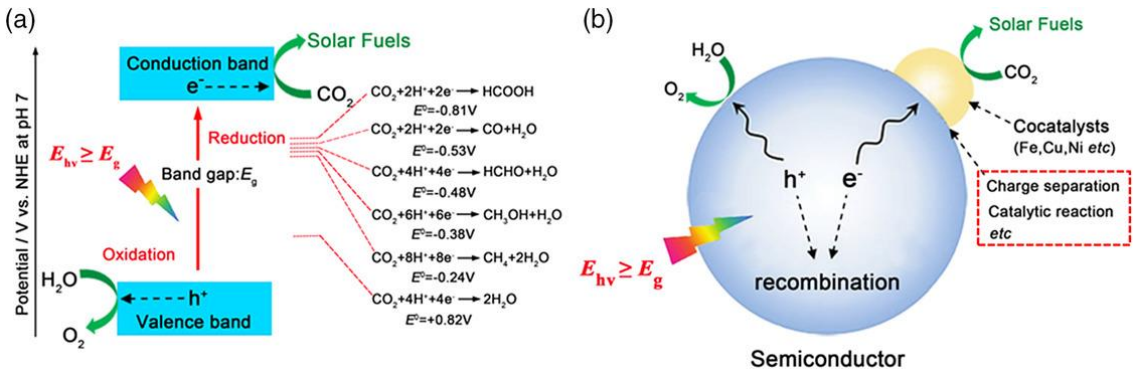

Figure 2: (a) Energy diagram for CO_2 reduction and water oxidation on a semiconductor. b) A schematic representation of the overal photocatalytic reaction

process, demonstrating elements that may influence photocatalytic performance. Reproduced with the permission from (Shen et al., 2020). Copy right 2020 Willey Library

3.1.1 Single metal nanoparticles

Plasmonic metal nanoparticles (NPs) such as Au, Ag, and Cu have a large optical extinction cross section and the ability to absorb significant visible light which accounts for up to 40% of solar irradiation to catalyze a wide range of photochemical reactions. As a result, , they offer several advantages over other conventional catalysts like Pt, Pd, Ru, and Rh, whose localized surface plasmon resonances (LSPRs) fall in the UV region of the solar spectrum. A single silver nanoparticles (AgNPs) photocatalyst was excited in a microfluidic reaction cell filled with CO_2 led to CO_2 reduction reaction CO_2RR, to CO and HCOOH. The synergy between photoexcited CO_2 and catalytic active sites, which is not clearly understood at the molecular level, was evidenced by *in-situ* surface-enhanced Raman spectroscopy (SERS) (Kumari et al., 2018). The SERS was used to physi-sorb CO_2 on nanoparticles, LSPR-triggered CO_2 activation to $HOCO^*$ (intermediate), followed by transformation of $HOCO^*$ to multiple products (H_2, CO, HCOOH, HCHO and CH_3OH), (see Figure 3). The real-time monitoring of CO_2RR activity by SERS shows that plasmonic AgNPs are selective for CO and HCOOH, with CO being the predominant product. On polyvinylpyrrolidone (PVP)-capped plasmonic AuNP-photocatalyst, photoexcited LSPR induced a multi-electron and multi-proton reduction of CO_2 to C_1 (methane) and C_2 (ethane) hydrocarbons, without formation of CO (Yu et al., 2018). The CO_2RR was conducted in isopropyl alcohol (IPA) saturated CO_2-aqueous solution to prevent h^+/e^- recombination during photoredox reaction, and the CO_2RR selectively produced CH_4 (6.8 NP^{-1}) and C_2H_6 (5.6 NP^{-1}) after 10 h of light irradiation. The results show that catalytic and selectivity of plasmonic gold

nanoparticles (AuNPs) for CO_2 transformation to C_1 and C_2 is modulated by laser excitation wavelength (photon energy), and photon flux (light intensity). Thus, the CH_4 production rate increased with decreasing excitation wavelength and with overall $8e^-$ process ($8H^+ + CO_2 \rightarrow CH_4 + 2H_2O$), while C_2H_6 production was only observed at lower excitation wavelength with $14e^-$ process ($14H^+ + 2CO_2 \rightarrow C_2H_6 + 4H_2O$). Zeng *et al.* (Zeng et al., 2021) embedded uniformly distributed plasmonic CuNPs into a triphenothiazine benzene ring (TPB) for photocatalytic CO_2 reduction to CO, H_2 and CH_4. CO evolution rates over TPB-Cu increased as the wt% of Cu bonded to TBP units increased, and CuNPs with 1wt% content yielded a CO evolution rate 3.2 times higher than bare CuNPs. Interestingly, the evolution rates of H_2 and CH_4 on TPB-Cu remained relatively constant, implying that incorporating plasmonic CuNPs into TPB increased the directional selectivity for CO formation over H_2 and CH_4. Plasmonic cupper NPs conjugated with TBP could provide a large contact area for hot electron migration, opening new doors for energy and carbon cycle processes.

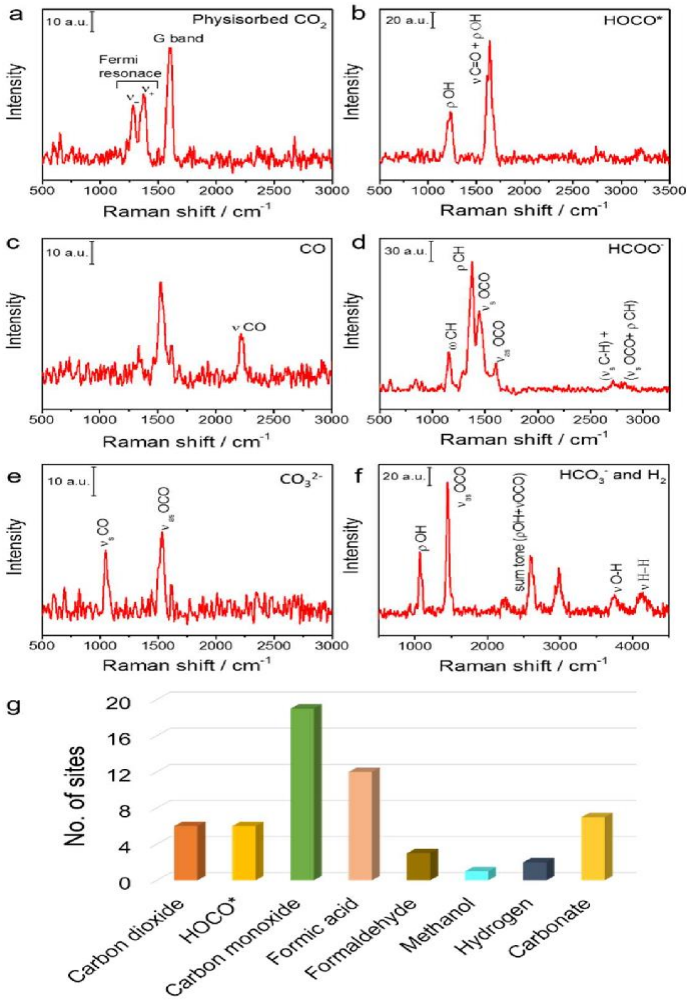

Figure 3: Representative SERS spectra that capture specific adsorbates or products observed in photocatalytic CO_2 reduction on Ag NPs. Specific species captured include (a) physisorbed CO_2, (b) $HOCO^*$ reaction intermediate, (c) carbon monoxide or CO, (d) formate ion or $HCOO^-$, (e) carbonate or CO_3^{2-}, (f) bicarbonate or HCO_3^-., adsorbed hydroxide or OH*, and H_2, and (g) Histogram of prevalence by the number of catalytic NPs on which each type of species was observed. Reproduced with permission from the American Chemical Society from ref. (Kumari et al., 2018).

3.1.2 Metal/metal oxide-based composites

In order to overcome the limitations of single-component plasmonic metal photocatalysts and to expand their light harvesting to UV region, researchers have

turned to multi-component semiconductors for a variety of applications. Decoration of metal oxide semiconductors with transition or plasmonic metals has been a huge success. Both plasmonic and transition metals on semiconductors can help harness UV and visible light by reducing energy band gaps, which play key roles in CO_2 activation and intermediates stabilization for CO_2RR.

For many years, the selective absolute conversion of CO_2 to CO has been a source of contention. In 2020, Nguyen *et al.* (Nguyen et al., 2020) constructed air-stable Z-scheme photocatalysts composed of Ag-decorated reduced titanium oxide/tungsten hybrid nanoparticles (TiO_2/WO_3-AgHNPs) for CO_2 reduction to CO (100%, without byproducts) and with an evolution rate of 1166.72 μmol g^{-1} h^{-1} after 7 h of light illumination. On one hand, the plasmonic Ag (1wt% Ag) increased the photocatalytic electron reaction rate up to 2333.44 μmol g^{-1} h^{-1}, and facilitated intense absorption light in the visible region of the catalysts due to its strong LSPR effect. The presence of Ti^{3+} states in the catalysts, on the other hand, facilitated the physisorption, stabilization, and reorientation of the intermediates formed during CO_2 reduction. Other gas products such as CH_4 and H_2 were produced in the absence of Ag deposition, suggesting the importance of using plasmonic Ag to achieve the formation of only CO.

Zhang *et al.* (Zhang et al., 2021) reported p-type Cu_2O photocatalysts with phase structures of 100 (100Cu_2O) and 111 (100Cu_2O) modified with Pd nanoparticles for CO_2RR activities. The well-matched band alignments between Pd and 100Cu_2O increased the work functions (Ws) of the 100Cu_2O-Pd composite, resulting in an enhanced photocatalytic CO generation at a production rate of 0.13 μmol/g.h, which is 3.0 times higher than bare 100Cu_2O nanoparticles. Pd nanoparticles (in 100Cu_2O-Pd) promoted efficient photoexcited electrons by acting as a photoinduced hole scavenger, and also improved photostability of 100Cu_2O-Pd by reducing photocorrosion.

However, 111Cu_2O-Pd composites lacked electron-hole mobility due to mismatched band structures between 111Cu_2O and Pd species, resulting in lower work function and poor photocatalytic CO_2RR compared to 100Cu_2O-Pd composites, emphasizing the importance of crystal surface structure and matched band structure construction for selective CO_2RR to CO.

Wang and co-workers demonstrated LSPR photo-assisted electron migration from plasmonic CuNPs to ZnO via metal-support interfaces in Cu/ZnO catalysts for CO_2 reduction to MeOH (Wang et al., 2019). In the photothermal process, the rate of MeOH formation was 2.13 μmol/g. min, compared to 1.38 μmol/g. min recorded in pure thermal process, and the apparent activation energy decreased from 82.4 to 49.4 kJ mol^{-1}. The rate-determining step in the thermal process was the formation of reaction intermediates (*HCOO, *HCOOH, and $^*H_2COOH$ species), followed by the hydrogenation of *HCOOH to MeOH. Formation of MeOH in photothermal process followed the same reaction pathway as thermal process, with the exception that induced hot electrons on CuNPs accelerated the conversion of intermediates to product (MeOH). Under visible light irradiation, the product selectivity over Cu/ZnO remained relatively constant and the decreased activation energy had no effect. Small amounts of Pt nanoparticles have also been used as co-catalyst on $ZnMn_2O_4$ nanorods as visible-light-driven catalysts for promoting CO_2 reduction to produce methane, as was the case in other studies (Alhaddad and Shawky, 2021) (see Figure 4a). The wt% of Pt species on ZMO nanorods influenced the catalytic activity and selectivity of Pt/ZMO catalysts, with 1.5% Pt/ZMO exhibiting the best photocatalytic performance for CO_2RR activity (Figure 4b). Band connection and surficial interactions between Pt species and ZMO nanorods with optimal Pt/ZMO at 1.5% Pt enhanced selective reduction of CO_2 to MeOH with an evolution rate of 1,906 μmol/g within 9 h.

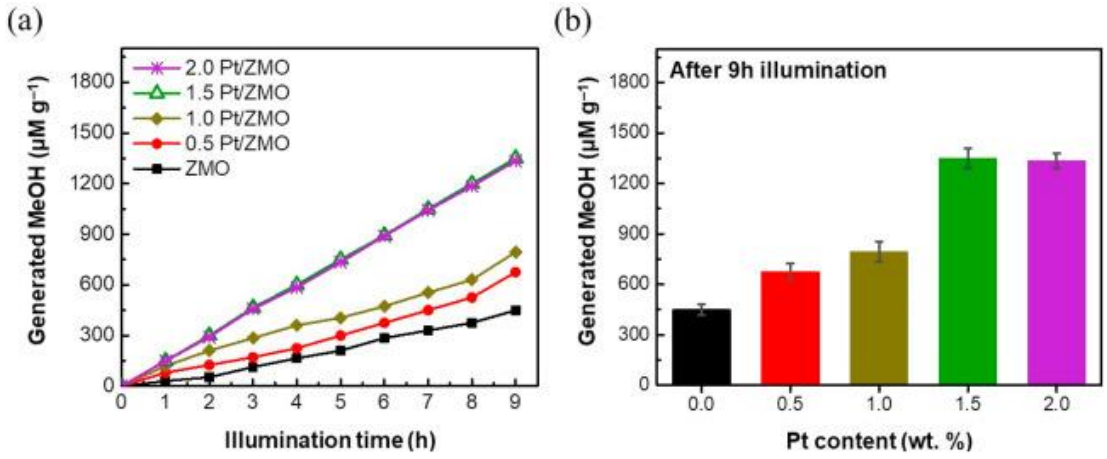

Figure 4: (a) Photocatalytic generation of methanol over Pt/ZMO nanocomposites at different illumination time, and (b) impact of Pt content in Pt/ZMO composite for a dose of 1.0 g/L for each within 9 h of light illumination. Reproduced from (Alhaddad and Shawky, 2021) with permission.

V, Cr, and Co loaded on TiO_2 were studied for CO_2RR to produce H_2, C_1 and C_{2+}. Higher photoconversion rates were observed compared to pristine TiO_2, which were found to be sensitive to the metal concentrations and TiO_2 crystallite size modification (Ola and Maroto-Valer, 2015). After 4 h of illumination, 1wt% Co-TiO_2 demonstrated the highest photoconversion rates of 62.91 μmol/g_{cat}h for H_2 and 26.12 μmol/g_{cat}h for MeOH (Figure 5). Ni-modified CeO_2, MgO, α-Al_2O_3 and TiO_2 NPs were studied for CO_2 methanation, and the effects of the solid supports were elucidated (Tada et al., 2012). CO_2 methanation pathways followed two steps: (i) reaction of CO_2 and H_2 at the meta/metal oxide interfaces to afford CO through reverse water gas shift reaction ($CO_2 + H_2 \rightarrow CO + H_2O$), and (ii) prompt methanation of CO with H_2 ($CO + 3H_2 \rightarrow CH_4 + H_2O$) at low temperature via the Fisher–Tropsch synthesis (FTs). CeO_2 has the highest number of CO_2 adsorption sites and exhibits the highest CO_2 methanation with near-unity CH_4 selectivity. Li and co-workers showed that partially oxidized metallic Fe NPs

(Fe and FeO_x) deposited on $MgO\text{-}Al_2O_3$ and then reduced under H_2 at different temperatures photothermally hydrogenated CO_2 into C_1 and C_{2+} hydrocarbons (Li et al., 2021). The Fe-500 sample (reduction performed at 500°C) showed the highest CO_2 conversion and excellent selectivity for C_{2+} hydrocarbons with 0% CO. The FeO_x phase promotes CO_2 reduction to CO via RGSW reaction and modulates the electronic properties of Fe phase to suppress CH_2 and CH_3 hydrogenation, thus enhancing C_{2+} hydrocarbon formation.

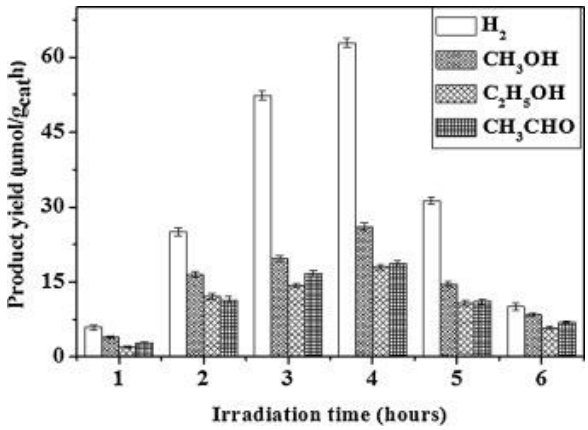

Figure 5: Irradiation time profile of 1 wt%Co–TiO_2 for CO_2 reduction to fuels. Reproduced from (Ola and Maroto-Valer, 2015) with permission.

The conjoining of metal, e.g. Ag and narrow band semiconductor e.g. InS_2 has been reported to improve photocatalytic reduction of CO_2 activity. Recently, a quaternary nanocomposite ($AgCuInS_2$) deposited on a graphene-TiO_2 based material presented excellent photoreduction activity of carbon dioxide in H_2O with the formation of mostly methanol, formaldehyde and formic acid. $AgCuInS_2$ combined with TiO_2 semiconductors ($AgCuInS_2$−TiO_2) absorb photon energy, which led to the excitation of electrons from valence band (VB) to conduction band (CB), creating electron−hole pair, and the graphene act as electron assimilates (Figure 6).

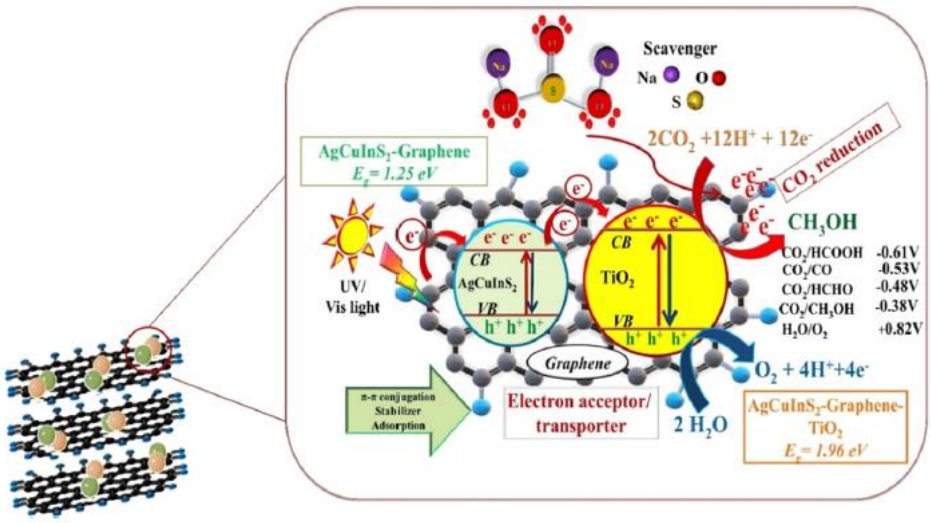

Figure 6: Mechanism of photocatalytic CO_2 reduction. Re-used with permission from (Otgonbayar et al., 2020). Copyright (2021) American Chemical Society.

3.1.3 Metal oxide/mesoporous oxides

Many metal-functionalized mesoporous aluminas and silicas have been studied as catalysts for CO_2 hydrogenation to CO via RWGS or CO methanation by Fischer Tropsch (FT) reactions. In terms of activity and selectivity, mesoporous materials with high Brunauer-Emett-Teller (BET) surface areas are important features for CO_2 adsorption and conversion (Petrovic et al., 2021). The nature of metal species immobilized on porous oxides also influences the CO_2RR selectivity for either CO or CH_4. Deposition of Ni on CaO-Al_2O_3 showed CO_2 conversion with 81% selectivity to CH_4; however, lower performance of the Ni-based catalyst in the subsequent methanation reaction (due to partial oxidation of Ni fractions) suggests that a better approach for CO_2RR on metal/mesoporous materials is required (Mutz et al., 2015). Addition of La as a second metal to Ni/-Al_2O_3, enhanced direct CO_2 methanation (CO_2 + H_2 → CO + H_2O) via the Sabatier reaction, increasing the CO_2 conversion rate to CH_4 from 42% to 80.3% (Rahmani et al., 2019). CO_2 methanation over mono and

bimetallic catalysts was temperature, feedstock (H_2/CO_2 ratio), and gas hourly space velocity (GHSV) sensitive. CO_2 was transformed into CO as a result of the RWGS reaction which occurred at higher GHSV values (between 6000-18,000 mL/(g_{cat}h)), 350^{o}C, and 3.5 H_2/CO_2 ratio, resulting in decreased CH_4 selectivity. In contrast, Bashiri and coworkers demonstrated that lowering the GHSV from 2000 to 1250 nml/min over a Ni-promoted iron catalyst on HZSM5-Al_2O_3 (Fe-Ni/HZSM5-Al_2O_3) increased CO_2 methanation significantly (Bashiri et al., 2018). The results also show that adding HZSM5 to Al_2O_3 increases the rate of CO_2 conversion to light hydrocarbons, CO, and CH_4 by 15.53%, indicating that combined supports have the potential to improve CO_2 conversion activity and selectivity.

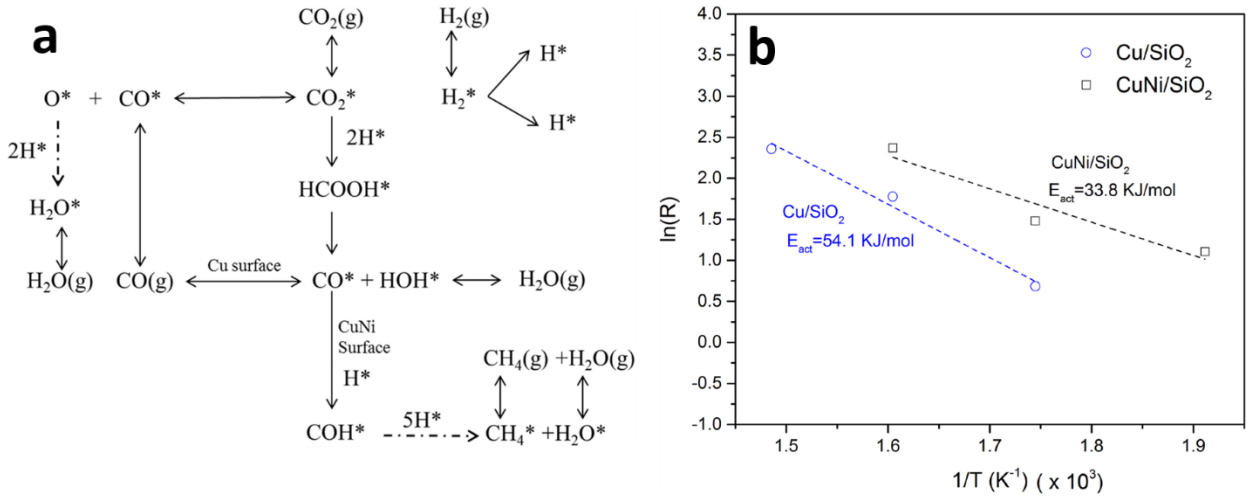

Figure 7: (a) Proposed reaction pathways on Cu/fumed-SiO_2 and CuNi/fumed-SiO_2 surface (b) Activation energy calculation for CO_2 conversion reaction over Cu/fumed-SiO_2 and CuNi/fumed-SiO_2. Reproduced from (Kumar et al., 2022) with permission.

Mesoporous siliceous materials are valuable supports because of their large number of active sites for supporting various metal ions to catalyze CO_2RR to renewable feedstocks. Single Cu-based catalytic systems are not suitable for direct CO_2

hydrogenation to either CH_4 or CH_3OH because they lead preferentially to the formation of CO via RWGS reaction. For example, CuNi/fumed-SiO_2 showed enhanced activity and selectivity for CO, as well as a tendency for methanation to CH_4 via interaction of CO and neighboring H, whereas Cu/fumed-SiO_2 showed only selectivity to CO due to decomposition of adsorbed formate intermediates to CO, Figure 7a (Kumar et al., 2022). The incorporation of Ni increases the system's catalytic active sites and lowers the activation barriers for CO_2RR to CO and CH_4, Figure 7b. Mesoporous Cu/SiO_2 doped with Ga and/or Zn had greater catalytic activity for direct CO_2 reduction to MeOH than undoped Cu/SiO_2 (Paris et al., 2020).

The strong promoting effects of dopants restricted the occurrence of RWGS reaction for CO formation while increasing selectivity for MeOH one. Both dopants provide more active sites on the catalysts, lowering the activation barrier of MeOH synthesis compared to CO formation, so methanol formation was preferred over CO formation. When mesoporous TiO_2/SiO_2 was irradiated with visible light without Cu species, CO was the main product of photo-transformation of CO_2/H_2O (Li et al., 2010). Cu deposition on TiO_2/SiO_2 improved photoreduction of CO_2 to CO, and CH_4 selectivity increased as well, peaking at 0.5wt% optimum Cu specie on TiO_2/SiO_2 (Figure 8). XPS allowed to identify the deposited Cu species as Cu_2O, which acts as a photoexcited electron sink, limiting the recombination of photoinduced holes and excited electrons and thus enhancing multi-electron photoredox reactions for CO_2 to CO and CH_4. Fu *et al.* designed photocatalytic systems based on CoO and Co_3O_4 nanoparticles to convert CO_2 to CO using bare CoONPs, CoO/s-SiO_2, CoO/s-SBA-15, and Co_3O_4/s-SBA-15 (Fu et al., 2019). Under similar photoredox conditions, CoO/s-SBA-15 exhibited the best activity for CO_2RR to CO with 85% selectivity at 14,147 μmol/hg after 2.5 h. Interfacial interactions between porous silica -OH groups and reaction substrates

enhance sorption and photocatalytic CO_2 reduction to CO over CoO/s-SBA-15 catalyst system.

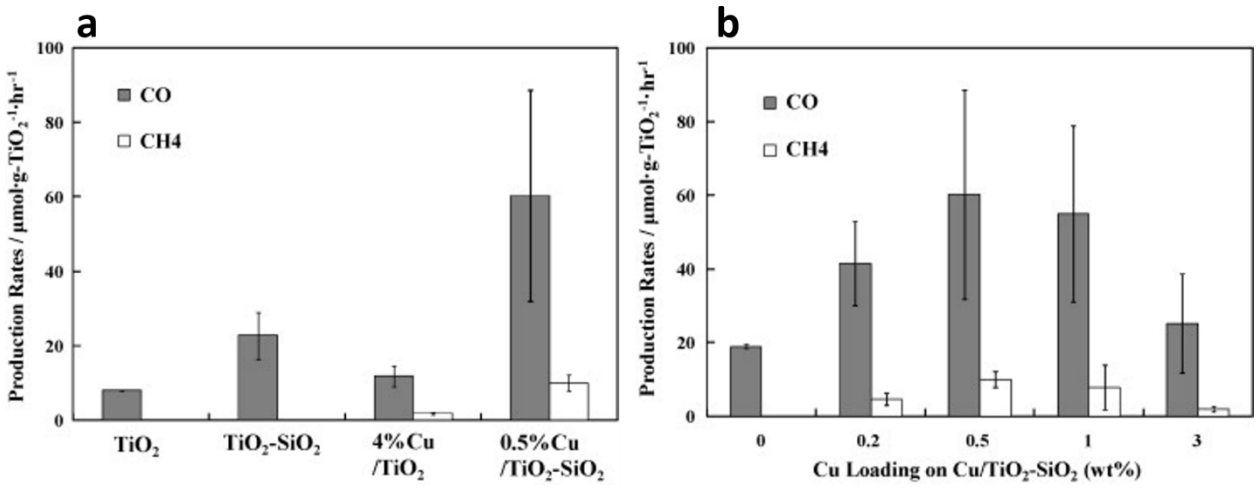

Figure 8: (a) Peak production rates of CO and CH_4 on various TiO_2-containing catalysts, and (b) Peak production rates of CO and CH_4 as a function of Cu loading in $Cu/TiO_2–SiO_2$ catalysts. Reproduced from (Li et al., 2010) with permission.

3.1.4 Inorganic/organic nanocomposites

3.1.4.1 Metal-organic frameworks (MOF) nanomaterials

MOFs are recognized as catalytic systems of choice for CO_2RR conversion to renewable energy feedstocks due to the large panel of surface functionalities and geometries, porosity as well as the possible customization these materials offer specifically for CO_2 capture and utilizations (CCUs). Architectural flexibility and ease of structural modification of MOFs through insertion of different metal ions (or metal clusters) together with interconnection of multidentate organic linkers with different functionalities are notable strategies to improve performance of MOF-based photocatalysts for CO_2 reduction (Ejeromedoghene et al., 2022). Wang and coworkers investigated the photocatalytic conversion of CO_2 to formate over a variety of amino-functionalized and unfunctionalized Fe-based MOFs. They found that amine-

functionalized Fe-based MOFs outperformed their respective parent MOFs in this transformation. NH_2-MIL-101(Fe), a framework composed of FeO clusters and 2-aminoterephthalic acid (H_2ATA) ligands prepared in dimethylformamide (DMF), exhibits the best catalytic activity, to generate $HCOO^-$ at the evolution rate of 178 µmol/g (Wang et al., 2014). Mechanistic pathways for enhanced activities include excitation of NH_2 functionality, electron transfer to the Fe center and direct excitation of Fe-O cluster (Scheme 2). Wei *et al.* reported visible-light induced CO evolution from CO_2RR over a series of UiO-based MOFs photocatalysts modified with different functional groups (F, NH_2, OCH_3, CH_3) (Wei et al., 2019). They observed an influence of the electron-withdrawing and electron-donating character of the introduced functional groups, CO evolution following the order UiO-68-F < UiO-68-NH_2 < UiO-68-CH_3 < UiO-68-OCH_3. The superior performance of UiO-68-OCH_3 was attributed to the pronounced charge separation efficiency of OCH_3. Crake et al. investigated applicability of titanium dioxide/carbon nitride (TiO_2/CNNS) nanosheet nanocomposites in photoreduction of CO_2 (Crake et al., 2019). They found that TiO_2/CNNS possessed improved CO_2 conversion and adsorption when compared to the individual materials used to make the composites (> 10 times). In addition, it was reported that the composite material with more {001} TiO_2 facets was the most catalytically active and this is attributed to enhanced charge transfer at the TiO_2/CNNS heterojunction interface. Previously, Crake et al (Crake et al. 2017) coupled NH_2-UiO-66 onto pre-formed TiO_2 nanosheets via *in situ* process to develop TiO_2/NH_2-UiO-66 heterojunction with permanent pore sizes and exposed catalytic actives sites for enhance CO_2 uptake and photoreduction of adsorbed CO_2 to CO under UV-visible light. The evolution rate of CO_2-to-CO conversion over the bound nanocomposite was 1.9 times more than that of pure TiO_2. Interestingly, the photoreduction efficiency of

mechanically blended TiO_2 and NH_2-UiO-66 is comparable to pure TiO_2, proving that *in situ* growth method was necessary for the enhanced catalytic activity. Transient absorption spectroscopy confirmed that the increased photoactivity of TiO_2/NH_2-UiO-66 was due to the efficient charge transfer at the interface of heterojunction.

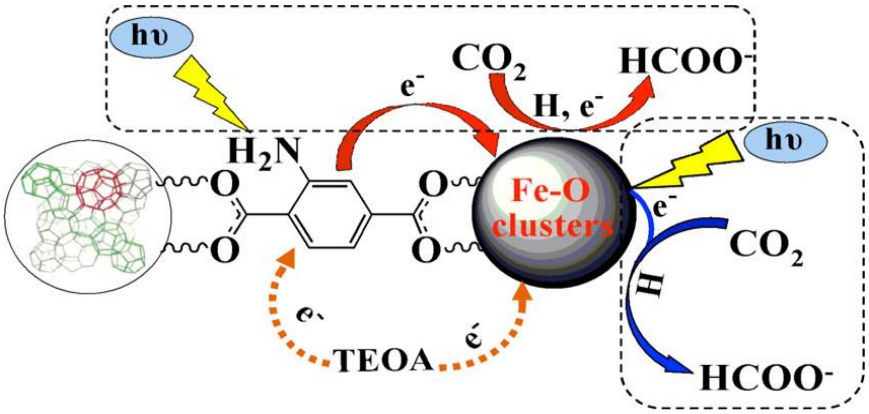

Scheme 2: Dual excitation pathways over amino-functionalized Fe-MOFs for photocatalytic reduction of CO_2 to formate. Reproduced from (Wang et al., 2014) with permission.

Besides the use of MOFs with multidentate linkers and different functional groups, multi-metallic MOFs can also offer improved stability and overall catalytic efficiency for CO_2 reduction in comparison to monometallic counterparts. Different MOFs with multi-metallic nodes have been explored for CO_2RR. For instance, bimetallic ZnCu MOF-74 outperformed monometallic Cu-MOF-74 when used as catalysts in methanol synthesis (Stolar et al., 2021). Selectivity for MeOH formation increased by 4.7 times upon incorporation of Zn into Cu-MOF-74 (c-ZnCU-MOF-74), and this value increased further to a factor of 8.3 upon amorphization of c-ZnCU-MOF-74. The findings highlight the significance of using heterometal nodes and amorphous MOF to get improved activity and selectivity. Fe-N-TiO_2/CPO-Cu MOF nanocomposites were fabricated where CPO-Cu-27MOF is supported on 0.12%Fe-0.5%N-codoped TiO_2

leading to effective photocatalytic reduction of CO_2 (khalilzadeh and Shariati, 2019). Reduction efficiency of Fe-N-TiO_2/CPO-Cu can be tuned by varying the amount of CPO-Cu-27 (CPO) in composites from 8 to 65wt.%, and the Fe-N-Ti@50CPO sample with 50wt% CPO yields the highest conversion of CO_2 to methane. The performance achieved is ca. 1.7 times higher than in the case of CO_2 methanation over Fe-NTiO_2. Liu *et al.* reported visible-light-driven CO_2 to CO conversion on hollow transition metal NPs-based MOFs (Liu et al., 2021). Their results show that Co-MOF-3 with two stacked piezoelectric phononic crystal nanoplates had a 2.5-fold higher CO_2 photoreduction efficiency than Co-MOF-1 with single nanoplate (Figure 9). The Co-MOF-3 homojunction system demonstrated a high CO_2 to CO conversion rate with 100% selectivity, outperforming most of the previously reported semiconductors for this reaction.

Polyoxometalates-based MOFs (POMOF) composites have also been studied for CO_2RR due to POM's unique ability to act as nodes or pillars, and more importantly, as high-efficiency catalytic sites in the MOF cages to adsorb reactants and improve MOF acidity, stability, and redox activity. Li et al. (Li et al., 2019) reported the use of a reductive POM and a hydrophobic fluorine-containing ligand to fabricate a stable POM-based MOF (NNU-29) composite as an effective CO_2 photoconversion catalytic system. The presence of a hydrophobic ligand improves the chemical stability of NNU-29 and reduces H_2 generation due to water attack to some extent, resulting in 98% selectivity for CO_2 reduction to HCOOH in aqueous solution after 16h of light irradiation. Wang *et al.* (Wang et al., 2021) recently proposed SO_3H-MIL-101-Cr (SO_3H-MOF) supported silicomolybdic acid (SMA) as a host-guest composite for CO_2 photoreduction. Pristine POM and MOF have negligible CO_2-to-CO activity compared to SO_3H-MOF. CO formation over POMOF composite, on other hand, achieved a

remarkable yield of 829.46 mol/g and selectivity of 93.2%. The superior reductive activity of POMOF was attributed to increased CO_2 affinity for silicomolybdic acid (SMA) and synergy between POF and MOF, resulting in enhanced charge carrier separation.

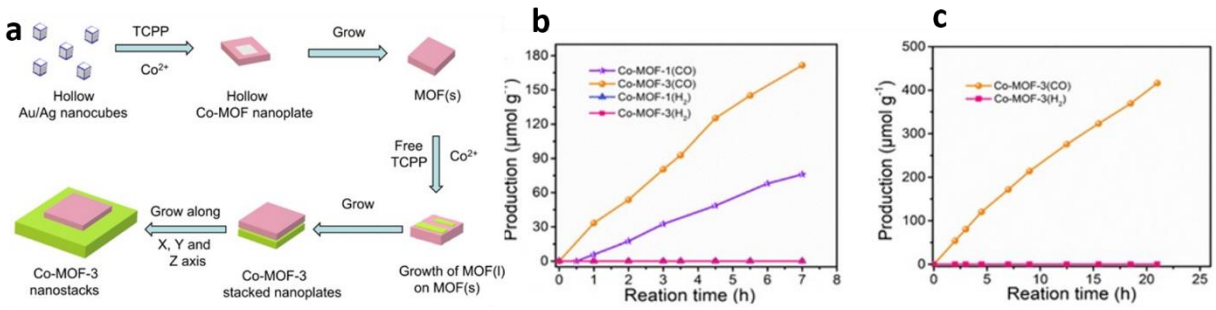

Figure 9: (a) Schematic view for the hollow Au/Ag directed formation of Co-MOF-3 nanocomposites. (b) Evolution of CO and H_2 as a function of reaction time during the CO_2 reduction under visible-light irradiation for Co-MOF-1 and Co-MOF-3 photocatalysts. (c) Stability of Co-MOF-3 during the continuous CO_2 reduction process. Reproduced with permission from ref. (Liu et al., 2021). Copyright 2021 Nature.

3.1.4.2 Metal-free nanomaterials

The high cost of production of metal-based nanomaterials, their susceptibility to deactivation in catalytic systems, environmental concerns about toxicity (Fall et al., 2022; Keller et al., 2017), and more often than not, their moderate catalytic performance in terms of activity and selectivity, have limited their use in CCUs. Graphene oxides, fullerenes, and graphitic carbon nitrides have recently emerged as valuable metal-free platforms for CO_2RR preparation, chemical inertness, and natural abundance (Yang et al., 2022). These materials are frequently used as a standalone material or in combination with other non-metal semiconducting materials to improve their CO_2RR performance (Shen et al., 2020). Several reports have shown that GO can

act by itself as a photocatalyst for CO_2 reduction either by adapting its method of preparation or through UV-Vis light-induced activation of pristine GO (Kuang et al., 2020). Hsu *et al.* (Hsu et al., 2013) studied the effect of volume of H_3PO_4 used as a mild oxidizer to prevent overoxidation of pristine GO on the CO2RR performance. Their results show that modified GOs have increased visible light absorption and improved CO_2 photoreduction to MeOH compared to pristine GO. The CO_2-to-MeOH conversion rate of GO-3 with excess H_3PO_4 was found 6-fold higher than with pure TiO_2. Kuang *et al.* (Kuang et al., 2020) reported on the photoreduction of CO_2 to CO over GO activated either by UV or simulated sunlight. GO activated by simulated-sunlight provided the highest CO_2 reduction efficiency, with a CO yield of 1.3-fold higher than the UV-activated GO and nearly 3 times higher than with pristine GO. The observed efficiency is due to light-induced increased defects and restoration of large π-conjugative systems. Compared to GO, reduced-GO (rGO) are superior solid supports for other semiconducting materials due to their high thermal and electrical conductivity. Yang *et al.* supported quinacridone (QA) NPs on rGO nanosheets through H-bonding and with different rGO contents and observed that this metal-free photocatalysts allowed photoreduction of CO_2 to CO and CH_4 under UV light (Yang et al., 2019). The sample containing 2% rGO had the highest CO_2 reduction efficiency and selectivity for CO and CH_4 due to the synergistic effects of QA as a photosensitizer and rGO as an electron acceptor to promote effective charge separation.

Based on the number of published articles on photocatalysis, graphitic carbon nitride (gCN) materials is the highest promising among the reported carbon-based materials for photoreduction of CO_2, due to its facile tunable synthetic routes, structural maneuverability, and tailorable morphology. However, they are limited due to their narrow visible light absorption window, low specific surface area, poor electrical

conductivity, and rapid recombination of photoexcited excitons (Shi et al., 2018). A variety of strategies, including structural modification via elemental doping, the attachment of a semiconducting motif, functional group modulation of gCN, and others, can significantly improve the photocatalytic CO_2 reduction (Alaghmandfard and Ghandi, 2022). Nonmetals like P, O, B, S, and N have become popular as interstitial or substitutional dopants on gCN for CO_2 photoreduction and other photocatalytic reactions.

Arumugam and coworkers synthesized a series of porous gCN doped with various nonmetals (B, O, P, and S) for photoreduction of CO_2/H_2O to gaseous fuels (Arumugam et al., 2022) among which S-doped gCN showed the highest CO_2-to-CH_4 conversion rate compared to others. Imaging studies showed that bare g-C_3N_4 has a thin-layered structure with irregular porosity, whereas S-doped g-C_3N_4 has a denser structure with a homogenous distribution of S atoms on the g-C_3N_4 matrix, suggesting that S atom can act as an electron sink for improved activity. Doping of S atoms into g-C_3N_4 did not enhance the surface area or modify the energy band gap of g-C_3N_4; rather, the remarkable boost in photoreduction efficiency was due to charge separation and migration processes. Mo et al. demonstrated that hydrothermal treatment of melamine and hydroxylammonium chloride precursors structurally transformed bulk g-C_3N_4 from an irregular morphology into a supramolecular hydrogen-bonded network intermediate; and that subsequent heating of the intermediate under NH_3 atmosphere led to the formation of porous TCN(NH_3) nanotubes with a 1D tubular structure. The structural transition from bulk gCN to 1D tubular structure was confirmed using XRD, FTIR, SEM, and TEM. The CO_2-to-CO conversion rate of porous TCN(NH_3) nanotubes was 17 and 15 times that of bulk g-C_3N_4 and TiO_2, respectively. Tubular structure of TCN(NH_3) has permanent porosity and a large surface area, which enhances solar light

utilization and spatially resisted photoinduced charge recombination, resulting in a better photoreduction efficiency than bulk g-C_3N_4. Huang *et al.* (Huang et al., 2015) successfully photoreduced CO_2 to CH_4 and MeOH over bulk g-C_3N_4 and amine-functionalized g-C_3N_4, which was prepared by heating g-C_3N_4 in monoethanolamine (MEA) solution. Both pure and functionalized g-C_3N_4 have a 2D lamellar structure with equal porosity, indicating that the amine functionalization has no effect on g-C_3N_4 morphology. The functionalized g-C_3N_4 heated in an oil bath for 5 hours had the highest CO_2 to fuel conversion rate. The CO_2 photoreduction efficiency over amine-functionalized g-C_3N_4 was significantly higher than pristine g-C_3N_4 due to the enhanced adsorption and destabilization of CO_2 by amine functional groups.

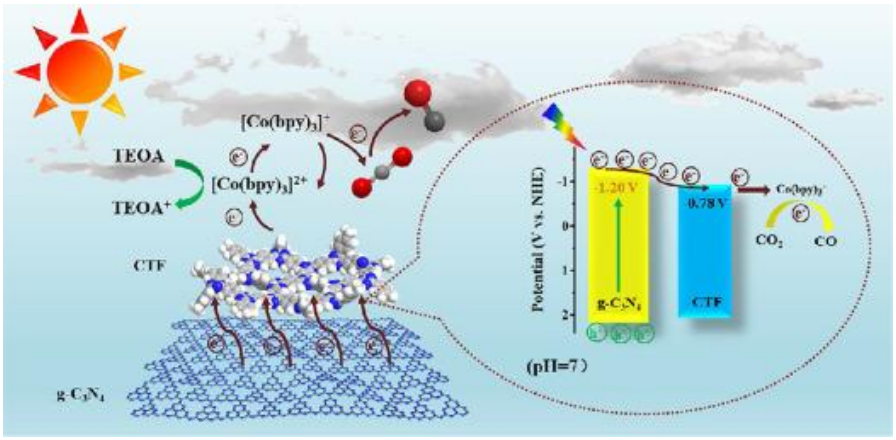

Figure 10: Schematic view and mechasism of CN/CTF heterostructure for photocatalytic CO_2 reduction. Reproduced with permission from ref. (He et al., 2022).

gCN has also been decorated with COFs and carbon dots (CDs) to fabricate metal-free composites for improved visible-light-induced CO_2 reduction. He *et al.* (He et al., 2022) reported for the first-time gCN/covalent triazine framework (2D/2D CN/CTF) heterostructures for CO_2 photoreduction. The TEM micrograph of CN/CTF reveals an overlaying lamellar structure of CN superimposed on an irregularly stratified

morphology of CTF, validating successful formulation of 2D/2D CN/CTF heterostructure. The optimal CN/CTF heterostructure is up to 25.5 and 2.5-fold more efficient in photoreduction of CO_2 to CO than CTF and CN, respectively. The enhanced reduction efficiency of CN/CTF was attributed to a lower probability of hole-electron recombination due to $[Co(bpy)_3]^{2+}$, which acts as electron harvester to accelerate charges separation, cleaving O=C=O to selectively produce CO (Figure 10). Wang *et al.* (Wang et al., 2022) reported van der Waals interfacial bonding between N-deficient gCN and Tp-Tta COF, demonstrating exceptional stability and selectivity for CO_2 photoreduction to CO. DFT calculations and EPR analysis confirmed the strong electronic coupling between gCN and Tp-Tta COF, which was responsible for improved photoreduction efficiency of the composite via large active sites for CO_2 capture and, an accelerated S-scheme charge separation system. Wang *et al.* (Wang et al., 2020) described carbon nanodots (CDs) electrostatically bounded to the surface of protonated gCN which demonstrated an excellent metal-free bifunctional photocatalysts to promote selective reduction of CO_2 to nearly 100% methanol. Structural elucidation reveals that the boundaries and edges of CN nanosheets, which possess a graphene-like structure, were coherently decorated by graphitic structure of ^{m}CDs, indicating strong electrostatic interactions between the two phases, which may have enhanced the composite's charge transfer process. In contrast, the amorphous structure of ^{s}CD was barely located in the phase structure of CN/^{s}CD composite following heterojunction formation, indicating weak interaction between the two phases. ^{m}CD features near-crystallized graphitic structures, whereas ^{s}CD is composed of amorphous carbons; hence, the photocatalytic functions of ^{m}CD/CN and ^{s}CD/CN are notably distinct. According to this study, ^{m}CD/CN photoreduces CO_2 to $6e^-$ product MeOH (Figure 11a), while ^{s}CD/CN favors formation of $2e^-$ product CO (Figure 11b). The authors

attributed the improved ^{m}CD/CN reduction efficiency to the hole-accepting role of ^{m}CD, which led to electron accumulation on CN surface and facilitated a multi-electron reduction process to produce MeOH with near-unity selectivity (Figure 11c).

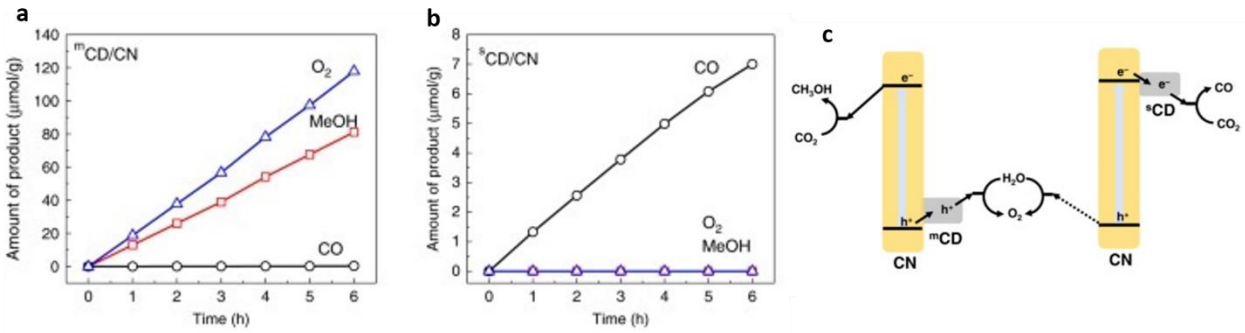

Figure 11: Photocatalytic activity of (a) ^{m}CD/CN for methanol formation, and (b) ^{s}CD/CN for CO formation measured under visible light ($\lambda > 420$ nm). (c) Schematic diagram of photocatalytic CO_2 reduction by the ^{m}CD/CN and ^{s}CD/CN. Reproduced with permission from ref (Wang et al., 2020). Copyright 2020 Nature.

Apart from all the aforementioned examples, this section also surveyed other recent/relevant research works on photocatalytic transformation of CO_2 (see Table S1 in the supplementary information)

3.2. Electrochemical transformation of CO_2

The electrochemical transformation of CO_2 to value added fuels has received considerable attention in recent years owing to its plethora benefits including energy production, storage, and others. The conversion process is located at the interface between the solid catalyst surface and the electrolyte, as is the case with all electrochemical reactions. A compact layer of ions next to the electrode, followed by a diffusion layer of solvated ions, can be used to describe the interface's structure (Rosen and Hod, 2018). The more the potential an electroactive species has, the more the

distance it can travel to the interface, and its relative orientation to the interface are all influenced by the bilayer structure which is thus essential for the rate and efficiency of the electrochemical CO_2RR. Electrochemical CO_2RR can produce useful chemicals and fuels including formaldehyde, CO, formic acid, ethylene, ethanol, methane, and methanol, depending on the electrical voltage supplied to the electrode (Chen et al., 2020).

The methods most frequently used for electroreduction of CO_2 are cyclic voltammetry (CV) and linear sweep voltammetry (LSV). The catalytic performance can also be evaluated using chronoamperometry. These CO_2 conversion operations are typically carried out at a specific reaction rate and ambient conditions of temperature and pressure (Nielsen et al., 2018). A coupled proton electron transfer that results in the protonation of the oxygen atom O (eq 1) or the carbon atom C (eq 2) triggers the adsorption of CO_2 on the electrode surface (eq 4) (Nielsen et al., 2018; Zhu et al., 2014). As such, this process requires the use of a large potential, which results in competing reactions such as the hydrogen evolution reaction (HER). In lieu of the above, integration of a catalyst in the system allows to reduce the overpotential and activate CO_2 conversion. In general, a heterogeneous catalyst deposited on the electrode surface or a homogeneous catalyst dissolved in solution are used in electrocatalytic CO_2 transformation. These catalysts will allow for a faster electron transfer coupled with protons, resulting in the observed products HCOOH (eq 2 and eq 3) or CO (eq 5 and eq 6) (Yin et al., 2019).

$$* + CO_2 + H^+ + e^- \rightarrow *OCHO \qquad \text{(Eq 1; a slow step)}$$

$$*OCHO + H^+ + e^- \rightarrow *HCOOH \qquad \text{(Eq 2; a fast step)}$$

$$*HCOOH \rightarrow * + HCOOH \qquad \text{(Eq 3)}$$

638 $* + CO_2 + H^+ + e^- \rightarrow *COOH$ (Eq4; a slow step)

639 $*COOH + H^+ + e^- \rightarrow *CO + H_2O$ (Eq 5; a fast step)

640 $*CO \rightarrow * + CO$ (Eq6)

641 As shown in Figure 12, various studies using different metal electrodes modified with
642 catalysts such as Sn, In, Au, Ag, Pd, Bi, Co, Mo, and others have been reported. As the
643 other side reactions (i.e. HER) can be almost suppressed, these materials exhibit
644 significant catalytic properties for the CO_2 transformation (Lu et al., 2019).
645 Furthermore, they present an extremely low energy barrier for the formation of the
646 intermediate, which must then be protonated at the carbon or oxygen atom before being
647 converted to formate or carbon monoxide.

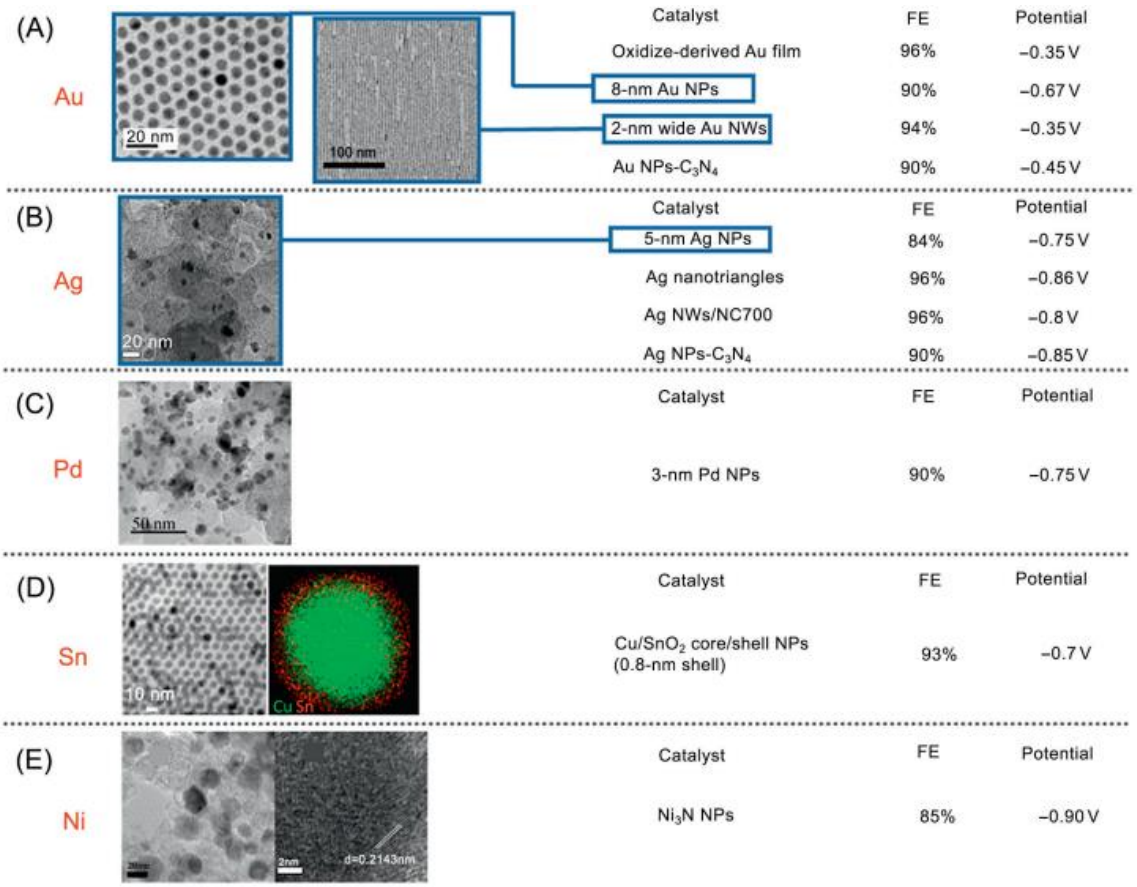

648

Figure 12: Overview of some typical Au, Ag, Pd, Sn, and Ni-based nanocatalysts for electrochemical reduction of CO_2 to CO. All potentials are contrasted with an electrode made of reversible hydrogen (RHE). NP stands for nanoparticle, whereas FE stands for faradic efficiency. Reprinted with the permission from (Yin et al., 2019). Copyright (2019) Elsevier.

Yang et al also investigated the CO_2RR on Ag, Pd, and Ag@Pd nanocubes. Pd nanocubes led to CO with high selectivity as a result of Pd turning into Pd hydride (PdH) during CO_2RR (Yang et al., 2022). In contrast, Ag@Pd makes the formation of PdH more difficult due to inhibited production of CO from the intermediate *HOCO which thus adjusts the reaction pathway towards HCOOH. The authors concluded that Ag nanocubes have high selectivity for H_2 with no phase transition during CO_2RR.

Li et al. (Z. Li et al., 2022) studied electrochemical CO_2RR to formate, which not only has the potential to reduce the issue of global warming brought on by CO_2, but also has the potential to be exploited for energy storage as intermittent renewable energy. A bimetallic BiSn nanomaterials were electrodeposited on copper mesh and tested as electrocatalysts for the conversion of CO_2 to formate. The resulting electrodes demonstrated excellent catalytic activity at 1.0 V vs. RHE, with a partial current density of 34.0 mA/cm^2 and an astonishingly high faradaic efficiency of roughly 94.8%. The production of formate at a remarkable rate of 634.3 mol/cm^{2}h -significantly higher than most rates previously reported- is noteworthy. The quick electron transfer of BiSn nanomaterials also contributed in the creation of the $CO2^{\bullet-}$ intermediate. Additionally, they produced a metastable metal oxide/metal interface that helped to stabilize the $CO_2^{\bullet-}$intermediate and suppress the HER side reaction. The pathway connected to the OCHO• intermediate was improved because of the optimized electronic structure of

673 BiSn, promoting the conversion of CO_2 to formate. According to these results, Bi/Sn
674 bimetallic catalysts are a viable option for very effective CO_2 reduction.

675 In contrast, the conversion of CO_2 to CO and formate is less difficult than CO_2RR to C-
676 H hydrocarbons, which are more significant scientifically and technologically but are
677 more difficult to manage. Concerning the synthesis of ethylene, Cu and Cu_2O are
678 regarded as the most common and effective electrocatalysts for CO_2RR. Multi-carbon
679 oxygenates, such as ethanol (the primary product), acetate, and n-propanol, can also be
680 produced in an alkaline electrolyte at -0.25 to -0.5 V vs RHE with a total EF of 57 %
681 (Li et al., 2014).

682 In order to achieve a lofty ultra-high selectivity of 82.4% for ethylene in an H-cell
683 system with good catalytic stability and material durability of 100 h, Sultan et al.
684 (Sultan et al., 2022) presented a completely redesigned electrocatalyst consisting of
685 Al_2CuO_4 nanosheets uniformly coated with CuO nanoparticles (CuAl-1: CuO/Al_2 CuO
686 4 -23) by phase. They found that Cu (CuAl-1) permitted high surface CO intermediate
687 coverages and improved CO adsorption for C-C coupling to *OCCO, a generation of
688 CO intermediate, and Cu (CuAl-1) also enabled high surface coverages of CO
689 intermediates.

690 Cu catalysts for CO_2RR can produce a wide range of hydrocarbons at a high catalytic
691 activity. For selective CO_2RR, Yin et al. (Yin et al., 2019) used a catalyst based on
692 copper nitride (Cu_3N) nanocubes (NC). With a FE of 60%, a mass activity of 34 A/g, a
693 C_2H_4/CH_4 molar ratio over than 2000, and strong selectivity and stability of CO_2RR
694 towards ethylene at -1.6 V vs. RHE, their 25 nm Cu_3N NCs showed good performance.
695 This lacks of product selectivity is a significant barrier to the use of these catalysts for

696 selective CO_2RR, and more research on the application of these substitute catalysts is
697 required for increased hydrocarbon yield.

698 In a related piece of study, Liu and coworkers noted the formation of exceptional
699 oxygen-rich ultrathin CuO nanoplate arrays that spontaneously transform into Cu/Cu_2O
700 heterogeneous surfaces after CO_2RR (Liu et al., 2022). The electrocatalyst displayed a
701 high ethylene energy efficiency of 84.5%, steady electrolysis for 55h, and a total cell
702 ethylene energy efficiency of 27.6% at 200 $mA.cm^{-2}$ in a flow cell with a neutral KCl
703 electrolyte. A density functional theory (DFT) investigation of the mechanism,
704 highlighted that stable nanostructures, stable Cu/Cu_2O interfaces, and improved
705 adsorption of the intermediate $^*OCCOH$ can enhance selectivity and amount of C_2H_4
706 produced.

707 Wang et al. developed CuBi NPs that showed a CH_4 FE as high as 70.6% at 1.2 Vs
708 RHE. According to their study, adding Bi NPs to the matrix (CuBi NPs) significantly
709 boosted the FE when compared to regular Cu NPs by almost 25 times (Wang et al.,
710 2020). DFT studies showed that alloying Cu with Bi lowers the energy required for the
711 rate-determining phase of $^*COH$ production, which provides an additional explanation
712 for the enhanced performance.

713 In addition to the aforementioned systems, other metal-based nanomaterials have been
714 investigated towards the production of hydrocarbon via the electrochemical reduction
715 of CO_2, which are outlined in Table 1 below.

716 Table 1. Selected examples of electroactive metal nanoparticles for converting CO_2 into hydrocarbon products

Nanoparticles	FE (%)	Current Density (mA/cm^2)	overpotential vs RHE (V)	Products	Remarks	Reference
Dibenzyldithiocarbamate functionalized AuNPs	100 ± 1	-	-0.8	CO	The hydrophobic nature of dibenzyl moites permit CO_2 to pass through	(L. Souza and H. B. Lima, 2021)
C_3N_4/Cu_2O-FeO nanocomposites	84.4	-	-0.24	CO	The interfacial interaction between g-C_3N_4	(Woyessa et al., 2021)

					and CU_2O-FeO are responsible for the efficient CO_2 reduction to CO	
Cu_xAu_y nanowire arrays	48	-	-0.5 to 0.7	EtOH	The selectivity of EtOH is attributed to the synergistic effect of morphology	(Zhu et al., 2019)
Iron dispersed on graphene doped with nitrogen	80	-	-0.57	CO with small traces of CH_4	Fe-N_4 increased CO_2 activation resulting from the incorporation	(Zhang et al., 2018)

					of trace Fe atoms to graphene matrices	
$ZnIn_2S_4$/silver (gold)/tetra(4-carboxyphenyl) porphyrin iron(III) chloride hybrids	-	-	-	CO and H_2	Au NPs favor H_2 generation, whilst Ag NPs serve as a promoter for interfacial charge transfer from ZnIn2S4 to the FeTCPP.	(P. Li et al., 2022)
Cu nanocrystals	-	-1.74	-0.95	n-propanol	The increased activity of the Cu	(Ren et al., 2015)

				nanocrystals toward the production of n-propanol was linked to the number of defect sites on their surface.
Composite of 64 ZrO_2 nanoparticles anchored on N-doped carbon sheets	2.6	-0.4	CO	The dispersion of ZrO_2 NPs with oxygen vacancies on the N-C responsible for the improved electrochemical (Miao et al., 2019)

					performance	
Cu nanowires	60, 17.4, 8 and 2	-	-1.1	H_2, ethylene, CO and ethene, respectively	Cu nanowire arrays can be tuned to systematically controlling hydrocarbon formation via the electrochemical reduction of CO_2.	(Ma et al., 2016a)
Mesoporous carbon modified CNT anchored	98	60	-0.81	CO	The dispersive Ni nanoparticles and N-doping	(Du et al., 2022)

by Ni NPs					active sites of mesoporous carbon is good for selective reduction of CO_2 to CO.	
C-supported Bi NPs	93 ± 2.5%	-	-1.6	$HCOO^-$	The electrode deactivates after about 70 h (in 3-h electrolysis experiments at different potentials).	(Ávila-Bolívar et al., 2019)

717 FE - Faradaic Efficiency; EtOH – Ethanol; FETCPP - Tetra(4-carboxyphenyl)porphyrin iron(III) chloride; $HCOO^-$ - Formate ion; NPs –Nanoparticles; AuNPs –

718 Gold nanoparticles

In the quest for additional electro-active nanoparticles for CO_2 reduction, non-metal NPs have been explored in order to speed up the reaction rate and increase the selectivity for products. For instance, boron phosphide NPs were shown by Mou et al. (Mou et al., 2019) to function remarkably as a non-metal electrocatalyst for the highly selective electrochemical conversion of CO_2 to CH_3OH. In comparison to RHE in 0.1 m $KHCO_3$, this catalyst achieves a high FE of 92% for CH_3OH at 0.5 V. According to DFT calculations, B and P synergistically facilitate the binding and activation of CO_2, and the $^*CO + {}^*OH$ to $^*CO + {}^*H_2O$ pathway, with a free energy change of 1.36 eV, is the rate-determining step for the CO_2RR. Liu et al. (Liu et al., 2022) reported B/N-doped sp^3/sp^2 hybridized nanocarbon, which consists of extremely small carbon NPs with an sp^3 carbon core surrounded by a sp^2 carbon shell, as an effective electrocatalyst for CO_2 to ethanol reduction at relatively low overpotentials. They claim that CO_2 reduction occurs during the synthesis of ethanol and acetate at 0.5 0.6 V (vs. RHE), with ethanol accounting for 51.6% - 56.0% of the total reduction. Due to the combined effects of sp^3/sp^2 carbon and B/N doping, there is a strong ethanol selectivity.

To perform electrocatalytic CO_2 reduction to liquid ethanol and acetone, Yuan and colleagues presented their findings. Yuan and colleagues used five pyridine derivatives, including pyridoxine, 4-hydroxypyridine, 4-aminopyridine, 8-hydroxyquionline, and 5-amino-1,10-phenanthroline, to functionalize graphene oxide (GRO) surfaces (Yuan et al., 2018). Surprisingly, the greatest catalyst for electrochemical CO_2 conversion is pyridoxine-modified GRO sheets with a pyridinic N concentration of 2.32% and an overall FE of 45.8%. Furthermore, the CO_2 reduction potentials of the other four pyridine derivatives functionalized GO varied with respect to ethanol and acetone. Li and colleagues described non-metal nanoporous S-doped and S,N-codoped carbons as catalysts for electrochemical transformation CO_2 (Li et al., 2016). The team found that

S,N-doped carbon has greater FE for conversion to CO and CH_4 compared to S-doped counterpart. The former revealed a maximum FE of 11.3% and 0.18%. for CO and CH_4 production, respectively. The S,N-nanoporous carbon was better at decreasing the overpotential of the reduction process.

Two-dimensional (2D) boron nitride nanosheets or meshes (BNs) doped with beryllium have been the subject of research by Azofra and coworkerss (Azofra et al., 2016). According to their mechanistic study, adding electron-deficient Be atoms to the 2D network significantly lowered the energy barriers for CO_2 fixation and the initial steps in hydrogenation. As a result of the exceptionally large hole created on the Be-doped surface environment, CO_2 was spontaneously absorbed (in terms of the Gibbs free binding energy).

Despite all the accomplishments in CO_2RR, it is worth to mention that high progress is still needed in the design of catalysts based on metal and non-metal for achieving a more performant CO_2 electrocatalytic transformation. The main challenge being the energy requirement for reducing CO_2 (due to its stability), an electrochemical potential [E°] of 1.9 V vs normal hydrogen electrode (NHE) at pH. Furthermore, due to the high reactivity of the one-electron reduction product ($CO_2^{\bullet-}$), regulating product selectivity is difficult. When a multi-electron process is combined with proton-coupled electron transfer, the potential for CO_2 reduction is greatly reduced, resulting in a variety of products depending on the number of electrons involved (Maeda, 2019). Finally, the quantum yield and current density reported thus far are extremely low, particularly for C_2^+ products, making commercial production extremely difficult. As a result, extensive and intensive research is required to overcome all of the aforementioned challenges.

3.3 Photo-electrochemical (PEC) reduction of CO_2

Photoelectrochemical (PEC) conversion of CO_2 can be described as a procedure mimicking the artificial photosynthesis technique. This method has been employed for the conversion of CO_2 to formate, formaldehyde, formic acid, methane, methanol, and ethanol (Kumaravel et al., 2020).This technique combines electrocatalytic and photocatalytic systems in which photogenerated electrons are transferred to the electrode surface under an applied electric field, thus reducing CO_2 in the process (Nandal et al., 2022).

During the 80s, Fisher et al. (Fisher and Eisenberg, 2002)and Inoue et al. (Inoue et al., 1979) studied the electrocatalytic reduction reactions that gave rise to studies of photo-electrocatalytic reduction of CO_2 on selected semiconductors. However, an extensive study using various metals and metal oxides requires large over potentials and suffers from hydrogen evolution (Benson et al., 2009; Qiao et al., 2014; Shen et al., 2015). Since then, it has become a promising technique for CO_2 conversion. In 2020, Arai et al. (Arai et al., 2010) reported the PEC conversion of CO_2 into HCOOH using a p-InP-Zn photocathode which has been modified with a Ru polymer. The conversion was achieved in the presence of visible light/ solar energy. Similarly, Kumaravel and his coleagues (Kumaravel et al., 2020) also synthesized a range of fuels and chemicals (Formic acid, methanol, ethanol, methane and ethane) from CO_2. They employed a catalyst-embedded microfluidic PEC reactor for the synthesis. The catalyst was activated in the presence of visible light irradiation. The schematic of the conversion is presented in Figure 13

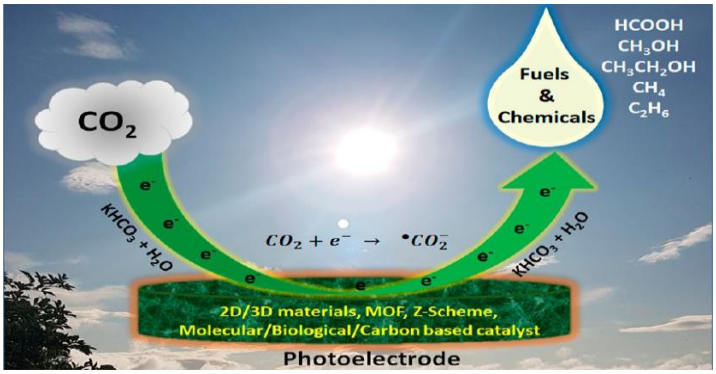

Figure 13: PEC Conversion of CO_2 into value-added product using solar irradiation. Adapted with permission from reference (Kumaravel et al., 2020). Copyright [2020], [American Chemical Society].

According to a recent study by Karim et al. (Rezaul Karim et al., 2018), single electron reduction of CO_2 to $^{\bullet}CO_2$ occurs at -1.90 V vs NHE at pH = 7 in aqueous solution at 25 ^{o}C under 1 atm pressure. The 2e- pathway of CO_2 reduction produces CO (E = -0.53 V vs NHE) and formate (E = -0.61 V vs NHE) while the 6e- pathway leads to the production of methanol (E= -0.38 V vs NHE) (Qiao et al., 2014; Rezaul Karim et al., 2018). The band varies depending on the type of metal coordination as shown in **Figure 14.**

In the electrochemical process, ultraviolet radiation on the semiconductor photocatalyst activates the metal center, thus forming an oxidation-reduction environment. During this process, electrons get excited from the VB to CB, leaving behind positive holes that oxidize water on the surface to form OH- radicals with strong oxidative decomposing power. Excited electrons from the CB get accepted by CO_2 to form $^{\bullet}CO_2$ radicals that react with the intermediate products of the oxidative reactions forming one or more of the products in **Table 2** depending on the bandgap of the photocatalysts (Ekambaram et al., 2007). Metal oxides present desirable bandgap and bandgap edge

positions, and their electronic structure plays a major role where the VB is fully filled by electrons and the CB is empty.

Table 2: The oxidation-reduction potential at pH=7 vs NHE and half-cell reactions (Ekambaram et al., 2007)

Reactants	**Products**	**EMF**
$CO_2 + 2e^- \rightarrow$	$^{\bullet}CO_2$	-1.90
$^{\bullet}CO_2 + 2H^+ + 2e^- \rightarrow$	HCOOH	-0.61
$^{\bullet}CO_2 + 2H^+ + 2e^- \rightarrow$	$CO + H_2O$	-0.53
$^{\bullet}CO_2 + 4H^+ + 4e^- \rightarrow$	$HCHO + H_2O$	-0.48
$^{\bullet}CO_2 + 6H^+ + 6e^- \rightarrow$	$CH_3OH + H_2O$	-0.38
$^{\bullet}CO_2 + 8H^+ + 8e^- \rightarrow$	$CH_4 + 2H_2O$	-0.24
$2H_2O + 4H^+ \rightarrow$	$O_2 + 4H^+$	+0.81
$H^+ + 2e^- \rightarrow$	H_2	-0.42

Therefore, the integration of electrocatalysis and photocatalysis generates a unique synergistic photo-electrochemical catalysis system (Huang et al., 2017; Rezaul Karim et al., 2018). The catalytic activity of a photocatalyst towards CO_2 reduction depends on its band gap and appropriate positioning of the conduction and valence bands (Handoko and Tang, 2013). Doping semiconductors have extensively been explored in the literature to enable visible-light-activated photocatalysis and the usage efficiency of solar light. Several published studies have used titanium for photocatalytic applications for organic compound decompositions due to its ability to oxidize organic and inorganic substances in water and air through a redox reaction (Xie et al., 2018). TiO_2 and ZnO absorb ultraviolet light of the solar spectrum due to their large bandgap's

energy (~380 nm and ~360 nm respectively) (Liu et al., 2010). The bandgap (the distance between the valence band and conduction band) of each semiconductor determines are shown in Figure 14, it shows the relationship between the bandgap and EMF at pH 7. Several alternative semiconductors such as Fe_2O_3, ZnO, WO_3, $SrTiO_3$, $NaTaO_3$, CdS, Ag_3PO_4, $BiPO_4$ and g-C_3N_4 have been reported to have promising electro-photocatalytic performance (Kubacka et al., 2011; L. White et al., 2015; Liu et al., 2010; Wang et al., 2009).

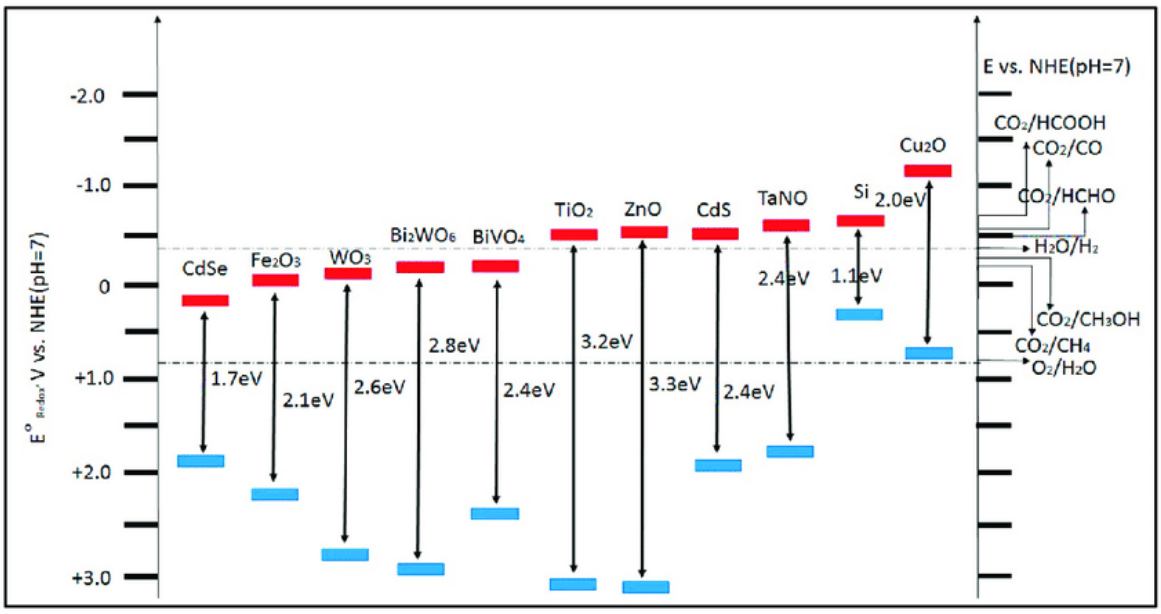

Figure 14: Band gap energy of various semiconductors (Wang et al., 2009). Copy right 2019

More recently, Nandal et al. (Nandal et al., 2022) performed a selective conversion of CO_2 into ethanol via a PEC method (see **Figure 15)**. The catalytic systems involve a mixture of Graphene oxide/Copper oxide and a copper-based MOF (GO/CuxO, Cu-MOF). The catalytic system was solar-driven and activated in the presence of sunlight. They reported an ethanol yield of 162 µM cm^{-1}. Most researchers believe that the PEC reduction technique is not only efficient, but it is also greener and sustainable. Other

PEC for CO_2 reduction surveyed in this section are listed in the supplementary file (Table S2)

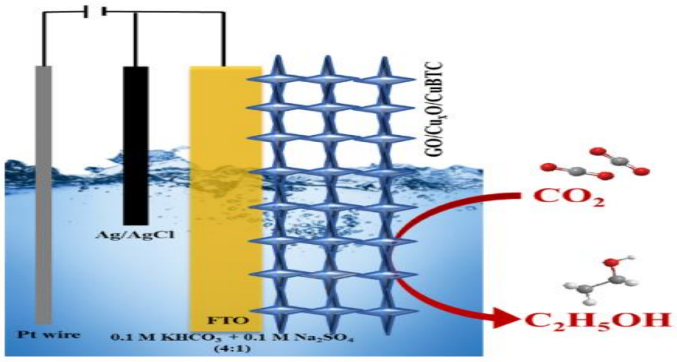

Figure 15: PEC reduction of CO_2 to ethanol. Adapted with permission from reference (Nandal et al., 2022). Copyright [2022], [Elsevier].

3.4 Photothermal heterogeneous catalysts for the hydrogenation of CO_2

The hydrogenation of CO_2 is gaining significant impetus in scientific investigations considering the large amount of CO_2 generated by the industrial processes and the associated environmental degradation. It facilitates the production of clean fuels and hydrocarbons such as CO, CH_4, and C_2^+ products (Fan and Tahir, 2022). The hydrogenation reaction can proceed via thermal catalysis, photocatalysis, and photothermal catalysis. While thermal and photocatalytic processes require the action of heat and light energies respectively, the photothermal catalytic approach combines both in a single reaction system. In photothermal catalytic systems, the CO_2 transformation reaction is driven by light energy into a thermally inspired catalytic reaction system or utilizing the photoinduced thermal effect of a catalyst. The light energy initiates a photoinduced redox reaction and a photoinduced thermally driven reaction (Oladoye et al., 2021). For instance, the exposure of a transition metal oxide-based catalyst to a sufficient amount of light energy causes an excitation of photons that produces electron-hole pairs in the conduction band (CB) and valence band (VB)

(Figure 16). These highly energetic electrons enter the anti-bonding orbitals of the reactants and activate the reactant molecules to stimulate a redox reaction. In other instances, the absorbed photon could be converted into heat energy (Liu et al., 2022). At an activated temperature, the active sites on the surface of the photothermal catalytic material could induce a thermally driven catalytic reaction. Several semiconducting metal oxides with tunable porosity and defective active sites have been designed for the hydrogenation of CO_2 into different hydrocarbon-based fuels (Table 3).

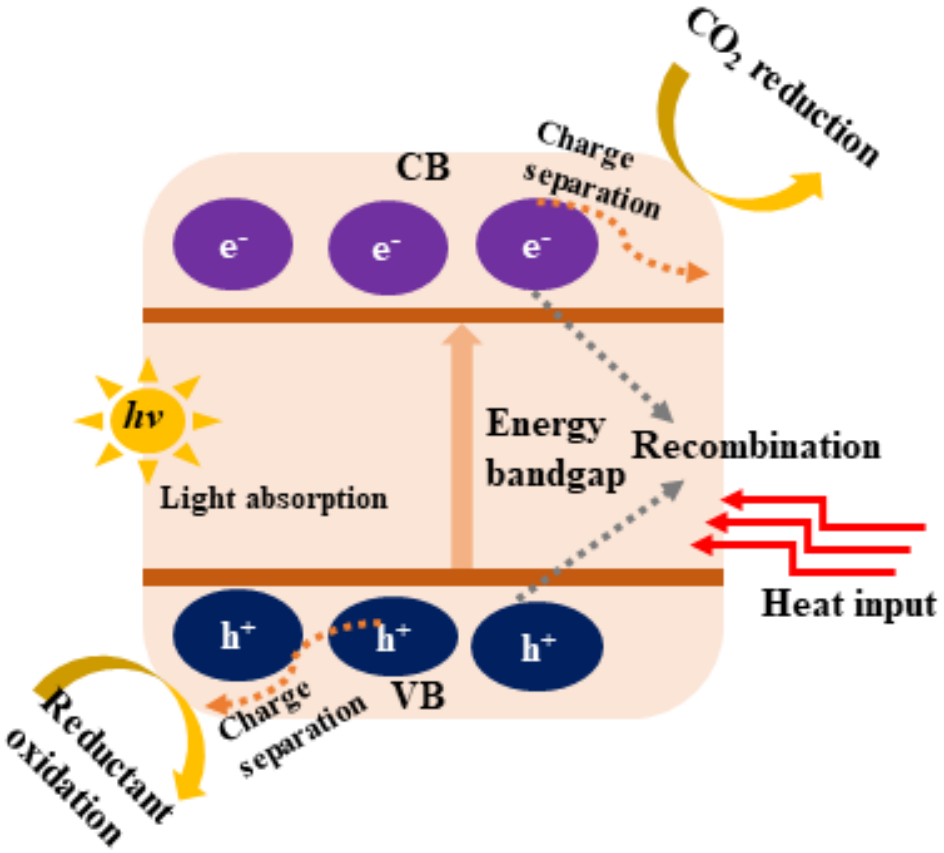

Figure 16: Scheme of the photothermal catalytic CO_2 reduction

869 Table 3: Examples of photothermal catalysts for the hydrogenation of CO_2 in fuels and hydrocarbons

Photothermal catalyst	**Light source**	**Reaction conditions**	**Selective products**	**Conversion rate ($mmol \cdot g^{-1} \cdot h^{-1}$)**	**Comments**	**References**
Pd/ZnO	Visible light	Low pressure (12 bar)	CH_3OH		Localized SPR of Pd contributed to the high yield of methanol	(Wu et al., 2019)
AuPt@UiO-66-NH_2	300 W Xe lamp	150°C, 4 h	CO	1451	Synergetic effect of plasmonic Au, doped active Pt, and encapsulation structure leading to the production of metal@MOF gives good hydrogenation performance	(Wang et al., 2022)

120 μm-SiNCs@Co nanoarray	300 W Xe arc lamp	Pressure (1 bar), power intensity (2.5 W cm^{-2})	CO	1780	Strong light-absorption ability over the entire solar spectrum due to the combination of the light-trapping effect of the nanoarray structures and the SPR of Co NPs increases the conversion rate	(Shen et al., 2022)
Ni/$TiO_{2-x}H_x$	300 W Xe lamp	Gas flow rate at 500 mL min^{-1} and purged for 10 min	CH_4		Abundant defects such as oxygen vacancies, active hydrogen species, and Ni active sites enhance the performance of the catalyst	(Y. Li et al., 2022)
Nb_2C-	300 W Xe	36-sun	CO	8.5 $mol \cdot g^{-1} \cdot h^{-1}$	Ni NPs greatly enhance the	(Wu et al.,

nanosheet-supported Ni NPs	arc lamp	illumination without external heating			activation of H_2 and accelerate CO_2 hydrogenation reactions; formation of Ni−H is vital for CO_2 conversion	2021)
Fe_3O_4	Xenon light source (200−1000 nm)	4 h of irradiation	CO	11.3	Fe-carbide and other Fe-based catalysts show excellent light-to-heat conversion performance and good light-harvesting properties	(Song et al., 2020)
θ-Fe_3C			CH_x	10.9		
α-MoC and β-Mo_2C mixed phases	300 W xenon lamp	130 °C, 5 h	CO and CH_4	25.8 $mL \cdot g^{-1} \cdot h^{-1}$	dissociation of light-promoted surface intermediate (formate species) was responsible for the enhanced activity of photothermal catalytic CO_2	(Zhao et al., 2021)

					hydrogenation	
Pd_2Cu alloy dispersed TiO_2	UV-Vis (350 to 750 nm)	150 °C	C_2H_5OH	4.1	Pd active sites utilize the electrons and hydrogenate the *CO to *HCO, which is a key step in the conversion process	(Elavarasan et al., 2022)
SNAs support on Co	300 W Xe arc lamp	Pressure (1 bar), power intensity (2.5 W cm^{-2})	CO	0.433	Photoexcited electron-hole pairs in the SNAs might be involved in the catalytic process	(D. Zhang et al., 2021)
Co@AAO	Sunlight	Power intensity (2.5 W cm^{-2})	CO	1666	A dual-pass AAO with a large channel size facilitates gas diffusion and thus boosts photothermal catalytic	(D. Lou et al., 2021)

					performance	
Au/CeO_2	Xe lamp	623 K	CO		Positive effect of light on CO_2 transformation is associated with the hydrogen dissociation step.	(B. Lu et al., 2019)

870 SPR-Surface plasmon resonance; MOF-Metal organic frameworks; SiNCs-Silica nanocones, NPs-Nanoparticles, SNA-Silicon
871 nanowires arrays, AAO-Anodic aluminum oxide

3.5 Thermochemical transformation of CO_2

The thermochemical transformation of CO_2 is an interesting strategy that has been gainfully explored for the reduction, splitting, or reforming of CO_2 to fuels/products such as carbon monoxide, methanol, methane, and dimethyl ether in the presence of suitable catalysts (Fuqiang et al., 2017; Roy et al., 2018). Although, there are many high-temperature thermochemical energy conversion processes for energy storage, energy conversion and water splitting reactions (Ali et al., 2020; Cheng et al., 2021; Lorentzou et al., 2014; Wu et al., 2018), the solar-induced thermochemical cyclic method is been emphasized as an outstanding approach for the efficient conversion of CO_2 (**Table 4**). This approach has produced intriguing results from several the experimental tests/designs conducted in different solar reactor models, which has given rise to more intensified research and technology development in this field (Guene Lougou et al., 2020). Many studies have shown that the solar thermochemical CO_2-transformation is a promising solution for solar energy harvesting and storage using materials like Fe-Ni alloy embedded in a perovskite (Hu et al., 2021), Ca- and Al-doped n$SmMnO_3$ perovskite (Gao et al., 2022), and ZrO_2-supported $NiFe_2O_4$ (Shuai et al., 2021), to convert CO_2 into CO with a 99% conversion rate of 381 mL g^{-1} min^{-1} at 850°C, high conversion of 595.56 mmol/g, and 37.89 mL of CO yield in 46 min, respectively. Meanwhile, Ni-doped $CaCO_3$ transformed 86.6% of CO_2 into syngas along with CH_4 in a fixed bed photo-reactor (Teng et al., 2022). The solar thermochemical process follows a two-step dissociation approach wherein the first step is an endothermic process that involves the production of O_2 by partially reducing a perovskite or metal oxide (MO) to a non-stoichiometric oxide with the assistance of high-temperature solar heat (Eq. 7). The second step usually occurs at low temperature via an exothermic process. At this stage, the reduced

perovskite or MO is oxidized with H_2O and/or CO_2 giving rise to the formation of H_2 and/or CO (Eq. 8-9), together with the stoichiometric oxide (Chen et al., 2022; Nair and Abanades, 2018).

$$MO + \text{solar heat} \rightarrow MO_{red} + O_2 \quad (7)$$

$$MO_{red} + CO_2 \rightarrow MO_{ox} + CO \quad (8)$$

$$CO_2 + \text{solar heat} \rightarrow CO + \tfrac{1}{2}O_2 \quad (9)$$

In the same vein, the photo-thermochemical (PTC) model produces photoinduced oxygen vacancies on the surface of the MO catalyst after exposure to UV-light energy (Eq. 10). Further, the oxygen vacancies are used to reduce CO_2 at temperatures below 873 K, thereby producing CO and O_2 (Eq. 5) (Xu et al., 2017, 2016).

$$2M_xO_y \rightarrow 2M_xO_{y-1} + O_2 \text{ (Photochemical step)} \quad (10)$$

$$2M_xO_{y-1} + CO_2\,(g) \rightarrow M_xO_y + CO \text{ (Thermochemical step)} \quad (11)$$

By exploring the Fisher Tropsh (F-T) technology, solar-assisted MOs can also afford carbon-free alternative fuels i.e. production of H_2 that can be used directly as a fuel or converted into other value-added chemicals (**Figure 17**) (G. Takalkar and Bhosale, 2019). Besides, other heterogeneous catalysts that change dynamically during the thermochemical reactions as well as possessing catalytic active sites and definite reaction pathways have been identified for CO_2 transformation (Feng et al., 2021). For example, the loading of IrO_x onto $LaFeO_3$ almost double the maximal CO release rate and increases the maximal O_2 evolution rate 0.5 times i.e. a 5-fold CO production (Jiang et al., 2016); meanwhile, the sol-gel synthesized $Co_xFe_{3-x}O$ achieved higher CO generation rate via CO_2 splitting (Takalkar and Bhosale, 2019).

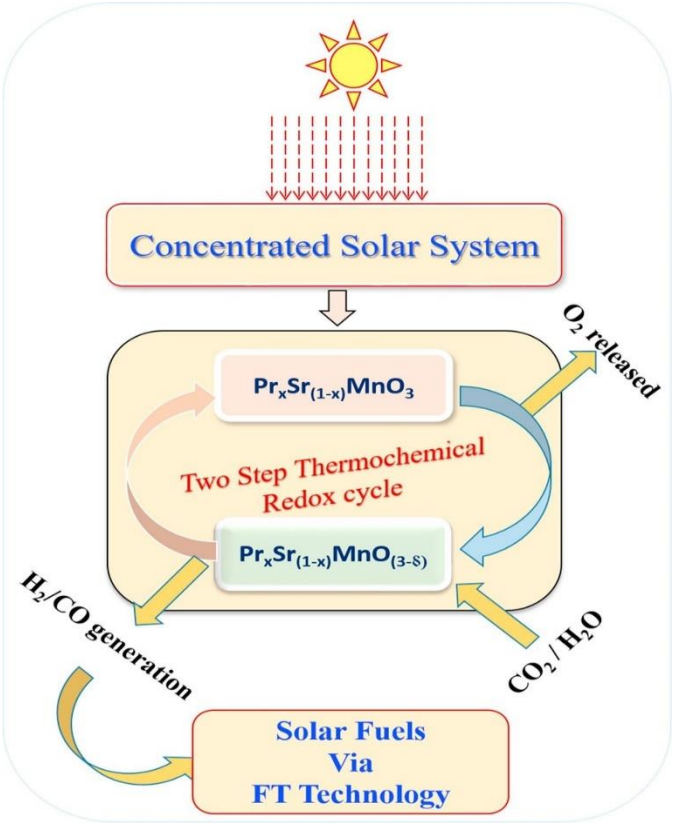

914

915 Figure 17: Solar-assisted thermochemical process for the production of hydrogen and syn gas by
916 the F-T approach. Reproduced from (Takalkar and Bhosale, 2019). Copyright 2019 Elsevier Ltd

917 Table 4: Some investigations on solar-assisted thermochemical transformation of CO_2

Fabricated thermochemical material	**Product(s) of the process**	**Condition**	**Conversion rate**	**References**
$NiFe_2O_4$@SiC	CO	1073–1273 K	18.1 %, 410 µmol/g	(Jiang et al., 2022)
Ni-phyllosilicate @CeO_2	H_2 and CO	100 h of irradiation	90.4 %, 120.90 and 136.84 mmol	(Shi et al., 2023)

			g_{cat} min^{-1}	
$CeO_{2-\delta}$	H_2 and CO	1400 °C	5.1 mL/g	(Haeussler et al., 2020)
Zn/ZnO	Syngas	900-2300 K	31.5-52.1%	(Loutzenhiser and Steinfeld, 2011)
Ni-ferrite	CO or CO/H_2	1100-1400 °C	0.07 mmol/g	(Lorentzou et al., 2014)
$NiFe_2O_4$@Alumina support	Fuels and chemicals	1300 K, 0.5 atm, and 0.4 m/s	98.22%	(Guene Lougou et al., 2020)
$La_{1-x}Ca_xMnO_3$	H_2 and CO	1000-1400 °C	137.5 μmol/g (1.6-fold increase)	(Dey et al., 2015)
Ceria pellets	H_2	1400 °C	2.3 $mL.g^{-1}.min^{-1}$	(Abanades and Haeussler, 2021)
Porous ceria	CO	2.8−3.8 kW and 1400 to 1600 °C	4.56 ± 0.12 mL g^{-1}	(Furler et al., 2012)
$LaCo_{0.7}Zr_{0.3}O_3$	CO	1000 C to 1300 °C, flow	75%	(Wang et al., 2020)

		rate of 40 sccm		

3.6 Non-thermal plasma (NTP) catalysis

Non-thermal plasma (NTP) catalysis is an auspicious technology that is gaining significance in C_1 chemistry. It has been postulated as an effective alternative to conventional thermal catalysis due to the unique interplay between the plasma and heterogeneous catalyst. Thus, this approach could overcome the kinetic limitation of conventional thermal catalysis without the need for any external heat sources (Parastaev et al., 2018). Typically, this process employs an electric discharge of partially ionized gas made up of electrons possessing average electron energy in the range of 1-10 eV (Chen et al., 2020c). These electrons have the capacity to activate stable C_1 molecules as well as denature their bonding structures in the gaseous phase under moderate conditions, thereby producing atoms, ions, and vibrationally-excited reactive species (Mehta et al., 2019). The NTP catalytic approach has the potential of accelerating many energy-intensive and kinetically and/or thermodynamically limited heterogeneous catalytic reactions such as CO_2 hydrogenation (Song et al., 2022), water–gas shift reaction (Xu et al., 2019), hydrocarbon reformation (Wu et al., 2018) and CO_2 splitting (Chen et al., 2019), amongst others.

In Chen et al. (Chen et al., 2020a) Ni NPs supported on silicalite-1 zeolites with suitable active sites and pore structures were comparably investigated in CO_2 hydrogenation under the thermal and NTP conditions. The comparative investigation showed that the hierarchical meso-microporous structures and the associated well-dispersion of Ni species were highly beneficial to the catalysis under the NTP conditions, especially at relatively high voltages. Using a dielectric barrier discharge (DBD) reactor at 150°C, Zeng and Tu (Zeng and Tu, 2017) showed that the presence of Ni in the reactor and injection of argon (up to 60%) in the reaction promotes the

conversion of CO_2 to CO and CH_4 (selectively, 85%) and the energy efficiency of the plasma process. In the reactor, Ar decelerates the breakdown voltage of the feed gas and accelerates charge transfer through the reactor. Furthermore, the NTP-activated hydrogenation of CO_2 in the presence of Ru/MgAl layered double hydroxide catalysts (having low activation energy) provided ~84 % of CH_4 yield at relatively low temperatures (Xu et al., 2020). In another approach, a MOF-supported Ni catalyst (15Ni/UiO-66) presented 99% selectively towards the conversion of CO_2 to CH_4 under NTP conditions and the catalyst was still stable after 20h of reaction (H. Chen et al., 2020b). The experimental investigations of Nizio et al. (Nizio et al., 2016) revealed that ceria and zirconia-promoted Ni-containing hydrotalcite-derived catalysts could yield high CH_4 under NTP conditions and temperatures < 330 °C.

4. Fuels generated from CO_2 conversion

The discovery and development of efficient technologies for the catalytic transformation of CO_2 is an exciting area of research (Ramírez-Valencia et al., 2021) as, in parallele of lowering the atmospheric CO_2, this would allow the access to essential chemicals and fuels such as formic acid (HCOOH), methanol (CH_3OH), carbon monoxide (CO), ethanol (CH_3CH_2OH) and methane (CH_4), among others, that are presently produced from fossil resources. **Figure 18** describes the potential products that could be derived from CO_2 conversion.

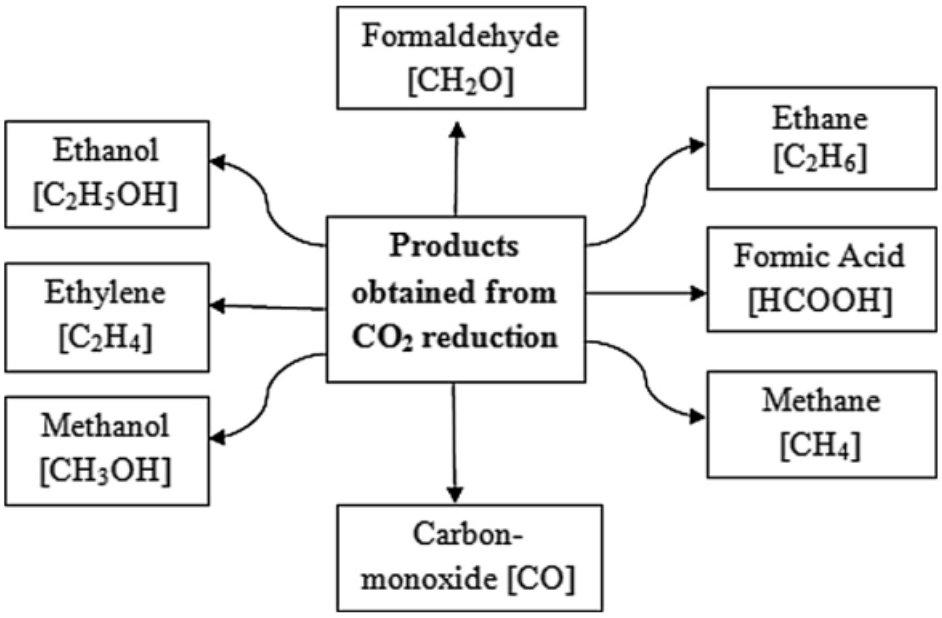

Figure 18: Potential products from CO_2 conversion (Ramírez-Valencia et al., 2021).

4.1 Formic acid

Among the myriad of products accessible from CO_2, formic acid is a valuable intermediate chemical and also used in the domain of energy for reversible hydrogen storage (**Figure 19**) (Moret et al., 2014). Formic acid is of great importance in textile industries, pharmaceuticals and food companies dues to its acidic nature and reducing properties (Afshar, 2014). In particular, the leather and tanning industries are one of the largest global consumers of formic acid (Pérez-Fortes et al., 2016). Other critical applications of formic acid include preservatives and antibacterial agents in animal feeds (Anadón et al., 2006). Therefore, formic acid is a highly valued product with little or no alternative.

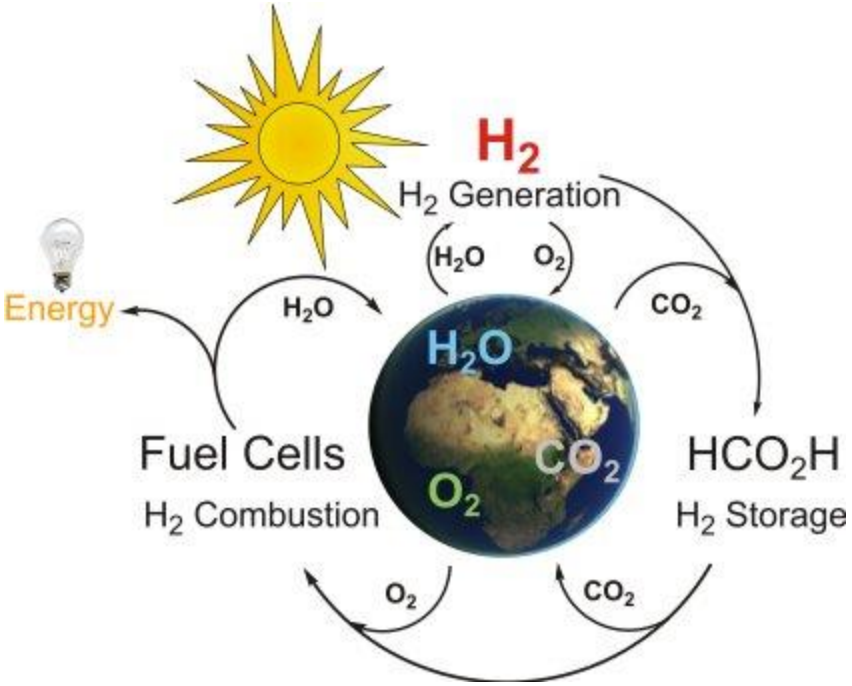

Figure 19: Reversible hydrogenation of CO_2 to formic acid (Li et al., 2002)

Several synthetic methods for the conversion of CO_2 to formic acid have been explored. This includes biochemical, photochemical, electrochemical, microwave-assisted, photosynthetic and catalytic reduction (Asiri and Lichtfouse, 2020; Hu et al., 2013; Lu et al., 2014; Scibioh and Viswanathan, 2004; Yadav et al., 2012). Catalytic conversion of CO_2 to formic acid was first reported by Inoue (Inoue et al., 1976) in 1976. Since then, CO_2 has become an attractive starting molecule for the synthesis of formic acid. Compared to other methodologies, the catalytic reduction method offers higher selectivity to targeted product, thus minimizing the risk of unwanted CO as a byproduct that may poison the fuel. However, the selectivity of the preferred product depends on the reduction method and the nature of the catalyst used.

Weilhard *et al.* reported the synthesis of formic acid from CO_2 feedstock using an ionic liquid as an alternative to expensive precious metal-based catalytic systems (Weilhard et al., 2021). As

shown in Scheme 3, the synthetic strategy consists of a mixture of CO_2 and H_2 in 1:1 molar ratio. The catalytic system consists of a homogeneous mixture of 1-butyl-2,3-dimethylimidazolium acetate (BMMI.OAc) and Scandium(III) trifluoromethanesulfonate ($Sc(OTf)_3$. They reported a very high catalytic efficiency with turnover numbers (TON) and turnover frequency (TOF) of 8 x 10^5 and 2.1 x 10^4 h^{-1}, respectively.

$$CO_2 + H_2 \xrightarrow[BMMI.OAc/\ (Sc(OTf)_3}]{\text{Dioxane/water}} HCOOH \qquad (12)$$

Moret *et al.* (Moret et al., 2014) applied a ruthenium-based homogeneous catalytic system to convert CO_2 feedstock into formic acid directly. The catalytic conversion was performed following the catalytic life cycle described in **Figure 20**. The reaction was performed at 40 °C using a mixture of water and dimethyl sulphoxide (DMSO) as the solvent.

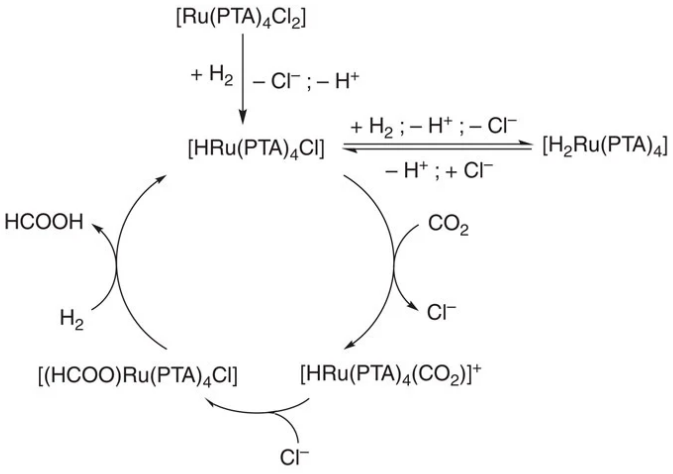

Figure 20: Catalytic cycle and hydrogenation of CO_2 into formic acid over $[HRu(PTA)_4Cl]$

They reported that the catalytic system is highly sustainable than the existing routes. In addition, it is highly recyclable and gives a higher yield of the target product. More recently, Mubarak *et*

al. (Mubarak et al., 2022) published a greener approach via photocatalytic transformation of CO_2 into formic acid. The catalytic procedure involves the breaking down of CO_2 into valuable chemicals in the presence of sunlight and Ag-doped TiO_2 NPs. This catalytic system iss highly selective with HCOOH as the single product, formic acid being obtained at a yield of 193 μM $cm^{-2}\,h^{-1}$.

4.2 Carbon monoxide

In the series of products derived from CO_2, carbon monoxide (CO) is one of the most critical chemicals and feedstock. It is a primary raw material along with H_2 gas for syngas production via Fischer-Tropsch synthesis to produce liquid fuels (Zeng et al., 2018). It is also valuable for the metallurgical industries (Liu et al., 2017). Most of the efforts concerning CO_2 reduction into CO efforts can be listed in two major categories, namely thermochemical reduction and electrochemical reduction (Porosoff et al., 2016). CO_2 being a very stable molecule, it requires a very high temperature (> 1200 °C) to decompose to CO (Equation 13). Therefore, this procedure is not thermodynamically favorable and must be catalytically driven.

$$CO_{2(g)} \rightarrow CO_{(g)} + \frac{1}{2}O_{2(g)}\ \Delta H = 279.8\ kJ/mol \qquad (13)$$

Various catalytic materials have been employed to reduce the energy cost of the catalytic conversion of CO_2 to CO. For example, Au nanocatalysts have shown tremendous potential in converting CO_2 to CO with a remarkable selectivity (Qi et al., 2019). Qi *et al.* (Qi et al., 2021) reported a successful electrochemical conversion of CO_2 to CO over Au nanocatalyst. Wen *et al.* (Wen et al., 2018) used a nanoporous Au leave electrocatalyst prepared by a de-alloying technique to reduce CO_2 to CO, achieving a very high catalytic efficiency to CO (90% FE).

While gold-based catalysts are the most successful catalysts for the conversion of CO_2 to CO, the high cost of Au may prevent large-scale industrial applications (Ma et al., 2016b) which requires

to find low-cost alternative catalysts. Metallic Ag is gaining considerable attention for CO_2 conversion because of its significantly lower cost compared to Au and also high selectivity to CO (Ma et al., 2016b). This has been demonstrated by Ma *et al.* (Ma et al., 2016b) who developed a Ag-based electrocatalyst comprising oxide-derived nanostructure silver (OD-Ag) and polycrystalline Ag. The proposed reduction mechanism is described in Scheme 3. The obtained catalytic efficiency was 80% Faradic efficiency which is comparable to the results obtained with Au electrocatalysts.

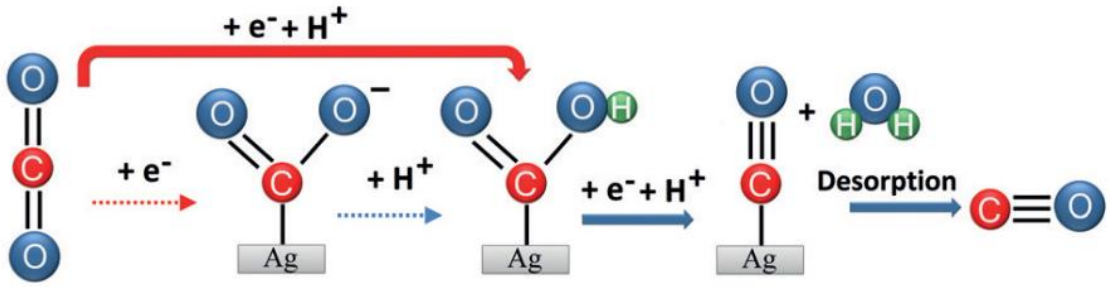

Scheme 3: Mechanism of the conversion of CO_2 to CO via electrochemical reduction proposed by (Ma et al., 2016b).

Dong *et al.* (Dong et al., 2021) reported the use of low-cost ZnOHF nanorods as a substitute to expensive Au and Ag metals for the reduction of CO_2 to CO by electrochemical reduction. They obtained a CO Faraday efficiency of 76.4% with the CO current density of 57.53mA/Cm^2. It is worth mentioning that the catalytic efficiency of this Zn-based catalyst is not as high as Au and Ag-based ones, but the price is significantly lower which may open avenues for a large-scale electrochemical reduction of CO_2 to CO.

4.3 Methanol

The conversion of CO_2 to MeOH has been drawing tremendous attention lately because of the vast applications of methanol (Olah, 2013). Methanol is a multipurpose chemical feedstock (Offermanns et al., 2014) for producing various value-added products and fuel. The current production rate of methanol is 98 million metric tons per year (Kajaste et al., 2018). It is also an important hydrogen carrier. The various applications and Carbon cycle of methanol are described in **Figure 21**.

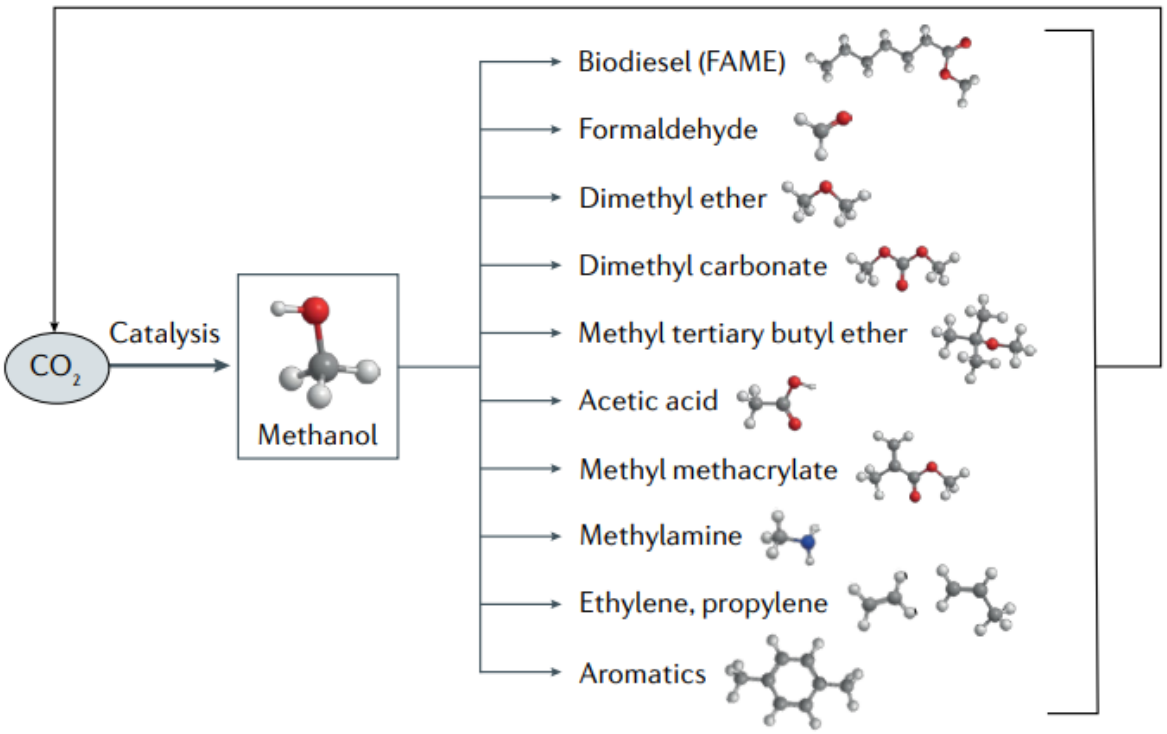

Figure 21: Main applications of methanol in industry

Considering the vast application of methanol (Figure 16), conversion of CO_2 to MeOH is a crucial research area. The production of methanol has been dominated by the conversion of syngas (a mixture of CO and H_2) and CO_2 (Nieminen et al., 2019). From the mechanistic point of view, the synthetic pathway may occur through direct CO_2 hydrogenation (eq 14) or via reverse water gas shift (RWGS) (eq 15) followed by CO hydrogenation (eq 16) (Gaikwad et al., 2020).

A challenge often characterized by this synthetic procedure is that it is performed at very high temperature and pressure (Bertau et al., 2014). In addition, it also suffers from poor selectivity and low yield (Jadhav et al., 2014).

To improve this procedure, various homogeneous and heterogeneous catalytic hydrogenation reactions as well as thermocatalysis, photocatalysis, electrocatalysis, and enzymatic catalysis have been explored with promising results (Navarro-Jaén et al., 2021).

$$CO_2 + 3H_2 \rightleftharpoons CH_3OH + H_2O \rightarrow \Delta H = -40.9 \text{ kJ mol}^{-1} \quad (14)$$

$$CO_2 + H_2 \rightleftharpoons CO + H_2O \rightarrow \Delta H = +49.8 \text{ kJ mol}^{-1} \quad (15)$$

$$CO + 2H_2 \rightleftharpoons CH_3OH \rightarrow \Delta H = -90.7 \text{ kJ mol}^{-1} \quad (16)$$

Conventionally, methanol production from syngas is usually catalyzed by a Cu-based heterogeneous catalyst at 513-533K temperature and 50-100 bar pressure (Bart and Sneeden, 1987). It is worth mentioning that Cu alone exhibits a very low activity; to enhance the activity, the Cu catalyst is usually tethered on support or promoters such as Al_2O_3, ZnO, and ZrO_2. In most cases, the synergy between the Cu catalyst and the promoters only achieves a conversion of approximately 30% due to a fast deactivation of the Cu catalyst (Navarro-Jaén et al., 2021). Although the activity is low, Cu-based catalysts are very cheap thus justifying their predominance in methanol synthesis. However, the growing demand for methanol induced emergence of new ideas for converting CO_2 to methanol.

For instance, Pd-based heterogeneous catalytic systems have been used to improve the synthesis of methanol. Díez-Ramírez *et al.* (Díez-Ramírez et al., 2016) reported the application of Pd/ZnO

catalyst to convert CO_2 to methanol under atmospheric conditions, observing a low conversion rate due to the side reactions from coke formation and water from the (RWGS) reaction (eq 15). Various attempts have been made to suppress side reactions from the (RWGS) reaction. Fiordaliso *et al.* (Fiordaliso et al., 2015) reported the use of supported Pd-Ga bimetallic catalysts, specifically, $GaPd_2/SiO_2$ for converting CO_2 to methanol, at low CO_2 pressure, and with a MeOH production rate of 0.12 mol%. Although the catalytic activity of this $GaPd_2/SiO_2$ was better than in previous studies, the major drawback is the Pd cost, thus limiting practical applications.

Ahmad *et al.* (Ahmad and Upadhyayula, 2019), developed an efficient, cheaper bimetallic catalyst Ga_3Ni_5 for CO_2 conversion and compared their results with those of Fiordaliso *et al.* (Fiordaliso et al., 2015). The activity of the Ga_3Ni_5 catalyst was found to be higher under the same experimental conditions, showing a MeOH conversion rate of 38.85 μmol g_{cat}^{-1} min^1 coupled to an impressive selectivity of 94 %.

While Ga, Zn, Cu, Al, Pd, Ni, Pt-based catalysts have been widely tested for MeOH synthesis, To motivate a cost-effective catalyst, scientists are considering an alternative to Pt and noble metals. For instance, CeO_2-based catalyst is getting attention due to its abundant oxygen and reversible valence charges (Ce^{4+} and Ce^{3+}) (F. Wang et al., 2016). This potential was demonstrated by Chang *et al.* (Chang et al., 2021), who applied a CeO_2-based catalyst Cu/ZnO–CeO_2 to convert CO_2 to methanol.

Perovskites have been also identified as low-cost approach for CO_2 conversion to methanol. This is described by Zhan *et al.* (Zhan et al., 2014), who employed a perovskite-based catalyst to produce methanol from CO_2. They reported an excellent catalytic efficiency with impressive stability of the prepared catalyst.

Apart from heterogeneous-based catalytic systems, homogeneous catalysts have been also reported for methanol synthesis from CO_2. Kothandaraman *et al.* (Kothandaraman et al., 2016) developed a Ru-based homogeneous catalytic system that showed a very good yield (79 %) in methanol. In addition, this catalyst also shows excellent recyclability with over five runs without a significant loss in activity. Zhou *et al.* (Zhou et al., 2022) published the use of a ruthenium pincer complex $[RuH_2(Me_2PCH_2SiMe_2)_2NH(CO)]$ which led to a good catalytic efficiency from the density functional theory (DFT) data.

Application of enzymes to reduce CO_2 to methanol is also getting considerable attention. Zhang *et al.* (Z. Zhang et al., 2021) reported the enzymatic conversion of CO_2 to methanol in the presence of nicotinamide adenine dinucleotide (NADH). The enzyme was immobilized on porous a MOF (ZIF-8) to improve CO_2 concentration. The prepared NADH/ZIF-8 composite was placed in the bio-electrochemical cell. The methanol conversion rate was 822 μmol g-1 h-1, and the catalytic system was found stable and environmentally friendly.

4.4 Ethanol

Ethanol is a valuable chemical in our daily life. In contrast to methanol, ethanol has some distinct advantages, such as higher energy density, lower toxicity, and transportation safety (D. Wang et al., 2016). As a result of these advantages, it intervenes in a wide range of domestic and industrial applications, including chemical raw material for chemical synthesis, in disinfectants, pharmaceuticals and cosmetics, plasticizers, polishes and dyes (An et al., 2021). In addition to its domestic and industrial applications, ethanol is a necessary fuel and hydrogen carrier (Pang et al., 2019). The United States are the world largest ethanol producer, accounting for 59% of global production. This is followed by brazil with 28% while the rest of the world accounts for 13% (**Figure 22**).

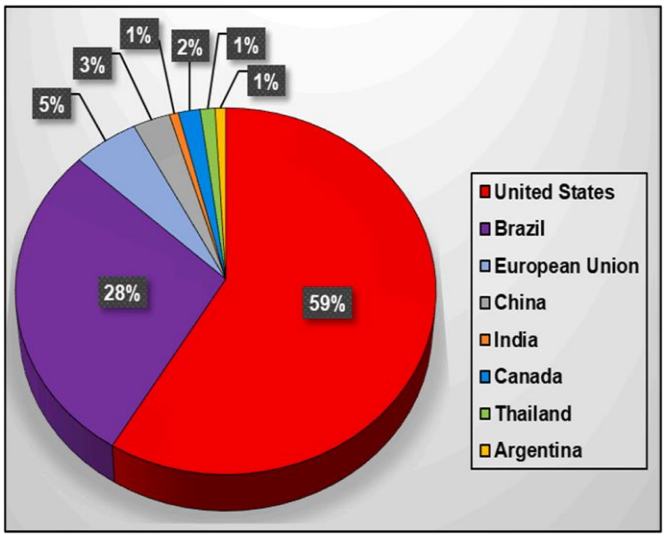

Figure 22: Ethanol production in various countries for the year 2020 (Cooper et al., 2021).

The high energy density and the compatibility of ethanol with existing and modern combustion engines make it a vital fuel. Ethanol is usually produced from the fermentation of starch and cellulose feedstock (Ali et al., 2022; Wang et al., 2021). With the population and increasing demand for food, the search for an alternative strategy for ethanol synthesis is highly urgent. That's why hydrogenation of CO_2 to ethanol has drawn a lot of attention.

Several catalytic systems have been used for CO_2 conversion to ethanol, notably Pt, Co, Fe, and Cu systems (Zheng et al., 2019). Cu-based catalysts have been used for hydrogenating CO_2 to ethanol due to their success in converting CO_2 to methanol; however, the selectivity to ethanol is very low (Cao et al., 2016). Recently, it has been found out that ethanol selectivity can be improved by using Cu^1 instead of Cu^o. Despite this success, the Cu-catalyst suffers from long-term use due to instability under the reaction conditions and operating conditions.

Other catalytic systems have been tested to improve the selectivity and yield of ethanol from CO_2, including Pt-based catalysts and their alloys; while good yield was obtained with these

catalysts, the high cost of the catalytic materials is an issue that limits their practical application (Choi and Liu, 2009). Lou *et al.* (Y. Lou et al., 2021) successfully applied a Pd/CeO_2 catalyst to convert CO_2 to ethanol. They reported a space yield time of 45.6 $g_{ethanol}\ g_{Pd}^{-1}\ h^{-1}$. Together with an excellent selectivity of 99.2 %. Zhang *et al.* (F. Zhang et al., 2021) reported the application of supported sodium-modified Rh NPs in zeolite to hydrogenate CO_2 to ethanol that showed a CO_2 conversion rate of 10 % and a selectivity of 24% to ethanol. Zheng *et al.* (Zheng et al., 2019) reported the conversion of CO_2 to ethanol using a $LaCo_{1-x}Ga_xO_3$ composite perovskite catalyst with a very good catalytic CO2 conversion of 9.8% and a 88.1% selectivity to ethanol.

Another challenge is catalyst separation from the product and recyclability; therefore, extensive research efforts are is devoted to develop effective and highly reusable catalysts in order to address this challenge.

4.5 Methane

Methane (CH_4) is a C_1 compound primarily used as fuel. Moreover, it is also used as a feedstock for chemical synthesis, especially as a synthetic natural gas and is also a major source of hydrogen storage (Koytsoumpa and Karellas, 2018). Therefore, the hydrogenation of CO_2 to methane is an effective strategy for CO_2 capture, utilization and conversion to valuable chemicals. Catalytic hydrogenation is the most widely studied route for CO_2 conversion to methane (Koytsoumpa and Karellas, 2018). This procedure is called methanation or Sabatier reaction (Lu et al., 2016) as it was first reported in 1902 by Sabatier *et al.* (Sabatier, 1902). According to the literature, two possible mechanisms have been proposed. The first mechanism is direct methanation (eq 17) which involves the reaction of CO_2 and H_2 with a nominal ratio of 1:4, respectively, while the second mechanism is the reaction of CO and H_2 in a ratio of 1:3 respectively (equation 2) (Dias and Perez-Lopez, 2021). As shown in equations 17 and 18, the

conversion of CO_2 to methane is a highly exothermic reaction which can proceed at a relatively lower temperature. However, given the thermodynamic stability of CO_2 molecules due to the presence of delocalized π bonds, the conversion of CO_2 to methane remains a serious challenge at a lower temperature (Álvarez et al., 2017).

$$CO_2 + 4H_2 \rightleftharpoons CH_4 + 2H_2O \quad \Delta H = -165 \text{ kJ mol}^{-1} \qquad (17)$$

$$CO + 3H_2 \rightleftharpoons CH_4 + H_2O \quad \Delta H = -206 \text{ kJ mol}^{-1} \qquad (18)$$

To overcome this challenge and permit activation of CO_2 at lower temperatures, highly active catalytic materials with good selectivity to methane and low deactivation must be developed. CO_2 methanation has been performed with transition metals such as Co, Ni, Fe, Cu, Ru, Rh, and Pd (Y.-T. Li et al., 2022). However, due to the cost and limited availability, these noble metals are not widely employed for methane synthesis, especially on an industrial scale. Therefore, a new generation of low-cost and efficient catalysts have been investigated for methanation reaction. Among them, Ni, Fe, and Co-based catalysts have been widely studied because of their low cost and catalytic efficiency for CO_2 methanation. Ni-based catalytic materials are the most studied for CO_2 methanation due to their low cost and availability (Fukuhara et al., 2017). Dias *et al.* (Dias and Perez-Lopez, 2021) reported the conversion of CO_2 to Methanol using Ni/SiO_2 catalyst promoted by Fe, Co, and Zn. They obtained a very high CO_2 conversion (73 %) and excellent selectivity (98.5 %) to methane.

It is generally believed that catalytic behavior depends on several factors, such as surface properties, metal support interaction, etc. Researchers are currently developing further catalytic supports to enhance the performance of catalytically active metal species. This was recently demonstrated by Li *et al.* (Y.-T. Li et al., 2022) who used a metal-organic framework (MOF) as a support to enhance the catalytic activity of NiFe for the hydrogenation of CO_2 to methane. MOFs

are highly porous coordination polymers that are characterized by high surface areas. As a result, they can enhance the catalytic activity in comparison to other traditional supports.

Li *et al.* (Y.-T. Li et al., 2022) obtained a very high CO_2 conversion (72.3 %) and impressive selectivity (99.3 %) with the NiFe/MOF catalytic material. Similarly, Hu *et al.* (Hu et al., 2022) also established the role of metal-support interaction using Ni supported on CeO_2 nanofibers. The oxygen vacancy enhanced the catalytic efficiency of Ni in CeO_2. The prepared catalyst recorded 82.3 % conversion of CO_2 at low temperatures (250 ^oC - 300 ^oC). In addition, they also reported impressive stability of the catalyst up to 60h. This result can be attributed to synergistic effects between the Ni NPs and the CeO_2 nanofibers.

4.6 Formaldehyde

The ease of availability of CO_2 has provided an opportunity for energy production and commodity products for the economy. Among other compounds which could be generated from CO_2 is formaldehyde (FMD). Formaldehyde, with the chemical formula HCHO, is a substance that has gained wide usage by millions of people, directly or indirectly, across the globe due to its versatility (Rauch et al., 2019; Subasi 2020; Usanmaz et al., 2002). Generally, FMD is produced industrially via three stages. These include the production of synthesis gas (a mixture of water gas, carbon(iv) oxide and hydrocarbons) by steam reforming natural gas, synthesis of MeOH, and the generation of FMD through the partial oxidation of MeOH (Bahmanpour et al., 2015). All these methods are energy-intensive procedures (Heim et al., 2017; Nguyen et al., 2020). Moreover, during these processes, CO_2 was contained in most of the products formed (Lervold et al., 2021), leading to increased pollution.

In a bid to curb the emission of CO_2, scientists have developed methods that could possibly convert CO_2 into useful products. Of these methods is the production of FMD (Friedlingstein 2015; Sümbelli et al., 2019). Although the generation of FMD from CO_2 is quite challenging, frantic efforts are being made to overcome this fall-out as CO_2 is resistant to chemical changes (Rauch et al., 2019). One of those efforts is the conversion of CO_2 at ambient temperature yielding the formation of FMD. The CO_2 reacts with triphenylsilane in the presence of a magnesium catalyst, resulting in an intermediate product formed, known as bis(silyl)acetal. This product is then converted to FMD in the presence of cesium fluoride (Eq 19) (Rauch et al., 2019).

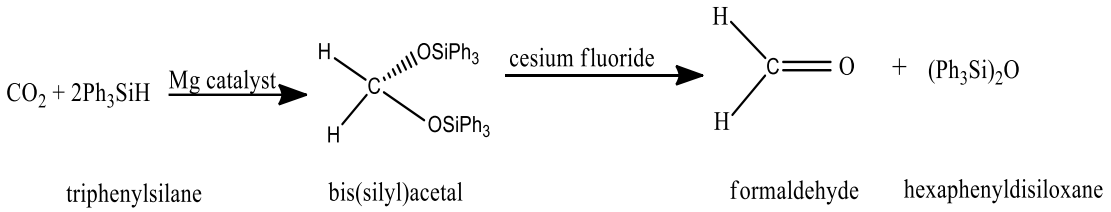

eq 19

Another way that allows to convert CO_2 into FMD is the hydrogenation process, which different researchers have debated to be dependent on the catalytic system (heterogeneous or homogeneous) involved (Dang et al., 2019; Nguyen et al., 2020; Studt et al., 2015). The most prevalent catalysts used for this reaction are heterogeneous Cu-based, such as Cu-ZnO-Al_2O_3 (Kobl et al., 2016) or Pt-promoted Cu/SiO_2 (Lee et al., 2001). This latter converts CO_2 to FMD at 150^{o}C for 120 min at 600 kPa. However, Lee and co-partners indicated some issues encountered with this catalyst (Lee et al., 2001). Moreso, a mesoporous graphitic carbon nitride (g-C_3N_4) material with specific crystallinity and surface area, has been shown to have a significant effect on the conversion of CO_2 to FMD. Since this discovery other photocatalytic mesoporous nanomaterials have been explored for the photocatalytic reduction of CO_2 (Park et al., 2012; Xu et al., 2013).

4.7 Hydrogen

Aside from FMD, a critical commodity product is hydrogen, being also a fuel, that could be generated from CO_2 via a process called carbon dioxide reforming. This process, represented on equation 20, consumes CO_2 and methane (CH_4), two greenhouse gases. This process requires high temperature, and as such, it is highly endothermic and also favored by low pressure (Wang et al., 1996).

$CO_2 + CH_4 \rightarrow 2CO + 2H_2 \qquad \Delta H_{(298)} = 247\ kJ/mol$ eq 20

Fan and coworkers reported this process has been catalyzed over a Ni-Co/MgO-ZrO_2 nanomaterial, (Fan et al., 2011). The effect of Ni-based catalysts on the CO_2 reforming of methane had earlier been investigated by Takano et al., (1994). This process produces green hydrogen a quality of hydrogen which is otherwise generated via the electrolysis of water using a renewable energy source (Acar and Dincer 2022; Luo et al., 2022). This process could solve the problem of CO_2 emission during hydrogen production from classical techniques (Madadi Avargani et al., 2022). However, there is a fall-out associated with the production of green hydrogen via the method mentioned above; it involves the release of carbon(ii)oxide as a by-product. Although CO has a significant value as a fuel and is crucial in manufacturing other chemicals, it has been known over the years for its highly hazardous nature (Prockop and Chichkova 2007; Rose et al., 2017; Wu and Juurlink 2014) and toxicity. Studies should focus more on the production of hydrogen from CO_2, as this process is not well explored. This will go a long way in tackling the issue of global warming.

4.8 Olefins and gasoline

The hydrogenation of CO_2 into high molecular weight hydrocarbons such as lower olefins and gasoline has become increasingly popular due to the necessity to use non-fossil carbon resources

as alternative to fossil oil for a sustainable production of liquid fuels and chemicals (Jiao et al., 2016; Yang et al., 2017; Zhong et al., 2016). This process requires input energy to form C-H bonds and to break C=O bonds (Dang et al., 2019) and efficient catalysts.

Processes based on different catalysts and producing unique products distribution have been developed in the past decades. A commonly used process is Fischer-Tropsch synthesis (FTS) that yields typically straight-chain hydrocarbons controlled by the Anderson–Schulz–Flory (ASF) product distribution, which restricts to C_2-C_4 hydrocarbon fraction of about 56.7% selectivity for desired lower olefins ($C_2^=$ - $C_4^=$) with 29.2% of undesired CH_4 selectivity (Scheme 4). If selective formation of lower olefins and low CH_4 formation can be achieved by proper catalyst modification and optimization of reaction conditions (Chen et al., 2015; Liu et al., 2015; Lu et al., 2014; Zhong et al., 2016; Zhou et al., 2015) achieve high selectivity for lower olefins and high stability, requires to develop new catalysts that operate away from Anderson–Schulz–Flory (ASF) distribution (Numpilai et al., 2017; Visconti et al., 2017; Zhang et al., 2015).

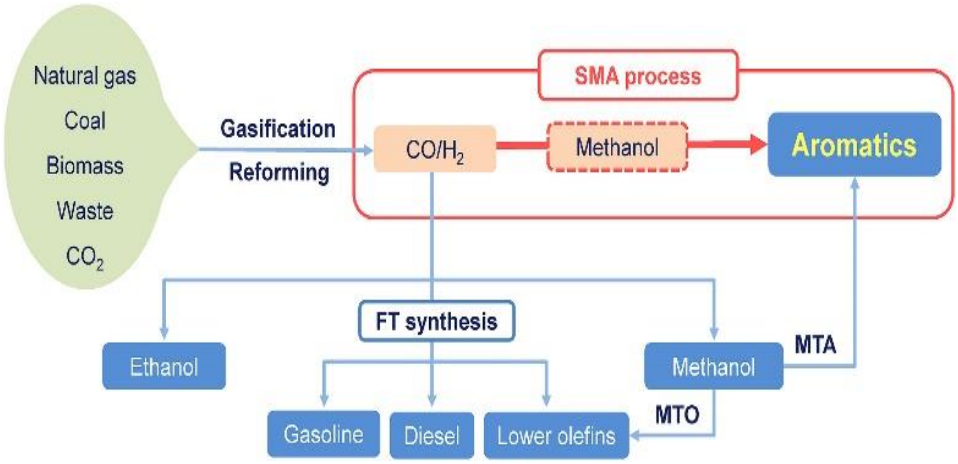

Scheme 4. Typical Reaction processes related to reduction of Syngas to hydrocarbons through Fischer-Tropsch synthesis and methanol-to-Olefins Technology. (Adapted without change from (Cheng et al., 2017)

In recent years, significant progress in the development of new catalysts that increase the selectivity of product formed has been made. For instance bifunctional catalysts such as oxide/zeolite have been shown to increase selectivity for lower olefins ($C_2^=$–$C_4^=$) with significant inhibition of CH_4 formation (Jiao et al., 2016; Li et al., 2019; Liu et al., 2017). Bifunctional catalysts typically consist of oxides and zeolites, which activate CO_2 and catalyze C-C coupling, respectively. In a recent work Gao et al. obtained 80% $C_2^=$–$C_4^=$ selectivity with ~ 4% CH_4 inhibition among all hydrocarbons using In-Zr composite based oxides and SAPO-34 zeolites (Gao et al., 2018; Dang et al., 2018). In addition, CO selectivity over the bifunctional catalysts could be jacked up to 85 % during CO_2 reduction to lower olefins at high temperature reversed water-gas shift (RWGS).

Moreover, the CO selectivity could be reduced if In_2O_3 is further modified by Zr and Zn promoters (Gao et al., 2017). The reduction of CO_2 to hydrocarbons over bifunctional catalysts involves hydrogenation of CO_2 to CH_xO species or intermediates on the oxygenated sites of the oxide component as the first step, and the migration of the intermediates to the zeolite component where they are transformed into various hydrocarbons at the acid sites of the zeolite (Cheng et al., 2017; Gao et al., 2017). The transport of the CH_xO intermediates plays a crucial role in suppressing the undesired RWGS side reaction and achieving a high selectivity and it can be improved by acid treatment of the zeolite crystals. The performance of bifunctional catalysts with and without acid treatment for In_2O_3-$ZnZrO_x$/SAPO-34 composite is summarized in **Table 5**. The maximum of $C_2^=$–$C_4^=$ selectivity is 85 % among all hydrocarbons with 1.6 % CH_4. Moreover, the decrease of zeolite crystal size (Dang et al., 2019) and shortening of the diffusion path of the methanol intermediates should favor the formation of lower olefins over the composite catalyst (Jiao et al., 2018; Yang et al., 2017).

Table 5: Performance of In_2O_3-$ZnZrO_x$ and SAPO-34 as bifunctional catalysts prior to and after treatment with nitric acid (Dang et al., 2019)

Entry	Catalyst type	Selectivity		CO_2 conversion (%)	Hydrocarbon distribution			
		HC	CO		$C_2^=$-$C_4^=$	C_2^o-C_4^o	C_{5+}	CH_4
1.	In_2O_3-$ZnZrO_x$/SAPO-34-S-a	17.0	44.2	55.8	85.0	11.1	2.3	1.6
2.	In_2O_3-$ZnZrO_x$/SAPO-34-S	17.9	45.0	55.0	79.6	13.9	5.2	1.3
3.	In_2O_3-$ZnZrO_x$/SAPO-34-S-H-a	17.0	46.6	53.4	84.5	11.0	3.3	1.2
4.	In_2O_3-$ZnZrO_x$/SAPO-34-H	17.4	45.9	54.1	79.0	16.5	3.3	1.2
5.	In_2O_3-$ZnZrO_x$/SAPO-	17.2	46.2	53.8	80.6	15.2	2.9	1.3

	34-C-a							
6.	In_2O_3-$ZnZrO_x$/SAPO-34-C	18.1	47.5	52.5	76.8	19.2	2.7	1.3

5. Conclusions and future outlook

Information gathered from recent literature confirms that continuous efforts are being made to reduce CO_2 in the environment. However, most articles are focused on its conversion to hydrocarbons, mainly methane, and other organic compounds, such as ethanol, methanol, and methanoic acid. Only limited articles were published on CO_2 reduction to either FMD (mostly as intermediates) or hydrogen. Thus, more reaction pathways that yield these products should be investigated. There are some challenges involved in CO_2 conversion into useful products, which should be considered. These include but are not limited to the production of harmful gases like CO, technological feasibilities in terms of more research as regards more-efficient conversion techniques, instability and low selectivity of the conversion products, and insufficient basic understanding of the catalytic processes (Sharma et al., 2022). Having pointed out these fall-outs, it is worth mentioning that scientists and other stakeholders should consider the project of CO_2 conversion as germane because it technically solves the problem of global warming and, in turn, impacts the economy of the worldwide system.

The use of nanomaterials-based technologies for the transformation of CO_2 is a relatively new area that scientists have to continue to explore. Unarguably, the demonstrated suitability, selectivity and applicability of nanomaterials for producing hydrocarbons and valued-added chemicals (methanol, ethanol, formic acid, formaldehyde, etc) have made nanomaterials

promising systems for the transformation of CO_2 into various fuels. The research findings so far are quite intriguing at the laboratory scale. However, the extension of these findings to industrial scale would be highly phenomenal. It is therefore recommended and/or suggested industrially suitable, and applicable catalyst (nanomaterials) be developed to selectively and efficiently transformed atmospheric CO_2 to value-added products.

Funding

This research exercise received no external funding

Acknowledgements

Alli, Y.A. would like to seize this opportunity to appreciate CNRS-Laboratory of Coordination Chemistry and Prof. Karine Philippot for providing him with laboratory space and enabling environment for postdoctoral research activities. Also, Oladoye, P.O. would like to appreciate Prof. Yong Cai for providing him with laboratory space and enabling environment for his doctoral research activities.

References

Abanades, S., Haeussler, A., 2021. Two-step thermochemical cycles using fibrous ceria pellets for H_2 production and CO2 reduction in packed-bed solar reactors. Sustainable Materials and Technologies 29. https://doi.org/10.1016/j.susmat.2021.e00328

Acar, C., Dincer, I., 2022. Selection criteria and ranking for sustainable hydrogen production options. International Journal of Hydrogen Energy. https://doi.org/10.1016/j.ijhydene.2022.07.137

Afolabi, T. Adeniyi, Ejeromedoghene, O., Olorunlana, G.E., Afolabi, T. Adeleke, Alli, Y.A., 2022. A selective and efficient chemosensor for the rapid detection of arsenic ions in aqueous medium. Res. Chem. Intermed. 48, 1747–1761. https://doi.org/10.1007/s11164-022-04665-1

Afshar, A.A.N., 2014. Chemical profile: formic acid. Webpage Summ. http//chemplan. biz/chemplan_demo/sample_reports/Formic_Acid_Profile. pdf (accessed Nov, 2017).

Ahmad, K., Upadhyayula, S., 2019. Conversion of the greenhouse gas CO 2 to methanol over supported intermetallic Ga–Ni catalysts at atmospheric pressure: thermodynamic modeling and experimental study. Sustain. Energy Fuels 3, 2509–2520.

Alaghmandfard, A., Ghandi, K., 2022. A Comprehensive Review of Graphitic Carbon Nitride (g-C3N4)–Metal Oxide-Based Nanocomposites: Potential for Photocatalysis and Sensing. Nanomaterials 12. https://doi.org/10.3390/nano12020294

Alhaddad, M., Shawky, A., 2021. Pt-decorated ZnMn2O4 nanorods for effective photocatalytic reduction of CO2 into methanol under visible light. Ceram. Int. 47, 9763–9770. https://doi.org/10.1016/j.ceramint.2020.12.116

Ali, Syed Saim, Ali, Syed Saif, Tabassum, N., 2022. A review on CO2 hydrogenation to ethanol: Reaction mechanism and experimental studies. J. Environ. Chem. Eng. 10, 106962.

Alli, Y.A., Adewuyi, S., Bada, B.S., Thomas, S., Anuar, H., 2021. Quaternary Trimethyl Chitosan Chloride Capped Bismuth Nanoparticles with Positive Surface Charges: Catalytic and Antibacterial Activities. J. Clust. Sci. 8. https://doi.org/10.1007/s10876-021-02156-8

Ali, N., Bilal, M., Nazir, M.S., Khan, A., Ali, F., Iqbal, H.M.N., 2020. Thermochemical and electrochemical aspects of carbon dioxide methanation: A sustainable approach to generate fuel via waste to energy theme. Science of the Total Environment 712. https://doi.org/10.1016/j.scitotenv.2019.136482

Alli, Y.A., Ejeromedoghene, O., Oladipo, A., Adewuyi, S., Amolegbe, S.A., Anuar, H., Thomas, S., 2022. Compressed Hydrogen-Induced Synthesis of Quaternary Trimethyl Chitosan-Silver Nanoparticles with Dual Antibacterial and Antifungal Activities. ACS Appl. Bio Mater. https://doi.org/10.1021/acsabm.2c00670

Álvarez, A., Borges, M., Corral-Pérez, J.J., Olcina, J.G., Hu, L., Cornu, D., Huang, R., Stoian, D., Urakawa, A., 2017. CO2 activation over catalytic surfaces. ChemPhysChem 18, 3135–3141.

An, K., Zhang, S., Wang, J., Liu, Q., Zhang, Z., Liu, Y., 2021. A highly selective catalyst of Co/La4Ga2O9 for CO2 hydrogenation to ethanol. J. Energy Chem. 56, 486–495.

Anadón, A., Martínez-Larrañaga, M.R., Martínez, M.A., 2006. Probiotics for animal nutrition in the European Union. Regulation and safety assessment. Regul. Toxicol. Pharmacol. 45, 91–95.

Arai, T., Sato, S., Uemura, K., Morikawa, T., Kajino, T., Motohiro, T., 2010. Photoelectrochemical reduction of CO 2 in water under visible-light irradiation by a p-type InP photocathode modified with an electropolymerized ruthenium complex. Chem. Commun. 46, 6944–6946.

Arumugam, M., Tahir, M., Praserthdam, P., 2022. Effect of nonmetals (B, O, P, and S) doped with porous g-C3N4 for improved electron transfer towards photocatalytic CO2 reduction with water into CH4. Chemosphere 286, 131765. https://doi.org/10.1016/j.chemosphere.2021.131765

Asiri, A.M., Lichtfouse, E., 2020. Conversion of Carbon Dioxide Into Hydrocarbons Vol. 2 Technology. Springer.

Ateka, A., Rodriguez-Vega, P., Ereña, J., Aguayo, A.T., Bilbao, J., 2022. A review on the valorization of CO2. Focusing on the thermodynamics and catalyst design studies of the direct synthesis of dimethyl ether. Fuel Processing Technology. https://doi.org/10.1016/j.fuproc.2022.107310

Atsbha, T.A., Yoon, T., Seongho, P., Lee, C.J., 2021. A review on the catalytic conversion of CO2using H2for synthesis of CO, methanol, and hydrocarbons. Journal of CO2 Utilization. https://doi.org/10.1016/j.jcou.2020.101413

Ávila-Bolívar, B., García-Cruz, L., Montiel, V., Solla-Gullón, J., 2019. Electrochemical reduction of CO2 to formate on easily prepared carbon-supported Bi nanoparticles. Molecules 24, 1–15. https://doi.org/10.3390/molecules24112032

Azofra, L.M., MacFarlane, D.R., Sun, C., 2016. An intensified π-hole in beryllium-doped boron nitride meshes: Its determinant role in CO2 conversion into hydrocarbon fuels. Chem. Commun. 52, 3548–3551. https://doi.org/10.1039/c5cc07942j

Bahmanpour, A.M., Hoadley, A., Tanksale, A., 2015. Formaldehyde production via hydrogenation of carbon monoxide in the aqueous phase. Green Chemistry 17, 3500-3507. 10.1039/C5GC00599J

Bart, J.C.J., Sneeden, R.P.A., 1987. Copper-zinc oxide-alumina methanol catalysts revisited.

Catal. Today 2, 1–124.

Bashiri, N., Royaee, S.J., Sohrabi, M., 2018. The catalytic performance of different promoted iron catalysts on combined supports Al2O3 for carbon dioxide hydrogenation. Res. Chem. Intermed. 44, 217–229. https://doi.org/10.1007/s11164-017-3099-9

Benson, E.E., Kubiak, C.P., Sathrum, A.J., Smieja, J.M., 2009. Electrocatalytic and homogeneous approaches to conversion of CO2 to liquid fuels. Chem. Soc. Rev. 38, 89–99. https://doi.org/10.1039/b804323j

Bertau, M., Offermanns, H., Plass, L., Schmidt, F., Wernicke, H.-J., 2014. Methanol: the basic chemical and energy feedstock of the future. Springer.

Boden, T., Andres, R., Marland, G. Global, regional, and national fossil-fuel co2 emissions (1751-2014)(v. 2017). Environmental System Science Data Infrastructure for a Virtual Ecosystem …, 2017.

Bousquet, P., Peylin, P., Ciais, P., Le Quéré, C., Friedlingstein, P., Tans, P.P., 2000. Regional changes in carbon dioxide fluxes of land and oceans since 1980. Science 290, 1342-1346.

Cao, A., Liu, G., Wang, L., Liu, J., Yue, Y., Zhang, L., Liu, Y., 2016. Growing layered double hydroxides on CNTs and their catalytic performance for higher alcohol synthesis from syngas. J. Mater. Sci. 51, 5216–5231.

Cassia, R., Nocioni, M., Correa-Aragunde, N., Lamattina, L., 2018. Climate change and the impact of greenhouse gasses: CO2 and NO, friends and foes of plant oxidative stress. Front. Plant Sci. https://doi.org/10.3389/fpls.2018.00273

Chang, S., Na, W., Zhang, J., Lin, L., Gao, W., 2021. Effect of the Zn/Ce ratio in Cu/ZnO–CeO 2 catalysts on CO 2 hydrogenation for methanol synthesis. New J. Chem. 45, 22814–22823.

Chen, H., Goodarzi, F., Mu, Y., Chansai, S., Mielby, J.J., Mao, B., Sooknoi, T., Hardacre, C.,

Kegnæs, S., Fan, X., 2020a. Effect of metal dispersion and support structure of Ni/silicalite-1 catalysts on non-thermal plasma (NTP) activated CO2 hydrogenation. Appl. Catal. B Environ. 272, 119013. https://doi.org/10.1016/j.apcatb.2020.119013

Chen, H., Mu, Y., Shao, Y., Chansai, S., Xiang, H., Jiao, Y., Hardacre, C., Fan, X., 2020b. Nonthermal plasma (NTP) activated metal–organic frameworks (MOFs) catalyst for catalytic CO2 hydrogenation. AIChE J. 66, 1–11. https://doi.org/10.1002/aic.16853

Chen, H., Mu, Y., Shao, Y., Chansai, S., Xu, S., Stere, C.E., Xiang, H., Zhang, R., Jiao, Y., Hardacre, C., Fan, X., 2019. Coupling non-thermal plasma with Ni catalysts supported on BETA zeolite for catalytic CO2 methanation. Catal. Sci. Technol. 9, 4135–4145. https://doi.org/10.1039/c9cy00590k

Chen, H., Mu, Y., Xu, Shanshan, Xu, Shaojun, Hardacre, C., Fan, X., 2020c. Recent advances in non-thermal plasma (NTP) catalysis towards C1 chemistry. Chinese J. Chem. Eng. 28, 2010–2021. https://doi.org/10.1016/j.cjche.2020.05.027

Chen, X., Deng, D., Pan, X., Hu, Y., Bao, X., 2015. N-doped graphene as an electron donor of iron catalysts for CO hydrogenation to light olefins. Chemical Communications 51, 217–220. https://doi.org/10.1039/c4cc06600f

Chen, Y., Vise, A., Klein, W.E., Cetinbas, F.C., Myers, D.J., Smith, W.A., Smith, W.A., Smith, W.A., Deutsch, T.G., Neyerlin, K.C., 2020. A Robust, Scalable Platform for the Electrochemical Conversion of CO2to Formate: Identifying Pathways to Higher Energy Efficiencies. ACS Energy Lett. 5, 1825–1833. https://doi.org/10.1021/acsenergylett.0c00860

Chen, Z., Jiang, Q., An, H., Zhang, J., Hao, S., Li, X., Cai, L., Yu, W., You, K., Zhu, X., Li, C., 2022. Platinum Group Metal Catalyst (RuO x , PtO x , and IrO x)-Decorated Ceria-

Zirconia Solid Solution as High Active Oxygen Carriers for Solar Thermochemical CO_2 Splitting . ACS Catal. 7719–7736. https://doi.org/10.1021/acscatal.2c02044

Cheng, F., Small, A.A., Colosi, L.M., 2021. The levelized cost of negative CO2 emissions from thermochemical conversion of biomass coupled with carbon capture and storage. Energy Conversion and Management 237, 114115. https://doi.org/10.1016/j.enconman.2021.114115

Cheng, K., Zhou, W., Kang, J., He, S., Shi, S., Zhang, Q., Pan, Y., Wen, W., Wang, Y., 2017. Bifunctional Catalysts for One-Step Conversion of Syngas into Aromatics with Excellent Selectivity and Stability. Chem 3, 334–347. https://doi.org/10.1016/j.chempr.2017.05.007

Choi, Y., Liu, P., 2009. Mechanism of Ethanol Synthesis from Syngas on Rh(111). J. Am. Chem. Soc. 131, 13054–13061. https://doi.org/10.1021/ja903013x

Cooper, G., McCaherty, J., Huschitt, E., Schwarck, R., Wilson, C., 2021. Ethanol industry outlook. Renew Fuels Assoc 2021, 1–40.

Crake, A., Christoforidis, K. C., Kafizas, A., Zafeiratos, S., Petit, C., 2017. CO2 capture and photocatalytic reduction using bifunctional TiO2/MOF nanocomposites under UV–vis irradiation. Appl. Catal. B. 210, 131-140. https://doi.org/10.1016/j.apcatb.2017.03.039

Crake, A., Christoforidis, K.C., Godin, R., Moss, B., Kafizas, A., Zafeiratos, S., Durrant, J.R., Petit, C., 2019. Titanium dioxide/carbon nitride nanosheet nanocomposites for gas phase CO2 photoreduction under UV-visible irradiation. Appl Catal B 242, 369–378. https://doi.org/10.1016/j.apcatb.2018.10.023

Dang, S., Li, S., Yang, C., Chen, X., Li, X., Zhong, L., Gao, P., Sun, Y., 2019. Selective Transformation of CO2 and H2 into Lower Olefins over In2O3-ZnZrOx/SAPO-34 Bifunctional Catalysts. ChemSusChem 12, 3582–3591. https://doi.org/10.1002/cssc.201900958

Dang, S., Yang, H., Gao, P., Wang, H., Li, X., Wei, W., Sun, Y., 2019. A review of research progress on heterogeneous catalysts for methanol synthesis from carbon dioxide hydrogenation. Catalysis Today 330, 61-75. https://doi.org/10.1016/j.cattod.2018.04.021

Dey, S., Naidu, B.S., Govindaraj, A., Rao, C.N.R., 2015. Noteworthy performance of La1-xCaxMnO$_3$ perovskites in generating H_2 and CO by the thermochemical splitting of H_2O and CO_2. Physical Chemistry Chemical Physics 17, 122–125. https://doi.org/10.1039/c4cp04578e

Dias, Y.R., Perez-Lopez, O.W., 2021. CO2 conversion to methane using Ni/SiO2 catalysts promoted by Fe, Co and Zn. J. Environ. Chem. Eng. 9, 104629.

Díez-Ramírez, J., Valverde, J.L., Sánchez, P., Dorado, F., 2016. CO2 hydrogenation to methanol at atmospheric pressure: influence of the preparation method of Pd/ZnO catalysts. Catal. Letters 146, 373–382.

Dong, W., ZHONG, D., HAO, G., LI, J., Qiang, Z., 2021. ZnOHF nanorods for efficient electrocatalytic reduction of carbon dioxide to carbon monoxide. J. Fuel Chem. Technol. 49, 1379–1388.

Du, J., Chen, A., Hou, S., Guan, J., 2022. CNT modified by mesoporous carbon anchored by Ni nanoparticles for CO2 electrochemical reduction. Carbon Energy 1–11. https://doi.org/10.1002/cey2.223

Ejeromedoghene, O., Oderinde, O., Okoye, C.O., Oladipo, A., Alli, Y.A., 2022. Microporous metal-organic frameworks based on deep eutectic solvents for adsorption of toxic gases and volatile organic compounds: A review. Chem. Eng. J. Adv. https://doi.org/10.1016/j.ceja.2022.100361

Ekambaram, S., Iikubo, Y., Kudo, A., 2007. Combustion synthesis and photocatalytic properties

of transition metal-incorporated ZnO. J. Alloys Compd. 433, 237–240. https://doi.org/10.1016/j.jallcom.2006.06.045

Elavarasan, M., Yang, W., Velmurugan, S., Chen, J.N., Yang, T.C.K., Yokoi, T., 2022. Highly Efficient Photothermal Reduction of CO2 on Pd2 Cu Dispersed TiO2 Photocatalyst and Operando DRIFT Spectroscopic Analysis of Reactive Intermediates. Nanomaterials 12. https://doi.org/10.3390/nano12030332

Fall, B., Gaye, C., Niang, M., Adekunle, Y., Abdou, A., Diagne, K., Modou, D., 2022. Removal of Toxic Chromium Ions in Aqueous Medium Using a New Sorbent Based on rGO @ CNT @ Fe 2 O 3. Chem. Africa. https://doi.org/10.1007/s42250-022-00499-x

Fan, M.-S., Abdullah, A.Z., Bhatia, S., 2011. Hydrogen production from carbon dioxide reforming of methane over Ni–Co/MgO–ZrO2 catalyst: Process optimization. International Journal of Hydrogen Energy 36, 4875-4886. https://doi.org/10.1016/j.ijhydene.2011.01.064

Fan, W.K., Tahir, M., 2022. Recent developments in photothermal reactors with understanding on the role of light/heat for CO2 hydrogenation to fuels: A review. Chem. Eng. J. 427, 131617. https://doi.org/10.1016/j.cej.2021.131617

Feely, R.A., Sabine, C.L., Lee, K., Berelson, W., Kleypas, J., Fabry, V.J., Millero, F.J., 2004. Impact of anthropogenic CO2 on the CaCO3 system in the oceans. Science (80-.). 305, 362–366.

Feng, K., Wang, Y., Guo, M., Zhang, J., Li, Z., Deng, T., Zhang, Z., Yan, B., 2021. In-situ/operando techniques to identify active sites for thermochemical conversion of CO2 over heterogeneous catalysts. J. Energy Chem. 62, 153–171. https://doi.org/10.1016/j.jechem.2021.03.054

1511 Fiordaliso, E.M., Sharafutdinov, I., Carvalho, H.W.P., Grunwaldt, J.-D., Hansen, T.W.,
1512 Chorkendorff, I., Wagner, J.B., Damsgaard, C.D., 2015. Intermetallic GaPd2 nanoparticles
1513 on SiO2 for low-pressure CO2 hydrogenation to methanol: Catalytic performance and in
1514 situ characterization. ACS Catal. 5, 5827–5836.
1515 Fisher, J. B., Eisenberg, R., 2002. Electrocatalytic reduction of carbon dioxide by using
1516 macrocycles of nickel and cobalt. J. Am. Chem. Soc. 102, 7361–7363.
1517 https://doi.org/10.1021/ja00544a035
1518 Friedlingstein, P., 2015. Carbon cycle feedbacks and future climate change. Philosophical
1519 Transactions of the Royal Society A: Mathematical, Physical and Engineering Sciences
1520 373, 20140421. 10.1098/rsta.2014.0421
1521 Fu, Z.C., Moore, J.T., Liang, F., Fu, W.F., 2019. Highly efficient photocatalytic reduction of
1522 CO2 to CO using cobalt oxide-coated spherical mesoporous silica particles as catalysts.
1523 Chem. Commun. 55, 11523–11526. https://doi.org/10.1039/c9cc01861a
1524 Fukuhara, C., Hayakawa, K., Suzuki, Y., Kawasaki, W., Watanabe, R., 2017. A novel nickel-
1525 based structured catalyst for CO2 methanation: A honeycomb-type Ni/CeO2 catalyst to
1526 transform greenhouse gas into useful resources. Appl. Catal. A Gen. 532, 12–18.
1527 Fuqiang, W., Ziming, C., Jianyu, T., Jiaqi, Z., Yu, L., Linhua, L., 2017. Energy storage
1528 efficiency analyses of CO2 reforming of methane in metal foam solar thermochemical
1529 reactor. Appl. Therm. Eng. 111, 1091–1100.
1530 https://doi.org/10.1016/j.applthermaleng.2016.10.025
1531 Furler, P., Scheffe, J., Gorbar, M., Moes, L., Vogt, U., Steinfeld, A., 2012. Solar thermochemical
1532 CO_2 splitting utilizing a reticulated porous ceria redox system. Energy and Fuels 26, 7051–
1533 7059. https://doi.org/10.1021/ef3013757

Gaikwad, R., Reymond, H., Phongprueksathat, N., Von Rohr, P.R., Urakawa, A., 2020. From CO or CO_2?: space-resolved insights into high-pressure CO_2 hydrogenation to methanol over $Cu/ZnO/Al_2O_3$. Catal. Sci. Technol. 10, 2763–2768.

Gao, K., Liu, X., Jiang, Z., Zheng, H., Song, C., Wang, X., Tian, C., Dang, C., Sun, N., Xuan, Y., 2022. Direct solar thermochemical CO_2 splitting based on Ca- and Al- doped $SmMnO_3$ perovskites: Ultrahigh CO yield within small temperature swing. Renew. Energy 194, 482–494. https://doi.org/10.1016/j.renene.2022.05.105

Gao, P., Li, S., Bu, X., Dang, S., Liu, Z., Wang, H., Zhong, L., Qiu, M., Yang, C., Cai, J., Wei, W., Sun, Y., 2017. Direct conversion of CO_2 into liquid fuels with high selectivity over a bifunctional catalyst. Nat Chem 9, 1019–1024. https://doi.org/10.1038/nchem.2794

Halder, P.K., Paul, N., Beg, M.R.A., 2014. Assessment of biomass energy resources and related technologies practice in Bangladesh. Renewable and Sustainable Energy Reviews. https://doi.org/10.1016/j.rser.2014.07.071

Guene Lougou, B., Shuai, Y., Zhang, H., Ahouannou, C., Zhao, J., Kounouhewa, B.B., Tan, H., 2020. Thermochemical CO_2 reduction over $NiFe_2O_4$@alumina filled reactor heated by high-flux solar simulator. Energy 197, 1–15. https://doi.org/10.1016/j.energy.2020.117267

Haeussler, A., Abanades, S., Julbe, A., Jouannaux, J., Drobek, M., Ayral, A., Cartoixa, B., 2020. Remarkable performance of microstructured ceria foams for thermochemical splitting of H_2O and CO_2 in a novel high–temperature solar reactor. Chemical Engineering Research and Design 156, 311–323. https://doi.org/10.1016/j.cherd.2020.02.008

Handoko, A.D., Tang, J., 2013. Controllable proton and CO_2 photoreduction over Cu_2O with various morphologies. Int. J. Hydrogen Energy 38, 13017–13022. https://doi.org/10.1016/j.ijhydene.2013.03.128

He, J., Wang, X., Jin, S., Liu, Z.Q., Zhu, M., 2022. 2D metal-free heterostructure of covalent triazine framework/g-C_3N_4 for enhanced photocatalytic CO_2 reduction with high selectivity. Chinese J. Catal. 43, 1306–1315. https://doi.org/10.1016/S1872-2067(21)63936-0

Heim, L.E., Konnerth, H., Prechtl, M.H.G., 2017. Future perspectives for formaldehyde: pathways for reductive synthesis and energy storage. Green Chemistry 19, 2347-2355. 10.1039/C6GC03093A

Herzer, D., 2022. The impact on domestic CO_2 emissions of domestic government-funded clean energy R&D and of spillovers from foreign government-funded clean energy R&D. Energy Policy 168, 113126. https://doi.org/10.1016/j.enpol.2022.113126

Hsu, H.C., Shown, I., Wei, H.Y., Chang, Y.C., Du, H.Y., Lin, Y.G., Tseng, C.A., Wang, C.H., Chen, L.C., Lin, Y.C., Chen, K.H., 2013. Graphene oxide as a promising photocatalyst for CO2 to methanol conversion. Nanoscale 5, 262–268. https://doi.org/10.1039/c2nr31718d

Hu, B., Guild, C., Suib, S.L., 2013. Thermal, electrochemical, and photochemical conversion of CO2 to fuels and value-added products. J. CO2 Util. 1, 18–27.

Hu, F., Ye, R., Jin, C., Liu, D., Chen, X., Li, C., Lim, K.H., Song, G., Wang, T., Feng, G., 2022. Ni nanoparticles enclosed in highly mesoporous nanofibers with oxygen vacancies for efficient CO2 methanation. Appl. Catal. B Environ. 317, 121715.

Hu, Y., Wu, J., Han, Y., Xu, W., Zhang, L., Xia, X., Huang, C., Zhu, Y., Tian, M., Su, Y., Li, L., Hou, B., Lin, J., Liu, W., Wang, X., 2021. Intensified solar thermochemical CO_2 splitting over iron-based redox materials via perovskite-mediated dealloying-exsolution cycles. Chinese J. Catal. 42, 2049–2058. https://doi.org/10.1016/S1872-2067(21)63857-3

Huang, Q., Yu, J., Cao, S., Cui, C., Cheng, B., 2015. Efficient photocatalytic reduction of CO_2 by amine-functionalized g-C 3 N 4. Appl. Surf. Sci. 358, 350–355.

https://doi.org/10.1016/j.apsusc.2015.07.082

Huang, Y., Yan, C.F., Guo, C.Q., Lu, Z.X., Shi, Y., Wang, Z. Da, 2017. Synthesis of GO-modified Cu2O nanosphere and the photocatalytic mechanism of water splitting for hydrogen production. Int. J. Hydrogen Energy 42, 4007–4016. https://doi.org/10.1016/j.ijhydene.2016.10.157

Inoue, T., Fujishima, A., Konishi, S., Honda, K., 1979. Photoelectrocatalytic reduction of carbon dioxide in aqueous suspensions of semiconductor powders [3]. Nature. https://doi.org/10.1038/277637a0

Inoue, Y., Izumida, H., Sasaki, Y., Hashimoto, H., 1976. Catalytic fixation of carbon dioxide to formic acid by transition-metal complexes under mild conditions. Chem. Lett. 5, 863–864.

Jadhav, S.G., Vaidya, P.D., Bhanage, B.M., Joshi, J.B., 2014. Catalytic carbon dioxide hydrogenation to methanol: A review of recent studies. Chem. Eng. Res. Des. 92, 2557–2567.

Jansen, D., Gazzani, M., Manzolini, G., Dijk, E. van, Carbo, M., 2015. Pre-combustion CO2 capture. International Journal of Greenhouse Gas Control 40, 167–187. https://doi.org/10.1016/j.ijggc.2015.05.028

Jiang, B., Guene Lougou, B., Zhang, H., Geng, B., Wu, L., Shuai, Y., 2022. Preparation and solar thermochemical properties analysis of $NiFe_2O_4$@SiC/ @Si_3N_4 for high-performance CO_2-splitting. Appl Energy 328, 120057. https://doi.org/10.1016/j.apenergy.2022.120057

Jiao, F., Li, Jinjing, Pan, X., Xiao, J., Li, H., Ma, H., Wei, M., Pan, Y., Zhou, Z., Li, M., Miao, S., Li, Jian, Zhu, Y., Xiao, D., He, T., Yang, J., Qi, F., Fu, Q., Bao, X., 2016. Selective conversion of syngas to light olefins Downloaded from. Catalysis 351, 1065–1067.

Jiao, F., Pan, X., Gong, K., Chen, Y., Li, G., Bao, X., 2018. Shape-Selective Zeolites Promote

Ethylene Formation from Syngas via a Ketene Intermediate. Angewandte Chemie 130, 4782–4786. https://doi.org/10.1002/ange.20180139Jiang, Q., Chen, Z., Tong, J., Yang, M., Jiang, Z., Li, C., 2016. Catalytic Function of IrOx in the Two-Step Thermochemical CO2-Splitting Reaction at High Temperatures. ACS Catal. 6, 1172–1180. https://doi.org/10.1021/acscatal.5b017747

Kajaste, R., Hurme, M., Oinas, P., 2018. Methanol-Managing greenhouse gas emissions in the production chain by optimizing the resource base. AIMS Energy 6, 1074–1102.

Kamkeng, A.D.N., Wang, M., Hu, J., Du, W., Qian, F., 2021. Transformation technologies for CO2 utilisation: Current status, challenges and future prospects. Chemical Engineering Journal. https://doi.org/10.1016/j.cej.2020.128138

Keller, A.A., Adeleye, A.S., Conway, J.R., Garner, K.L., Zhao, L., Cherr, G.N., Hong, J., Gardea-Torresdey, J.L., Godwin, H.A., Hanna, S., Ji, Z., Kaweeteerawat, C., Lin, S., Lenihan, H.S., Miller, R.J., Nel, A.E., Peralta-Videa, J.R., Walker, S.L., Taylor, A.A., Torres-Duarte, C., Zink, J.I., Zuverza-Mena, N., 2017. Comparative environmental fate and toxicity of copper nanomaterials. NanoImpact 7, 28–https://doi.org/10.1016/j.impact.2017.05.003

Khalilzadeh, A., Shariati, A., 2019. Fe-N-TiO2/CPO-Cu-27 nanocomposite for superior CO2 photoreduction performance under visible light irradiation. Sol. Energy 186, 166–174. https://doi.org/10.1016/j.solener.2019.05.009

Kobl, K., Thomas, S., Zimmermann, Y., Parkhomenko, K., Roger, A.-C., 2016. Power-law kinetics of methanol synthesis from carbon dioxide and hydrogen on copper–zinc oxide catalysts with alumina or zirconia supports. Catalysis Today 270, 31-42. https://doi.org/10.1016/j.cattod.2015.11.020

Kothandaraman, J., Goeppert, A., Czaun, M., Olah, G.A., Prakash, G.K.S., 2016. Conversion of CO2 from air into methanol using a polyamine and a homogeneous ruthenium catalyst. J. Am. Chem. Soc. 138, 778–781.

Kovačič, Ž., Likozar, B., Huš, M., 2020. Photocatalytic CO2 Reduction: A Review of Ab Initio Mechanism, Kinetics, and Multiscale Modeling Simulations. ACS Catal. 10, 14984–15007. https://doi.org/10.1021/acscatal.0c02557

Koytsoumpa, E.I., Karellas, S., 2018. Equilibrium and kinetic aspects for catalytic methanation focusing on CO2 derived Substitute Natural Gas (SNG). Renew. Sustain. Energy Rev. 94, 536–550.

Kuang, Y., Shang, J., Zhu, T., 2020. Photoactivated Graphene Oxide to Enhance Photocatalytic Reduction of CO2. ACS Appl. Mater. Interfaces 12, 3580–3591. https://doi.org/10.1021/acsami.9b18899

Kubacka, A., Fernández-García, M., Colón, G., 2011. Advanced Nanoarchitectures for Solar Photocatalytic Applications. Chem. Rev. 112, 1555–1614. https://doi.org/10.1021/cr100454n

Kumar, A., Mohammed, A.A.A., Saad, M.A.H.S., Al-Marri, M.J., 2022. Effect of nickel on combustion synthesized copper/fumed-SiO2 catalyst for selective reduction of CO2 to CO. Int. J. Energy Res. 46, 441–451. https://doi.org/10.1002/er.6586

Kumaravel, V., Bartlett, J., Pillai, S.C., 2020. Photoelectrochemical conversion of carbon dioxide (CO2) into fuels and value-added products. ACS Energy Lett. 5, 486–519.

Kumari, G., Zhang, X., Devasia, D., Heo, J., Jain, P.K., 2018. Watching visible light-driven CO2 reduction on a plasmonic nanoparticle catalyst. ACS Nano 12, 8330–8340. https://doi.org/10.1021/acsnano.8b03617

L. Souza, M., H. B. Lima, F., 2021. Dibenzyldithiocarbamate-Functionalized Small Gold Nanoparticles as Selective Catalysts for the Electrochemical Reduction of CO2 to CO. ACS Catal. 11, 12208–12219. https://doi.org/10.1021/acscatal.1c00591

Lee, D.-K., Kim, D.-S., Kim, S.-W., 2001. Selective formation of formaldehyde from carbon dioxide and hydrogen over PtCu/SiO2. Applied Organometallic Chemistry 15, 148-150. https://doi.org/10.1002/1099-0739(200102)15:2<148::AID-AOC104>3.0.CO;2-N

Lervold, S., Lødeng, R., Yang, J., Skjelstad, J., Bingen, K., Venvik, H.J., 2021. Partial oxidation of methanol to formaldehyde in an annular reactor. Chemical Engineering Journal 423, 130141. https://doi.org/10.1016/j.cej.2021.130141

Li, B., Duan, Y., Luebke, D., Morreale, B., 2013. Advances in CO2 capture technology: A patent review. Appl Energy. https://doi.org/10.1016/j.apenergy.2012.09.009

Li, C.W., Ciston, J., Kanan, M.W., 2014. Electroreduction of carbon monoxide to liquid fuel on oxide-derived nanocrystalline copper. Nature 508, 504–507. https://doi.org/10.1038/nature13249

Li, J., Yu, T., Miao, D., Pan, X., Bao, X., 2019. Carbon dioxide hydrogenation to light olefins over ZnO-Y2O3 and SAPO-34 bifunctional catalysts. Catal Commun 129. https://doi.org/10.1016/j.catcom.2019.105711

Li, P., Jia, X., Zhang, Jinping, Li, J., Zhang, Jinqiang, Wang, L., Wang, J., Zhou, Q., Wei, W., Zhao, X., Wang, S., Sun, H., 2022. The roles of gold and silver nanoparticles on ZnIn2S4/silver (gold)/tetra(4-carboxyphenyl)porphyrin iron(III) chloride hybrids in carbon dioxide photoreduction. J. Colloid Interface Sci. https://doi.org/10.1016/J.JCIS.2022.08.097

Li, Q., Jiang, L., Lin, Q., Zhou, G., Zhan, F., Zheng, Q., Wei, X., 2002. Properties of hydrogen storage alloy Mg~ 2Ni produced by hydriding combustion synthesis. CHINESE J.

NONFERROUS Met. 12, 914–918.

Li, W., Seredych, M., Rodríguez-Castellón, E., Bandosz, T.J., 2016. Metal-free Nanoporous Carbon as a Catalyst for Electrochemical Reduction of CO2 to CO and CH4. ChemSusChem 9, 606–616. https://doi.org/10.1002/cssc.201501575

Li, X.X., Liu, J., Zhang, L., Dong, L.Z., Xin, Z.F., Li, S.L., Huang-Fu, X.Q., Huang, K., Lan, Y.Q., 2019. Hydrophobic Polyoxometalate-Based Metal-Organic Framework for Efficient CO2 Photoconversion. ACS Appl. Mater. Interfaces 11, 25790–25795. https://doi.org/10.1021/acsami.9b03861

Li, Y., Wang, W.N., Zhan, Z., Woo, M.H., Wu, C.Y., Biswas, P., 2010. Photocatalytic reduction of CO2 with H2O on mesoporous silica supported Cu/TiO2 catalysts. Appl. Catal. B Environ. 100, 386–392. https://doi.org/10.1016/j.apcatb.2010.08.015

Li, Y., Zeng, Z., Zhang, Y., Chen, Y., Wang, W., Xu, X., Du, M., Li, Z., Zou, Z., 2022. Deactivation and Stabilization Mechanism of Photothermal CO2Hydrogenation over Black TiO2. ACS Sustain. Chem. Eng. https://doi.org/10.1021/acssuschemeng.2c01081

Li, Y.-T., Zhou, L., Cui, W.-G., Li, Z.-F., Li, W., Hu, T.-L., 2022. Iron promoted MOF-derived carbon encapsulated NiFe alloy nanoparticles core-shell catalyst for CO2 methanation. J. CO2 Util. 62, 102093.

Li, Z., Feng, Y., Li, Y., Chen, X., Li, N., He, W., Liu, J., 2022. Fabrication of Bi/Sn bimetallic electrode for high-performance electrochemical reduction of carbon dioxide to formate. Chem. Eng. J. 428. https://doi.org/10.1016/j.cej.2021.130901

Li, Z., Liu, J., Shi, R., Waterhouse, G.I.N., Wen, X.D., Zhang, T., 2021. Fe-Based Catalysts for the Direct Photohydrogenation of CO2 to Value-Added Hydrocarbons. Adv. Energy Mater. 11, 1–9. https://doi.org/10.1002/aenm.202002783

Lingampalli, S.R., Ayyub, M.M., Rao, C.N.R., 2017. Recent Progress in the Photocatalytic Reduction of Carbon Dioxide. ACS Omega 2, 2740–2748. https://doi.org/10.1021/acsomega.7b00721

Liu, H., Gao, X., Shi, D., He, D., Meng, Q., Qi, P., Zhang, Q., 2022. Recent Progress on Photothermal Heterogeneous Catalysts for CO2 Conversion Reactions. Energy Technol. 10, 1–18. https://doi.org/10.1002/ente.202100804

Liu, K., Sakurai, M., Aono, M., 2010. ZnO-based ultraviolet photodetectors. Sensors 10, 8604–8634. https://doi.org/10.3390/s100908604

Liu, S., Tao, H., Zeng, L., Liu, Qi, Xu, Z., Liu, Qingxia, Luo, J.-L., 2017. Shape-dependent electrocatalytic reduction of CO2 to CO on triangular silver nanoplates. J. Am. Chem. Soc. 139, 2160–2163.

Liu, W., Zhai, P., Li, A., Wei, B., Si, K., Wei, Y., Wang, X., Zhu, G., Chen, Q., Gu, X., Zhang, R., Zhou, W., Gong, Y., 2022. Electrochemical CO2 reduction to ethylene by ultrathin CuO nanoplate arrays. Nat. Commun. 13. https://doi.org/10.1038/s41467-022-29428-9

Liu, X., Wang, M., Zhou, C., Zhou, W., Cheng, K., Kang, J., Zhang, Q., Deng, W., Wang, Y., 2017. Selective transformation of carbon dioxide into lower olefins with a bifunctional catalyst composed of ZnGa2O4 and SAPO-34. Chemical Communications 54, 140–143. https://doi.org/10.1039/c7cc08642c

Liu, Y., Chen, C., Valdez, J., Motta Meira, D., He, W., Wang, Y., Harnagea, C., Lu, Q., Guner, T., Wang, H., Liu, C.H., Zhang, Q., Huang, S., Yurtsever, A., Chaker, M., Ma, D., 2021. Phase-enabled metal-organic framework homojunction for highly selective CO2 photoreduction. Nat. Commun. 12, 1–13. https://doi.org/10.1038/s41467-021-21401-2

Liu, Y., Chen, J.F., Bao, J., Zhang, Y., 2015. Manganese-modified Fe3O4 microsphere catalyst

with effective active phase of forming light olefins from syngas. ACS Catal 5, 3905–3909. https://doi.org/10.1021/acscatal.5b00492

Lorentzou, S., Karagiannakis, G., Pagkoura, C., Zygogianni, A., Konstandopoulos, A.G., 2014. Thermochemical CO2 and CO2/H2O splitting over NiFe2O4 for solar fuels synthesis. Energy Procedia 49, 1999–2008. https://doi.org/10.1016/j.egypro.2014.03.212

Lou, D., Xu, A.B., Fang, Y., Cai, M., Lv, K., Zhang, D., Wang, X., Huang, Y., Li, C., He, L., 2021. Cobalt-Sputtered Anodic Aluminum Oxide Membrane for Efficient Photothermal CO2 Hydrogenation. ChemNanoMat 7, 1008–1012. https://doi.org/10.1002/cnma.202100162

Lou, Y., Zhu, W., Wang, L., Yao, T., Wang, S., Yang, Bo, Yang, Bing, Zhu, Y., Liu, X., 2021. CeO2 supported Pd dimers boosting CO2 hydrogenation to ethanol. Appl. Catal. B Environ. 291, 120122.

Loutzenhiser, P.G., Steinfeld, A., 2011. Solar syngas production from CO2 and H2O in a two-step thermochemical cycle via Zn/ZnO redox reactions: Thermodynamic cycle analysis. Int J Hydrogen Energy 36, 12141–12147. https://doi.org/10.1016/j.ijhydene.2011.06.128

Low, J., Cheng, B., Yu, J., 2017. Surface modification and enhanced photocatalytic CO 2 reduction performance of TiO 2 : a review. Appl Surf Sci 392, 658–686. https://doi.org/10.1016/j.apsusc.2016.09.093

Lu, B., Quan, F., Sun, Z., Jia, F., Zhang, L., 2019. Photothermal reverse-water-gas-shift over Au/CeO2 with high yield and selectivity in CO2 conversion. Catal. Commun. 129, 105724. https://doi.org/10.1016/j.catcom.2019.105724

Lu, H., Yang, X., Gao, G., Wang, J., Han, C., Liang, X., Li, C., Li, Y., Zhang, W., Chen, X., 2016. Metal (Fe, Co, Ce or La) doped nickel catalyst supported on ZrO2 modified

mesoporous clays for CO and CO2 methanation. Fuel 183, 335–344.

Lu, J., Yang, L., Xu, B., Wu, Q., Zhang, D., Yuan, S., Zhai, Y., Wang, X., Fan, Y., Hu, Z., 2014. Promotion effects of nitrogen doping into carbon nanotubes on supported iron fischer-tropsch catalysts for lower olefins. ACS Catal 4, 613–621. https://doi.org/10.1021/cs400931z

Lu, P., Gao, D., He, H., Wang, Q., Liu, Z., Dipazir, S., Yuan, M., Zu, W., Zhang, G., 2019. Facile synthesis of a bismuth nanostructure with enhanced selectivity for electrochemical conversion of CO2 to formate. Nanoscale 11, 7805–7812. https://doi.org/10.1039/c9nr01094g

Lu, X., Leung, D.Y.C., Wang, H., Leung, M.K.H., Xuan, J., 2014. Electrochemical reduction of carbon dioxide to formic acid. ChemElectroChem 1, 836–849.

Luo, Z., Wang, X., Wen, H., Pei, A., 2022. Hydrogen production from offshore wind power in South China. International Journal of Hydrogen Energy 47, 24558-24568. https://doi.org/10.1016/j.ijhydene.2022.03.162

Ma, M., Djanashvili, K., Smith, W.A., 2016a. Controllable Hydrocarbon Formation from the Electrochemical Reduction of CO2 over Cu Nanowire Arrays. Angew. Chemie - Int. Ed. 55, 6680–6684. https://doi.org/10.1002/anie.201601282

Ma, M., Trześniewski, B.J., Xie, J., Smith, W.A., 2016b. Selective and efficient reduction of carbon dioxide to carbon monoxide on oxide-derived nanostructured silver electrocatalysts. Angew. Chemie 128, 9900–9904.

Madadi Avargani, V., Zendehboudi, S., Cata Saady, N.M., Dusseault, M.B., 2022. A comprehensive review on hydrogen production and utilization in North America: Prospects

and challenges. Energy Conversion and Management 269, 115927. https://doi.org/10.1016/j.enconman.2022.115927

Maeda, K., 2019. Metal-Complex/Semiconductor Hybrid Photocatalysts and Photoelectrodes for CO2 Reduction Driven by Visible Light. Adv. Mater. 31. https://doi.org/10.1002/adma.201808205

Mehta, P., Barboun, P., Go, D.B., Hicks, J.C., Schneider, W.F., 2019. Catalysis Enabled by Plasma Activation of Strong Chemical Bonds: A Review. ACS Energy Lett. 4, 1115–1133. https://doi.org/10.1021/acsenergylett.9b00263

Miao, Z., Hu, P., Nie, C., Xie, H., Fu, W., Li, Q., 2019. ZrO2 nanoparticles anchored on nitrogen-doped carbon nanosheets as efficient catalyst for electrochemical CO2 reduction. J. Energy Chem. 38, 114–118. https://doi.org/10.1016/j.jechem.2019.01.010

Mo, Z., Zhu, X., Jiang, Z., Song, Y., Liu, D., Li, Hongping, Yang, X., She, Y., Lei, Y., Yuan, S., Li, Huaming, Song, L., Yan, Q., Xu, H., 2019. Porous nitrogen-rich g-C3N4 nanotubes for efficient photocatalytic CO2 reduction. Appl. Catal. B Environ. 256, 117854. https://doi.org/10.1016/j.apcatb.2019.117854

Mondal, M.K., Balsora, H.K., Varshney, P., 2012. Progress and trends in CO2 capture/separation technologies: A review. Energy 46, 431–441. https://doi.org/10.1016/j.energy.2012.08.006

Moret, S., Dyson, P.J., Laurenczy, G., 2014. Direct synthesis of formic acid from carbon dioxide by hydrogenation in acidic media. Nat. Commun. 5, 1–7.

Mou, S., Wu, T., Xie, J., Zhang, Y., Ji, L., Huang, H., Wang, T., Luo, Y., Xiong, X., Tang, B., Sun, X., 2019. Boron Phosphide Nanoparticles: A Nonmetal Catalyst for High-Selectivity Electrochemical Reduction of CO2 to CH3OH. Adv. Mater. 31. https://doi.org/10.1002/adma.201903499

Mubarak, S., Dhamodharan, D., Byun, H.-S., Pattanayak, D.K., Arya, S.B., 2022. Efficient photoelectrocatalytic conversion of CO2 to formic acid using Ag-TiO2 nanoparticles formed on the surface of nanoporous structured Ti foil. J. Ind. Eng. Chem.

Mustafa, A., Lougou, B.G., Shuai, Y., Wang, Z., Tan, H., 2020. Current technology development for CO2 utilization into solar fuels and chemicals: A review. Journal of Energy Chemistry. https://doi.org/10.1016/j.jechem.2020.01.023

Mutz, B., Carvalho, H.W.P., Mangold, S., Kleist, W., Grunwaldt, J.D., 2015. Methanation of CO2: Structural response of a Ni-based catalyst under fluctuating reaction conditions unraveled by operando spectroscopy. J. Catal. 327, 48–53. https://doi.org/10.1016/j.jcat.2015.04.006

Nair, M.M., Abanades, S., 2018. Experimental screening of perovskite oxides as efficient redox materials for solar thermochemical CO 2 conversion. Sustain. Energy Fuels 2, 843–854. https://doi.org/10.1039/c7se00516d

Nandal, N., Prajapati, P.K., Abraham, B.M., Jain, S.L., 2022. CO2 to ethanol: A selective photoelectrochemical conversion using a ternary composite consisting of graphene oxide/copper oxide and a copper-based metal-organic framework. Electrochim. Acta 404, 139612.

Navarro-Jaén, S., Virginie, M., Bonin, J., Robert, M., Wojcieszak, R., Khodakov, A.Y., 2021. Highlights and challenges in the selective reduction of carbon dioxide to methanol. Nat. Rev. Chem. 5, 564–579.

Nguyen, C.T.K., Quang Tran, N., Seo, S., Hwang, H., Oh, S., Yu, J., Lee, J., Anh Le, T., Hwang, J., Kim, M., Lee, H., 2020. Highly efficient nanostructured metal-decorated hybrid semiconductors for solar conversion of CO2 with almost complete CO selectivity. Mater.

Today 35, 25–33. https://doi.org/10.1016/j.mattod.2019.11.005

Nguyen, T.D., Van Tran, T., Singh, S., Phuong, P.T.T., Bach, L.G., Nanda, S., Vo, D.-V.N. Conversion of Carbon Dioxide into Formaldehyde. In: Inamuddin, Asiri AM, Lichtfouse E, editors. Conversion of Carbon Dioxide into Hydrocarbons Vol. 2 Technology. Springer International Publishing, Cham, 2020, pp. 159-183.

Nielsen, D.U., Hu, X.M., Daasbjerg, K., Skrydstrup, T., 2018. Chemically and electrochemically catalysed conversion of CO2 to CO with follow-up utilization to value-added chemicals. Nat. Catal. https://doi.org/10.1038/s41929-018-0051-3

Nieminen, H., Laari, A., Koiranen, T., 2019. CO2 hydrogenation to methanol by a liquid-phase process with alcoholic solvents: a techno-economic analysis. Processes 7, 405.

Nizio, M., Benrabbah, R., Krzak, M., Debek, R., Motak, M., Cavadias, S., Gálvez, M.E., Da Costa, P., 2016. Low temperature hybrid plasma-catalytic methanation over Ni-Ce-Zr hydrotalcite-derived catalysts. Catal. Commun. 83, 14–17. https://doi.org/10.1016/j.catcom.2016.04.023

Numpilai, T., Witoon, T., Chanlek, N., Limphirat, W., Bonura, G., Chareonpanich, M., Limtrakul, J., 2017. Structure–activity relationships of Fe-Co/K-Al2O3 catalysts calcined at different temperatures for CO2 hydrogenation to light olefins. Appl Catal A Gen 547, 219–229. https://doi.org/10.1016/j.apcata.2017.09.006

Offermanns, H., Plass, L., Bertau, M., 2014. From Raw Materials to Methanol, Chemicals and Fuels. Methanol Basic Chem. Energy Feed. Futur. Springer Heidelberg/Berlin, Ger. 1–7.

Ola, O., Maroto-Valer, M.M., 2015. Transition metal oxide based TiO2 nanoparticles for visible light induced CO2 photoreduction. Appl. Catal. A Gen. 502, 114–121. https://doi.org/10.1016/j.apcata.2015.06.007

Oladoye, P.O., Adegboyega, S.A., Giwa, A.-R.A., 2021. Remediation potentials of composite metal-organic frameworks (MOFs) for dyes as water contaminants: A comprehensive review of recent literatures. Environ Nanotechnol Monit Manag 16, 100568. https://doi.org/10.1016/j.enmm.2021.100568

Olah, G.A., 2013. Towards oil independence through renewable methanol chemistry. Angew. Chemie Int. Ed. 52, 104–107.

Omoregbe, O., Mustapha, A.N., Steinberger-Wilckens, R., El-Kharouf, A., Onyeaka, H., 2020. Carbon capture technologies for climate change mitigation: A bibliometric analysis of the scientific discourse during 1998–2018. Energy Reports 6, 1200–1212. https://doi.org/10.1016/j.egyr.2020.05.003

Otgonbayar, Z., Youn Cho, K., Oh, W.-C., 2020. Novel Micro and Nanostructure of a AgCuInS2–Graphene–TiO2 Ternary Composite for Photocatalytic CO2 Reduction for Methanol Fuel. ACS Omega 5, 26389–26401. https://doi.org/10.1021/acsomega.0c02498

Pang, J., Zheng, M., Zhang, T., 2019. Synthesis of ethanol and its catalytic conversion, in: Advances in Catalysis. Elsevier, pp. 89–191.

Parastaev, A., Hoeben, W.F.L.M., van Heesch, B.E.J.M., Kosinov, N., Hensen, E.J.M., 2018. Temperature-programmed plasma surface reaction: An approach to determine plasma-catalytic performance. Appl. Catal. B Environ. 239, 168–177. https://doi.org/10.1016/j.apcatb.2018.08.011

Paris, C., Karelovic, A., Manrique, R., Le Bras, S., Devred, F., Vykoukal, V., Styskalik, A., Eloy, P., Debecker, D.P., 2020. CO2 Hydrogenation to Methanol with Ga- and Zn-Doped Mesoporous Cu/SiO2 Catalysts Prepared by the Aerosol-Assisted Sol-Gel Process**. ChemSusChem 13, 6409–6417. https://doi.org/10.1002/cssc.202001951

Park, H.-a., Choi, J.H., Choi, K.M., Lee, D.K., Kang, J.K., 2012. Highly porous gallium oxide with a high CO2 affinity for the photocatalytic conversion of carbon dioxide into methane. Journal of Materials Chemistry 22, 5304-5307. 10.1039/C2JM30337J

Pawelec, B., Guil-López, R., Mota, N., Fierro, J.L.G., Navarro Yerga, R.M., 2021. Catalysts for the conversion of co2 to low molecular weight olefins—a review. Materials. https://doi.org/10.3390/ma14226952

Peiseler, L., Cabrera Serrenho, A., 2022. How can current German and EU policies be improved to enhance the reduction of CO2 emissions of road transport? Revising policies on electric vehicles informed by stakeholder and technical assessments. Energy Policy 168, 113124. https://doi.org/10.1016/j.enpol.2022.113124

Pérez-Fortes, M., Schöneberger, J.C., Boulamanti, A., Harrison, G., Tzimas, E., 2016. Formic acid synthesis using CO2 as raw material: Techno-economic and environmental evaluation and market potential. Int. J. Hydrogen Energy 41, 16444–16462.

Petrovic, B., Gorbounov, M., Masoudi Soltani, S., 2021. Influence of surface modification on selective CO2 adsorption: A technical review on mechanisms and methods. Microporous Mesoporous Mater. https://doi.org/10.1016/j.micromeso.2020.110751

Porosoff, M.D., Yan, B., Chen, J.G., 2016. Catalytic reduction of CO 2 by H 2 for synthesis of CO, methanol and hydrocarbons: challenges and opportunities. Energy Environ. Sci. 9, 62–73.

Prockop, L.D., Chichkova, R.I., 2007. Carbon monoxide intoxication: An updated review. Journal of the Neurological Sciences 262, 122-130. https://doi.org/10.1016/j.jns.2007.06.037

Purwanto, Deshpande, R.M., Chaudhari, R.V., Delmas, H., 1996. Solubility of Hydrogen, Carbon Monoxide, and 1-Octene in Various Solvents and Solvent Mixtures. Journal of Chemical & Engineering Data 41, 1414-1417. 10.1021/je960024e

Qi, Z., Biener, J., Biener, M., 2019. Surface oxide-derived nanoporous gold catalysts for electrochemical CO2-to-CO reduction. ACS Appl. Energy Mater. 2, 7717–7721.

Qi, Z., Biener, M.M., Kashi, A.R., Hunegnaw, S., Leung, A., Ma, S., Huo, Z., Kuhl, K.P., Biener, J., 2021. Electrochemical CO2 to CO reduction at high current densities using a nanoporous gold catalyst. Mater. Res. Lett. 9, 99–104.

Qiao, J., Liu, Y., Hong, F., Zhang, J., 2014. A review of catalysts for the electroreduction of carbon dioxide to produce low-carbon fuels. Chem. Soc. Rev. https://doi.org/10.1039/c3cs60323g

Rahmani, S., Meshkani, F., Rezaei, M., 2019. Preparation of Ni-M (M: La, Co, Ce, and Fe) catalysts supported on mesoporous nanocrystalline γ-Al2O3 for CO2 methanation. Environ. Prog. Sustain. Energy 38, 118–126. https://doi.org/10.1002/ep.13040

Ramírez-Valencia, L.D., Bailón-García, E., Carrasco-Marín, F., Pérez-Cadenas, A.F., 2021. From CO2 to value-added products: a review about carbon-based materials for electro-chemical CO2 conversion, Catalysts. MDPI.

Rauch, M., Strater, Z., Parkin, G., 2019. Selective Conversion of Carbon Dioxide to Formaldehyde via a Bis(silyl)acetal: Incorporation of Isotopically Labeled C1 Moieties Derived from Carbon Dioxide into Organic Molecules. Journal of the American Chemical Society 141, 17754-17762. 10.1021/jacs.9b08342

Ren, D., Tee Wong, N., Denny Handoko, A., Huang, Y., Siang Yeo, B., 2015. Mechanistic Insights into the Enhanced Activity and Stability of Agglomerated Cu Nanocrystals for the

Electrochemical Reduction of Carbon Dioxide to n-Propanol. J. Phys. Chem. Lett. 7, 20–24. https://doi.org/10.1021/acs.jpclett.5b02554

Rezaul Karim, K.M., Ong, H.R., Abdullah, H., Yousuf, A., Cheng, C.K., Rahman Khan, M.M., 2018. Photoelectrochemical reduction of carbon dioxide to methanol on p-type CuFe2O4 under visible light irradiation. Int. J. Hydrogen Energy 43, 18185–18193. https://doi.org/10.1016/j.ijhydene.2018.07.174

Rose, J.J., Wang, L., Xu, Q., McTiernan, C.F., Shiva, S., Tejero, J., Gladwin, M.T., 2017. Carbon Monoxide Poisoning: Pathogenesis, Management, and Future Directions of Therapy. Am J Respir Crit Care Med 195, 596-606. 10.1164/rccm.201606-1275CI

Rosen, B.A., Hod, I., 2018. Tunable Molecular-Scale Materials for Catalyzing the Low-Overpotential Electrochemical Conversion of CO2. Adv. Mater. 30, 1–7. https://doi.org/10.1002/adma.201706238

Roy, S., Cherevotan, A., Peter, S.C., 2018. Thermochemical CO2 Hydrogenation to Single Carbon Products: Scientific and Technological Challenges. ACS Energy Lett. 3, 1938–1966. https://doi.org/10.1021/acsenergylett.8b00740

Sabatier, P., 1902. New synthesis of methane. Comptes Rendus 134, 514–516.

Schimel, D., Stephens, B.B., Fisher, J.B., 2015. Effect of increasing CO2 on the terrestrial carbon cycle. Proceedings of the National Academy of Sciences 112, 436-441. 10.1073/pnas.1407302112

Scibioh, M.A., Viswanathan, B., 2004. Electrochemical reduction of carbon dioxide: a status report, in: Proc Indian Natn Sci Acad. pp. 1–56.

Sha, F., Han, Z., Tang, S., Wang, J., Li, C., 2020. Hydrogenation of Carbon Dioxide to Methanol over Non−Cu-based Heterogeneous Catalysts. ChemSusChem.

https://doi.org/10.1002/cssc.202002054

Sharma, D., Sharma, R., Chand, D., Chaudhary, A., 2022. Nanocatalysts as potential candidates in transforming CO2 into valuable fuels and chemicals: A review. Environmental Nanotechnology, Monitoring & Management 18, 100671. https://doi.org/10.1016/j.enmm.2022.100671

Shen, H., Peppel, T., Strunk, J., Sun, Z., 2020. Photocatalytic Reduction of CO 2 by Metal-Free-Based Materials: Recent Advances and Future Perspective. https://doi.org/10.1002/solr.201900546

Shen, Q., Chen, Z., Huang, X., Liu, M., Zhao, G., 2015. High-Yield and Selective Photoelectrocatalytic Reduction of CO2 to Formate by Metallic Copper Decorated Co3O4 Nanotube Arrays. Environ. Sci. & Technol. 49, 5828–5835. https://doi.org/10.1021/acs.est.5b00066

Shen, X., Li, C., Wu, Z., Tang, R., Shen, J., Chu, M., Xu, A., Zhang, B., He, L., Zhang, X., 2022. Rationally designed nanoarray catalysts for boosted photothermal CO2 hydrogenation. Nanoscale 14, 11568–11574. https://doi.org/10.1039/d2nr02680e

Shi, H., Tian, C., Liu, X., Sun, N., Song, C., Zheng, H., Gao, K., Wang, X., Jiang, Z., Xuan, Y., Ding, Y., 2023. Ni-phyllosilicate nanotubes coated by CeO2 for ultra-efficiency of 36.9% and near-limit CO2 conversion in solar-driven conversion of CO2-to-fuel. Chemical Engineering Journal 454, 140063. https://doi.org/10.1016/j.cej.2022.140063

Shi, L., Yang, L., Zhou, W., Liu, Y., Yin, L., Hai, X., Song, H., Ye, J., 2018. Photoassisted Construction of Holey Defective g-C3N4 Photocatalysts for Efficient Visible-Light-Driven H2O2 Production. Small 14. https://doi.org/10.1002/smll.201703142

Shuai, Y., Zhang, H., Guene Lougou, B., Jiang, B., Mustafa, A., Wang, C.H., Wang, F., Zhao, J.,

2021. Solar-driven thermochemical redox cycles of ZrO2 supported NiFe2O4 for CO2 reduction into chemical energy. Energy 223, 120073. https://doi.org/10.1016/j.energy.2021.120073

Solomon, S., Daniel, J.S., Sanford, T.J., Murphy, D.M., Plattner, G.K., Knutti, R., Friedlingstein, P., 2010. Persistence of climate changes due to a range of greenhouse gases. Proc. Natl. Acad. Sci. U. S. A. 107, 18354–18359. https://doi.org/10.1073/pnas.1006282107

Solomon, S., Plattner, G.K., Knutti, R., Friedlingstein, P., 2009. Irreversible climate change due to carbon dioxide emissions. Proc. Natl. Acad. Sci. U. S. A. 106, 1704–1709. https://doi.org/10.1073/pnas.0812721106

Song, C., Liu, X., Xu, M., Masi, D., Wang, Y., Deng, Y., Zhang, M., Qin, X., Feng, K., Yan, J., Leng, J., Wang, Z., Xu, Y., Yan, B., Jin, S., Xu, D., Yin, Z., Xiao, D., Ma, D., 2020. Photothermal Conversion of CO2with Tunable Selectivity Using Fe-Based Catalysts: From Oxide to Carbide. ACS Catal. 10, 10364–10374. https://doi.org/10.1021/acscatal.0c02244

Song, C., Wang, J., Wang, X., AlQahtani, M.S., Knecht, S.D., Bilen, S.G., Chu, W., 2022. Synergetic Effect of Nonthermal Plasma and Supported Cobalt Catalyst in Plasma-Enhanced Co2 Hydrogenation. SSRN Electron. J. 138661. https://doi.org/10.2139/ssrn.4070252

Stolar, T., Prašnikar, A., Martinez, V., Karadeniz, B., Bjelić, A., Mali, G., Friščić, T., Likozar, B., Užarević, K., 2021. Scalable mechanochemical amorphization of bimetallic Cu-Zn MOF-74 catalyst for selective CO2reduction reaction to methanol. ACS Appl. Mater. Interfaces 13, 3070–3077. https://doi.org/10.1021/acsami.0c21265

Studt, F., Behrens, M., Kunkes, E.L., Thomas, N., Zander, S., Tarasov, A., Schumann, J., Frei, E., Varley, J.B., Abild-Pedersen, F., Nørskov, J.K., Schlögl, R., 2015. The Mechanism of

CO and CO2 Hydrogenation to Methanol over Cu-Based Catalysts. ChemCatChem 7, 1105-1111. https://doi.org/10.1002/cctc.201500123

Subasi, N.T., 2020. Formaldehyde Advantages and Disadvantages: Usage Areas and Harmful Effects on Human Beings. Biochemical Toxicology-Heavy Metals. DOI: 10.5772/intechopen.89299

Sultan, S., Lee, H., Park, S., Kim, M.M., Yoon, A., Choi, H., Kong, T.H., Koe, Y.J., Oh, H.S., Lee, Z., Kim, H., Kim, W., Kwon, Y., 2022. Interface rich CuO/Al2CuO4 surface for selective ethylene production from electrochemical CO2 conversion. Energy Environ. Sci. https://doi.org/10.1039/d1ee03861c

Sümbelli, Y., Biçen Ünlüer, Ö., Ersöz, A., Say, R., 2019. Synergistic effect of binanoenzyme and cryogel column on the production of formic acid from carbondioxide. Journal of Industrial and Engineering Chemistry 76, 251-257. https://doi.org/10.1016/j.jiec.2019.03.049

Tada, S., Shimizu, T., Kameyama, H., Haneda, T., Kikuchi, R., 2012. Ni/CeO2 catalysts with high CO2 methanation activity and high CH4 selectivity at low temperatures. Int. J. Hydrogen Energy 37, 5527–5531. https://doi.org/10.1016/j.ijhydene.2011.12.122

Takalkar, G., Bhosale, R.R., 2019. Solar thermocatalytic conversion of CO2 using PrxSr(1−x)MnO3−Δ perovskites. FuelFuel 254, 115624. https://doi.org/10.1016/j.fuel.2019.115624

Takalkar, G.D., Bhosale, R.R., 2019. Application of cobalt incorporated Iron oxide catalytic nanoparticles for thermochemical conversion of CO2. Appl. Surf. Sci. 495, 143508. https://doi.org/10.1016/j.apsusc.2019.07.250

Takano, A., Tagawa, T., Goto, S., 1994. Carbon dioxide reforming of methane on supported nickel catalysts. Journal of chemical engineering of Japan 27, 727-731.

Teng, L., Xuan, Y., Da, Y., Sun, C., Liu, X., Ding, Y., 2022. Direct solar-driven reduction of greenhouse gases into hydrocarbon fuels incorporating thermochemical energy storage via modified calcium looping. Chem. Eng. J. 440, 135955. https://doi.org/10.1016/j.cej.2022.135955

Usanmaz, S.E., Akarsu, E.S., Vural, N., 2002. Neurotoxic effects of acute and subacute formaldehyde exposures in mice. Environmental Toxicology and Pharmacology 11, 93-100. https://doi.org/10.1016/S1382-6689(01)00109-0

Visconti, C.G., Martinelli, M., Falbo, L., Infantes-Molina, A., Lietti, L., Forzatti, P., Iaquaniello, G., Palo, E., Picutti, B., Brignoli, F., 2017. CO2 hydrogenation to lower olefins on a high surface area K-promoted bulk Fe-catalyst. Appl Catal B 200, 530–542. https://doi.org/10.1016/j.apcatb.2016.07.047

Wang, L., Ma, T., Dai, S., Ren, T., Chang, Z., Fu, M., Li, X., Li, Y., 2020. Solar thermochemical CO2 splitting with doped perovskite LaCo0.7Zr0.3O3: Thermodynamic performance and solar-to-fuel efficiency. RSC Adv 10, 35740–35752. https://doi.org/10.1039/d0ra05709f

Wang, D., Bi, Q., Yin, G., Zhao, W., Huang, F., Xie, X., Jiang, M., 2016. Direct synthesis of ethanol via CO 2 hydrogenation using supported gold catalysts. Chem. Commun. 52, 14226–14229.

Wang, D., Huang, R., Liu, W., Sun, D., Li, Z., 2014. Fe-based MOFs for photocatalytic CO2 reduction: Role of coordination unsaturated sites and dual excitation pathways. ACS Catal. 4, 4254–4260. https://doi.org/10.1021/cs501169t

Wang, F., Wei, M., Evans, D.G., Duan, X., 2016. CeO 2-based heterogeneous catalysts toward catalytic conversion of CO 2. J. Mater. Chem. A 4, 5773–5783.

Wang, J., Yu, Y., Cui, J., Li, X., Zhang, Y., Wang, C., Yu, X., Ye, J., 2022. Defective g-

C3N4/covalent organic framework van der Waals heterojunction toward highly efficient S-scheme CO2 photoreduction. Appl. Catal. B Environ. 301, 120814. https://doi.org/10.1016/j.apcatb.2021.120814

Wang, S., Lu, G.Q., Millar, G.J., 1996. Carbon Dioxide Reforming of Methane To Produce Synthesis Gas over Metal-Supported Catalysts: State of the Art. Energy & Fuels 10, 896-904. 10.1021/ef950227t

Wang, W., Ciais, P., Nemani, R.R., Canadell, J.G., Piao, S., Sitch, S., White, M.A., Hashimoto, H., Milesi, C., Myneni, R.B., 2013. Variations in atmospheric CO2 growth rates coupled with tropical temperature. Proceedings of the National Academy of Sciences 110, 13061-13066. 10.1073/pnas.1219683110

Wang, X., Maeda, K., Thomas, A., Takanabe, K., Xin, G., Carlsson, J.M., Domen, K., Antonietti, M., 2009. A metal-free polymeric photocatalyst for hydrogen production from water under visible light. Nat. Mater. 8, 76–80. https://doi.org/10.1038/nmat2317

Wang, X.X., Duan, Y.H., Zhang, J.F., Tan, Y.S., 2022. Catalytic conversion of CO2 into high value-added hydrocarbons over tandem catalyst. Ranliao Huaxue Xuebao/Journal of Fuel Chemistry and Technology. https://doi.org/10.1016/S1872-5813(21)60181-0

Wang, Y., Liu, X., Han, X., Godin, R., Chen, J., Zhou, W., Jiang, C., Thompson, J.F., Mustafa, K.B., Shevlin, S.A., Durrant, J.R., Guo, Z., Tang, J., 2020. Unique hole-accepting carbon-dots promoting selective carbon dioxide reduction nearly 100% to methanol by pure water. Nat. Commun. 11, 1–9. https://doi.org/10.1038/s41467-020-16227-3

Wang, Y., Wang, K., Zhang, B., Peng, X., Gao, X., Yang, G., Hu, H., Wu, M., Tsubaki, N., 2021. Direct conversion of CO2 to ethanol boosted by intimacy-sensitive multifunctional catalysts. ACS Catal. 11, 11742–11753.

Wang, Y., Xie, Y., Deng, M., Liu, T., Yang, H., 2021. Incorporation of Polyoxometalate in Sulfonic Acid-modified MIL-101-Cr for Enhanced CO2 Photoreduction Activity. Eur. J. Inorg. Chem. 2021, 681–687. https://doi.org/10.1002/ejic.20200101

Wang, Y., Zhang, X., Chang, K., Zhao, Z., Huang, J., Kuang, Q., 2022. MOF Encapsulated AuPt Bimetallic Nanoparticles for Improved Plasmonic-induced Photothermal Catalysis of CO2 Hydrogenation. Chem. - A Eur. J. 28. https://doi.org/10.1002/chem.202104514

Wang, Z., Yuan, Q., Shan, J., Jiang, Z., Xu, P., Hu, Y., Zhou, J., Wu, L., Niu, Z., Sun, J., Cheng, T., A. Goddard III, W., 2020. Highly Selective Electrocatalytic Reduction of CO2 into Methane on Cu–Bi Nanoalloys. J. Phys. Chem. Lett. 11, 7261–7266. https://doi.org/10.1021/acs.jpclett.0c01261

Wang, Zhou jun, Song, H., Pang, H., Ning, Y., Dao, T.D., Wang, Zhuan, Chen, H., Weng, Y., Fu, Q., Nagao, T., Fang, Y., Ye, J., 2019. Photo-assisted methanol synthesis via CO2 reduction under ambient pressure over plasmonic Cu/ZnO catalysts. Appl. Catal. B Environ. 250, 10–16. https://doi.org/10.1016/j.apcatb.2019.03.003

Wei, Y.P., Liu, Y., Guo, F., Dao, X.Y., Sun, W.Y., 2019. Different functional group modified zirconium frameworks for the photocatalytic reduction of carbon dioxide. Dalt. Trans. 48, 8221–8226. https://doi.org/10.1039/c9dt01767d

Weilhard, A., Argent, S.P., Sans, V., 2021. Efficient carbon dioxide hydrogenation to formic acid with buffering ionic liquids. Nat. Commun. 12, 1–7.

Wen, X., Chang, L., Gao, Y., Han, J., Bai, Z., Huan, Y., Li, M., Tang, Z., Yan, X., 2018. A reassembled nanoporous gold leaf electrocatalyst for efficient CO2 reduction towards CO. Inorg. Chem. Front. 5, 1207–1212.

Woyessa, G.W., dela Cruz, J. ar B., Rameez, M., Hung, C.H., 2021. Nanocomposite catalyst of

graphitic carbon nitride and Cu/Fe mixed metal oxide for electrochemical CO2 reduction to CO. Appl. Catal. B Environ. 291, 120052. https://doi.org/10.1016/j.apcatb.2021.120052

Wu, D., Deng, K., Hu, B., Lu, Q., Liu, G., Hong, X., 2019. Plasmon-Assisted Photothermal Catalysis of Low-Pressure CO 2 Hydrogenation to Methanol over Pd/ZnO Catalyst. ChemCatChem 11, 1598–1601. https://doi.org/10.1002/cctc.201802081

Wu, S., Zhou, C., Doroodchi, E., Nellore, R., Moghtaderi, B., 2018. A review on high-temperature thermochemical energy storage based on metal oxides redox cycle. Energy Conversion and Management 168, 421–453. https://doi.org/10.1016/j.enconman.2018.05.017

Wu, J., Huang, Y., Ye, W., Li, Y., 2017. CO2 Reduction: From the Electrochemical to Photochemical Approach. Advanced Science. https://doi.org/10.1002/advs.201700194

Wu, P.E., Juurlink, D.N., 2014. Carbon monoxide poisoning. Cmaj 186, 611. 10.1503/cmaj.130972

Wu, Z., Hao, X., Zhou, W., Yao, S., Han, J., Tang, X., Zhang, X., 2018. N-pentane activation and products formation in a temperature-controlled dielectric barrier discharge reactor. Plasma Sources Sci. Technol. 27. https://doi.org/10.1088/1361-6595/aae701

Wu, Z., Li, C., Li, Z., Feng, K., Cai, M., Zhang, D., Wang, S., Chu, M., Zhang, C., Shen, J., Huang, Z., Xiao, Y., Ozin, G.A., Zhang, X., He, L., 2021. Niobium and Titanium Carbides (MXenes) as Superior Photothermal Supports for CO2Photocatalysis. ACS Nano 15, 5696–5705. https://doi.org/10.1021/acsnano.1c00990

Xie, W., Li, R., Xu, Q., 2018. Enhanced photocatalytic activity of Se-doped TiO2 under visible light irradiation. Sci. Rep. 8, 1–10. https://doi.org/10.1038/s41598-018-27135-4

Xu, C., Zhang, Y., Pan, F., Huang, W., Deng, B., Liu, J., Wang, Z., Ni, M., Cen, K., 2017. Guiding effective nanostructure design for photo-thermochemical CO2 conversion: From DFT calculations to experimental verifications. Nano Energy 41, 308–319. https://doi.org/10.1016/j.nanoen.2017.09.023

Xu, H., Ouyang, S., Li, P., Kako, T., Ye, J., 2013. High-Active Anatase TiO2 Nanosheets Exposed with 95% {100} Facets Toward Efficient H2 Evolution and CO2 Photoreduction. ACS Applied Materials & Interfaces 5, 1348-1354. 10.1021/am302631b

Xu, L., Jiang, Q., Xiao, Z., Li, X., Huo, J., Wang, S., Dai, L., 2016. Plasma-Engraved Co3O4 Nanosheets with Oxygen Vacancies and High Surface Area for the Oxygen Evolution Reaction. Angew. Chemie - Int. Ed. 55, 5277–5281. https://doi.org/10.1002/anie.201600687

Xu, S., Chansai, S., Stere, C., Inceesungvorn, B., Goguet, A., Wangkawong, K., Taylor, S.F.R., Al-Janabi, N., Hardacre, C., Martin, P.A., Fan, X., 2019. Sustaining metal–organic frameworks for water–gas shift catalysis by non-thermal plasma. Nat. Catal. 2, 142–148. https://doi.org/10.1038/s41929-018-0206-2

Xu, Shanshan, Chansai, S., Shao, Y., Xu, Shaojun, Wang, Y. chi, Haigh, S., Mu, Y., Jiao, Y., Stere, C.E., Chen, H., Fan, X., Hardacre, C., 2020. Mechanistic study of non-thermal plasma assisted CO2 hydrogenation over Ru supported on MgAl layered double hydroxide. Appl. Catal. B Environ. 268, 118752. https://doi.org/10.1016/j.apcatb.2020.118752

Yadav, R.K., Baeg, J.-O., Oh, G.H., Park, N.-J., Kong, K., Kim, J., Hwang, D.W., Biswas, S.K., 2012. A photocatalyst–enzyme coupled artificial photosynthesis system for solar energy in production of formic acid from CO2. J. Am. Chem. Soc. 134, 11455–11461.

Yang, J., Pan, X., Jiao, F., Li, J., Bao, X., 2017. Direct conversion of syngas to aromatics. Chemical Communications 53, 11146–11149. https://doi.org/10.1039/c7cc04768a

Yang, P., Guo, S., Yu, X., Zhang, F., Yu, B., Zhang, H., Zhao, Y., Liu, Z., 2019. Photocatalytic Reduction of Carbon Dioxide over Quinacridone Nanoparticles Supported on Reduced Graphene Oxide. Ind. Eng. Chem. Res. 58, 9636–9643. https://doi.org/10.1021/acs.iecr.9b00242

Yang, X., Lee, J.H., Kattel, S., Xu, B., Chen, J.G., 2022. Tuning Reaction Pathways of Electrochemical Conversion of CO2 by Growing Pd Shells on Ag Nanocubes. Nano Lett. 22, 4576–4582. https://doi.org/10.1021/acs.nanolett.2c01667

Yang, X., Li, K., Wang, G., Li, X., Zhou, P., Ding, S., Lyu, Z., Chang, Y., Zhou, Y., Zhu, W., 2022. 2D Catalysts for CO 2 Photoreduction: Discussing Structure Efficiency Strategies and Prospects for Scaled Production Based on Current Progress. Chem. – A Eur. J. https://doi.org/10.1002/chem.202201881

Yin, Z., Palmore, G.T.R., Sun, S., 2019. Electrochemical Reduction of CO2 Catalyzed by Metal Nanocatalysts. Trends Chem. https://doi.org/10.1016/j.trechm.2019.05.004

Yu, S., Wilson, A.J., Heo, J., Jain, P.K., 2018. Plasmonic Control of Multi-Electron Transfer and C-C Coupling in Visible-Light-Driven CO2 Reduction on Au Nanoparticles. Nano Lett. 18, 2189–2194. https://doi.org/10.1021/acs.nanolett.7b05410

Yuan, J., Zhi, W.Y., Liu, L., Yang, M.P., Wang, H., Lu, J.X., 2018. Electrochemical reduction of CO2 at metal-free N-functionalized graphene oxide electrodes. Electrochim. Acta 282, 694–701. https://doi.org/10.1016/j.electacta.2018.06.107

Zeng, J., Bejtka, K., Ju, W., Castellino, M., Chiodoni, A., Sacco, A., Farkhondehfal, M.A., Hernández, S., Rentsch, D., Battaglia, C., 2018. Advanced Cu-Sn foam for selectively converting CO2 to CO in aqueous solution. Appl. Catal. B Environ. 236, 475–482.

Zeng, Y., Tu, X., 2017. Plasma-catalytic hydrogenation of CO2 for the cogeneration of CO and

CH4 in a dielectric barrier discharge reactor: Effect of argon addition. J. Phys. D. Appl. Phys. 50. https://doi.org/10.1088/1361-6463/aa64bb

Zeng, Z., Huang, H., Fu, Z., Lai, H., Long, B., Ali, A., Song, T., Deng, G.J., 2021. Plasmonic Cu NPs-embedded phenothiazine benzene with tunable bonding units for superior photocatalytic CO2 reduction. Appl. Surf. Sci. 550, 149361. https://doi.org/10.1016/j.apsusc.2021.149361

Zhan, H., Li, F., Gao, P., Zhao, N., Xiao, F., Wei, W., Sun, Y., 2014. Influence of element doping on La–Mn–Cu–O based perovskite precursors for methanol synthesis from CO 2/H 2. Rsc Adv. 4, 48888–48896.

Zhang, C., Yang, S., Wu, J., Liu, M., Yazdi, S., Ren, M., Sha, J., Zhong, J., Nie, K., Jalilov, A.S., Li, Z., Li, H., Yakobson, B.I., Wu, Q., Ringe, E., Xu, H., Ajayan, P.M., Tour, J.M., 2018. Electrochemical CO2 Reduction with Atomic Iron-Dispersed on Nitrogen-Doped Graphene. Adv. Energy Mater. 8. https://doi.org/10.1002/aenm.201703487

Zhang, D., Lv, K., Li, C., Fang, Y., Wang, S., Chen, Z., Wu, Z., Guan, W., Lou, D., Sun, W., Yang, D., He, L., Zhang, X., 2021. All-Earth-Abundant Photothermal Silicon Platform for CO2 Catalysis with Nearly 100% Sunlight Harvesting Ability. Sol. RRL 5, 1–7. https://doi.org/10.1002/solr.202000387

Zhang, F., Zhou, W., Xiong, X., Wang, Yuhao, Cheng, K., Kang, J., Zhang, Q., Wang, Ye, 2021. Selective Hydrogenation of CO2 to Ethanol over Sodium-Modified Rhodium Nanoparticles Embedded in Zeolite Silicalite-1. J. Phys. Chem. C 125, 24429–24439.

Zhang, J., Lu, S., Su, X., Fan, S., Ma, Q., Zhao, T., 2015. Selective formation of light olefins from CO2 hydrogenation over Fe-Zn-K catalysts. Journal of CO2 Utilization 12, 95–100. https://doi.org/10.1016/j.jcou.2015.05.004

Zhang, X., Zhao, X., Chen, K., Fan, Y., Wei, S., Zhang, W., Han, D., Niu, L., 2021. Palladium-modified cuprous(i) oxide with {100} facets for photocatalytic CO2reduction. Nanoscale 13. https://doi.org/10.1039/d0nr07703h

Zhang, Z., Li, J., Ji, M., Liu, Y., Wang, N., Zhang, X., Zhang, S., Ji, X., 2021. Encapsulation of multiple enzymes in a metal–organic framework with enhanced electro-enzymatic reduction of CO 2 to methanol. Green Chem. 23, 2362–2371.

Zhao, J., Bai, Y., Liang, X., Wang, T., Wang, C., 2021. Photothermal catalytic CO2hydrogenation over molybdenum carbides: Crystal structure and photothermocatalytic synergistic effects. J. CO2 Util. 49, 101562. https://doi.org/10.1016/j.jcou.2021.101562

Zheng, J., Kang, A.N., WANG, J., Jing, L.I., Yuan, L.I.U., 2019. Direct synthesis of ethanol via CO2 hydrogenation over the Co/La-Ga-O composite oxide catalyst. J. Fuel Chem. Technol. 47, 697–708.

Zhong, L., Yu, F., An, Y., Zhao, Y., Sun, Y., Li, Z., Lin, T., Lin, Y., Qi, X., Dai, Y., Gu, L., Hu, J., Jin, S., Shen, Q., Wang, H., 2016. Cobalt carbide nanoprisms for direct production of lower olefins from syngas. Nature 538, 84–87. https://doi.org/10.1038/nature19786

Zhou, Xiangping, Ji, J., Wang, D., Duan, X., Qian, G., Chen, D., Zhou, Xinggui, 2015. Hierarchical structured α-Al2O3 supported S-promoted Fe catalysts for direct conversion of syngas to lower olefins. Chemical Communications 51, 8853–8856. https://doi.org/10.1039/c5cc00786k

Zhou, Y., Zhao, Y., Shi, X., Tang, Y., Yang, Z., Pu, M., Lei, M., 2022. A theoretical study on the hydrogenation of CO 2 to methanol catalyzed by ruthenium pincer complexes. Dalt. Trans. 51, 10020–10028.

Zhu, W., Zhang, Y.J., Zhang, H., Lv, H., Li, Q., Michalsky, R., Peterson, A.A., Sun, S., 2014.

Active and selective conversion of CO2 to CO on ultrathin Au nanowires. J. Am. Chem. Soc. 136, 16132–16135. https://doi.org/10.1021/ja5095099

Zhu, W., Zhao, K., Liu, S., Liu, M., Peng, F., An, P., Qin, B., Zhou, H., Li, H., He, Z., 2019. Low-overpotential selective reduction of CO2 to ethanol on electrodeposited CuxAuy nanowire arrays. J. Energy Chem. 37, 176–182. https://doi.org/10.1016/j.jechem.2019.03.030